On Properties of Spots in Jets and Channel Flows

PhD Thesis

Bharat Thakarshi Dodia

Department of Mathematics

University College London

UNIVERSITY OF LONDON

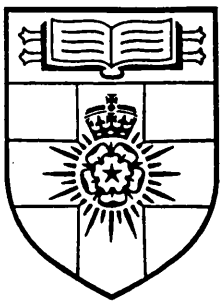

September 23, 1994

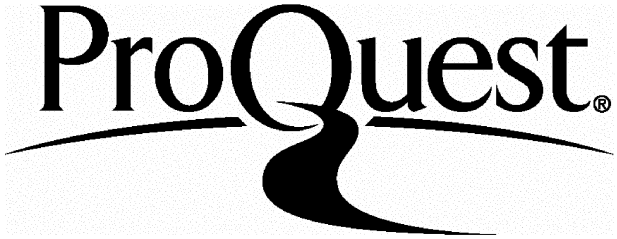

ABSTRACT

This thesis examines theoretically the structure of unsteady three-dimensional disturbances mainly in wall-jet flows and partly in channel flows, these disturbances having a spot-like character sufficiently far downstream of the initial disturbance. A start is made by using an approach similar to that in recent work by Doorly and Smith (1992), Smith (1992).

The inviscid initial-value formulation taken, involving the three-dimensional unsteady Euler equations for an incompressible fluid, allows considerable analytical progress on the nonlinear side, as well as being suggested by some of the experimental evidence on turbulent spots and by previous related theory. The behaviour at large scaled times and large scaled distances is associated with two major length scales, proportional to $(time)^{1/3}$ and to $(time)$, in the evolving spot. Within both scales it is found that nonlinear effects first enter the reckoning in the edge-layer(s) or caustic region(s) of the spot disturbance. The amplitude acquires the form of a nonlinearly distorted Airy function in this edge-layer, decaying exponentially outside the wing-tip region but approximately sinusoidally inside. As the typical amplitudes increase the nonlinear effects move towards the middle of the spot.

Numerical solutions for the governing nonlinear amplitude equations in the $(time)^{1/3}$ region are shown for two different amplitude levels. The computational results and accompanying analysis confirm that the positions of maximum amplitude gradually move towards the middle of the spot's trailing edge. As the amplitudes are increased further the governing equations for the wall-jet spot become analogous with those for the boundary-layer spot, and comparisons are made. The edge-layer properties further downstream are also examined.

Table of contents

List of figures

ACKNOWLEDGEMENTS

This thesis would not have been possible without the help and support of many friends and colleagues. Among those most deserving of thanks are first and foremost my supervisor Prof. Frank. T. Smith, for his superb and friendly guidance, for initially encouraging me to do some research and for his patience. I thank Professor S. N. Brown, Professor E. R. Johnson, Dr R. G. A. Bowles, Dr R. I. Bowles and Dr S. N. Timoshin for many useful discussions. Also finally I would like to thank my family for all their support.

Bharat T. Dodia, September 23, 1994

This work was supported by SERC, U.K, which is gratefully acknowledged.

CHAPTER 1

INTRODUCTION

§1.0 BRIEF HISTORICAL REVIEW OF TURBULENCE

In recent years much time and effort has been spent on examining nonlinear systems in nature and in general, such as in weather prediction, stock market analysis, turbulence modeling and so on, using numerous techniques ranging from experimental and computational studies to analytical studies; some of these techniques as applied to turbulence modeling of fluid flows are described below. Indeed in this introduction we will concentrate specifically on transitional/turbulent flows only, as regards examining nonlinear systems. However before discussing these points we should note that interest in turbulence as a phenomenon is as old as recorded history. For example, the Bible contains several references to turbulence or chaos; Publius Ovidus Naso in his classic masterpiece the Metamorphoses writes, *Before there was any earth or sea, before the canopy of heaven stretched overhead, Nature presented the same aspect the world over, that to which man has given the name of Chaos ...*; Leonardo da Vinci was intrigued by turbulence, as his sketch reproduced in fig 1.0.1 indicates.

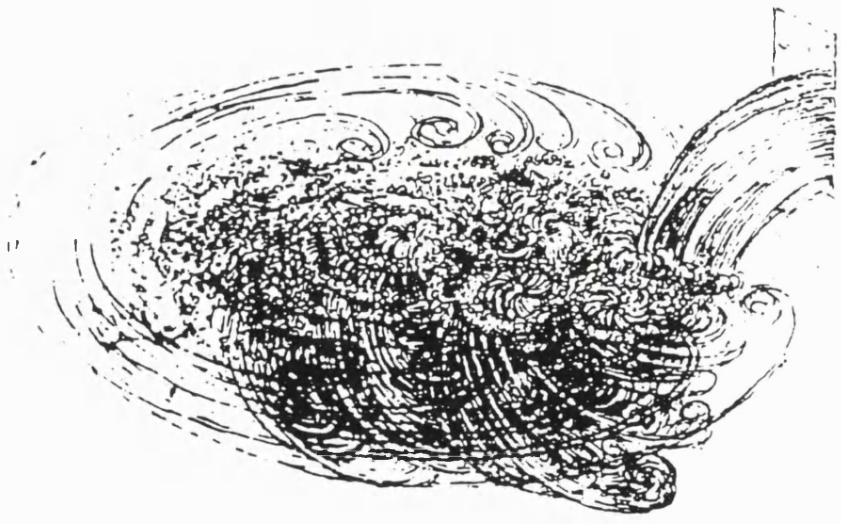

fig 1.0.1

Very early observations of turbulence – sketch by Leonardo da Vinci circa 1500

But the modern scientific study of turbulence dates form the late 1800s with the work of Osborne Reynolds. Early investigations on transition from laminar to turbulent flow were made by Reynolds (1883) and in his classic paper on the instability of flow down a pipe he writes as follows.

The .... experiments were made on three tubes .... The diameters of these were nearly 1 inch, 1/2 inch and 1/4 inch. They were all about 4 feet 6 inches long, and fitted with trumpet mouthpieces, so that water might enter without disturbance. The water was drawn through the tubes out of a large glass tank, in which the tubes were immersed, arrangements being made so that a streak or streaks of highly coloured water entered the tubes with the clear water.

The general results were as follows:

(1) When the velocities were sufficiently low, the streak of colour extended in a beautiful straight line through the tube (see fig 1.0.2*a*).

(2) If the water in the tank had not quite settled to rest, at sufficiently low velocities, the streak would shift about the tube, but there was no appearance of sinuosity.

(3) As the velocity was increased by small stages, at some point in the tube, always at a considerable distance from the trumpet or intake the colour band would all at once mix-up with the surrounding water, and fill the rest of the tube with a mass of coloured water (see fig 1.0.2*b*). *Any increase in the velocity caused the point of breakdown to approach the trumpet, but with no velocities that were tried did it reach this. On viewing the tube by the light of an electric spark, the mass of colour resolved itself into a mass of more or less distinct curls, showing eddies* (see fig 1.0.2*c*) (Acheson 1990).

With these observations in mind O. Reynolds theoretically decomposed the velocity field into a mean-flow plus a perturbation, and time averaged the Navier-Stokes equations on the basis of this decomposition. The equations he obtained are now called the Reynolds-averaged Navier-Stokes equations. The averages of the products of the perturbation terms appear in the mean-flow equations as virtual stresses, which are usually known as Reynolds stresses.

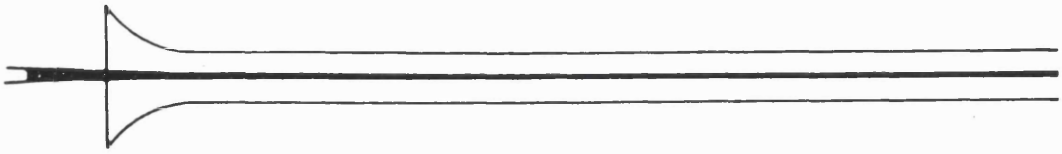

fig 1.0.2a

For low velocities a straight line is observed

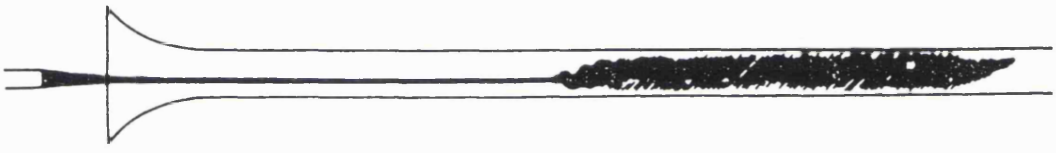

fig 1.0.2b

At higher velocities the colour band mixes with the surrounding fluid

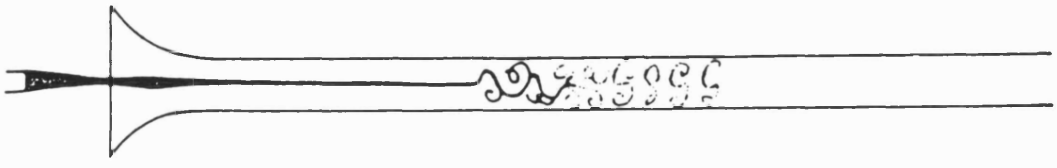

fig 1.0.2c

Eddies are seen when the tube is observed by the light of an electric spark

These Reynolds stresses represent the nonlinear effect of the fluctuating flow on the mean-flow, for the above decomposition. From the above Reynolds was able to gauge in a fairly decent way some of the important parameters controlling the breakdown of laminar flow.

§1.1 THEORETICAL AND EXPERIMENTAL DEVELOPMENTS

The onset of turbulent flow in a boundary layer requires the presence of sufficiently strong disturbances, but the required strength of the disturbances depends on their form and the Reynolds number. In the absence of such sources of finite disturbance as surface excrescences or waviness and with a low level of turbulence in the external flow (Tu less than about 0.1 %, where Tu is a simple measure of the turbulence intensity in the free stream, i.e. $Tu = (\frac{\bar{u'^2}+\bar{v'^2}+\bar{w'^2}}{3})^{1/2}/u_e$. (u', v', w') are the perturbation components of the velocity vector in the streamwise, normal and spanwise directions and u_e is the free stream velocity.) the process begins with the amplification of unsteady Tollmien-Schlichting waves on quasi-flat surfaces and/or the appearance of streamwise Taylor-Görtler vortices associated with surface or streamwise curvature. These in turn depend on the Reynolds number and the pressure distribution. However, there may then be a large streamwise distance between the positions at which these waves or vortices first appear and the onset of turbulence, and our knowledge of the physics of the process (the transition) that develops within that distance is far from complete.

An important line of attack that has been pursued for many years is to extend the classical small-perturbation stability theory to disturbances of finite amplitude, by including the nonlinear terms in the equations of the perturbed flow, e.g Stuart (1960), Reynolds and Potter (1967). This brings into play harmonics of the basic sinusoidal disturbance considered and demonstrates that, even for conditions of stability to linear modes, the instantaneous velocity profiles resulting from the combined mean and disturbance velocities can readily be sufficiently inflected to be destabilized (over a part of the disturbance wave) with an associated strong amplification rate. The wavelengths of the distur-

bances that are destabilized tend to be large relative to the boundary layer thickness ($\simeq 10\delta$, where δ is the boundary layer thickness) so that the inflected profiles can be present over a significant extent of the surface and for time intervals of the order $10\delta/u_e$. These regions of inflected profiles can introduce the possibility of a chain of instabilities developing over a wide spectrum, leading to a flow that could be described as turbulent, with a mean flow differing markedly from the original laminar flow.

However, alternative and, in some quarters, more readily accepted ideas on the development of the transition process in certain configurations , from the appearance of Tollmien-Schlichting waves to turbulence, have emerged from the work of Emmons (1951), Schubauer and Klebanoff (1956) and the subsequent work of Narasimha (1957). The ideas concern so-called turbulent spots. Although in fact there are many transition paths (depending on the particular input disturbances) and numerous corresponding theoretical ideas (e.g above), our concern in this thesis is primarily with understanding the properties of spots. From observations of the flow on a water table, Emmons formulated the view that turbulence is not initiated along a continuous front but starts in the form of randomly distributed 'spots' of turbulence, each of which expands as it moves downstream. Fully developed turbulent flow then begins when these expanded regions of turbulence merge across the whole span. The transition region can therefore be said to begin at the streamwise position where the spots first appear and to end where they have merged to form a continuous front. Emmons first suggested that the probability of the generation of spots is constant with distance x downstream from the beginning of the transition region but later modified this by assuming the probability is proportional to x^n where $n \geq 1$.

In a purely laminar region the probability is zero, while in the turbulent region the probability is unity and the fraction of time over which the flow at a point in the transition region is turbulent is referred to as the 'intermittency factor' (γ). For a flat plate at zero incidence it is found that γ can be described

as a function of ξ, where $\xi = (x - x_t)/\lambda$ and $\lambda = x_{\gamma=0.75} - x_{\gamma=0.25}$, while x_t marks the beginning of transition. However, Narasimha (1957) has shown that Emmons's (1951) hypothesis for the generation of spots over the transition region leads to a distribution of γ that does not fit the experimental data. Narasimha (1957) then postulated that spots form at a preferred streamwise position but randomly in time and spanwise location. This postulate led to a relation for a flat plate at zero incidence, $\gamma = 1 - exp(-0.412\xi^2)$, which is in better agreement with the experimental data. Adverse pressure gradients, noise, turbulence in the external flow, increases in the Reynolds number and other such destabilizing factors increase the rate of generation of spots.

Experimental studies have shown that from a small surface excrescence a continuous stream of spots is generated which expand as they move downstream to form a wedge of turbulence of semi-apex angle $\simeq 10°$ in boundary layer flows. Such wedges have long been observed in wind tunnels with the aid of suitable flow visualization techniques, for example by Carlson, Widnall and Peeters (1982) who have studied spot generation in channel flows; see below.

Schubauer and Klebanoff (1955) studied experimentally spots in a boundary layer on a flat plate. Details of the geometry of the spots and their growth with movement downstream were demonstrated in the experiments by Schubauer and Klebanoff. A spot was introduced into a laminar boundary layer on a flat plate in a wind tunnel by means of an electrical spark discharge normal to the surface through the boundary layer. The spot's development and growth downstream is illustrated below (see Stuart (1963)), where it is seen that its forward apex moves downstream at close to the main stream velocity, but its rear edge convects downstream at about half that speed. Hot-wire records within the growing 'triangular' region are much the same as those of fully developed turbulent flow but upstream of this region at any instant the flow is smooth and laminar. Consistent with this, it was found that the instantaneous velocity profiles in the transition region are for part of the time characteristic of turbulent flow, and at other times they are those of a laminar boundary

layer; hence the concept of intermittency.

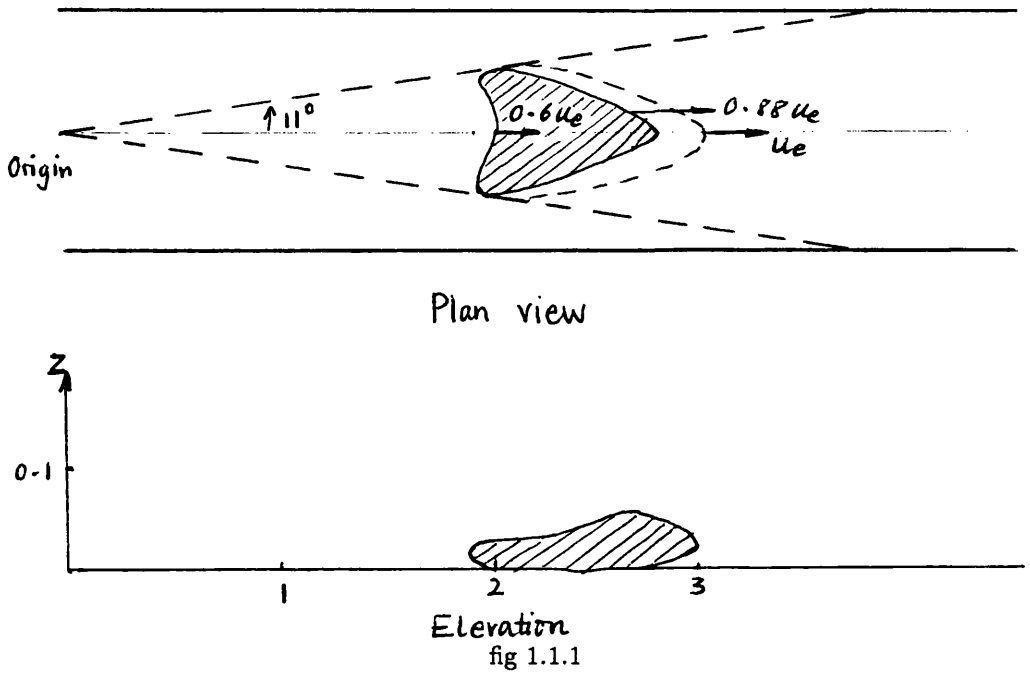

fig 1.1.1

We note that even in nominally two-dimensional flow the Tollmien-Schlichting waves that develop in regions of instability do not remain rectilinear but show evidence of spanwise warping or bending which becomes increasingly marked with movement downstream. See experiments by Klebanoff, Tidstrom and Sargent (1962) and recent theory by Stewart and Smith (1992). The warping appears to arise from initially small irregularities in the main flow. Hence the associated disturbance vorticity develops streamwise components which grow as the warping increases, and these in turn induce secondary flows to and from the surface which help to intensify the warping. The disturbance vorticity lines thus form hairpin-like bends and as the bends grow the vorticity lines stretch and strengthen along the inclined sides of the bends. This results in 'peaks' and 'hollows' of high and low disturbance intensity with higher amplification rates at the 'peaks'. At some stage the hot wire records at a peak show 'spikes' of a kind that can be identified as due to turbulence and we can infer that a spot is born (see Stuart (1963), Stewart and Smith (1992)). The above description is illustrated below in fig 1.1.2. We note that the process described

above in which turbulent spots eventually appear is forced, as opposed to introducing a small amplitude disturbance into the flow and letting it develop freely into a transitional/turbulent spot. Indeed this is what is assumed below in the work that follows. We also note that surface excrescences, external turbulence and noise can in some measure bypass the initial Tollmien-Schlichting wave stage of the above process, since they can introduce directly disturbances of sufficiently large amplitude associated with highly unstable three-dimensional flow patterns which can readily generate 'spots'.

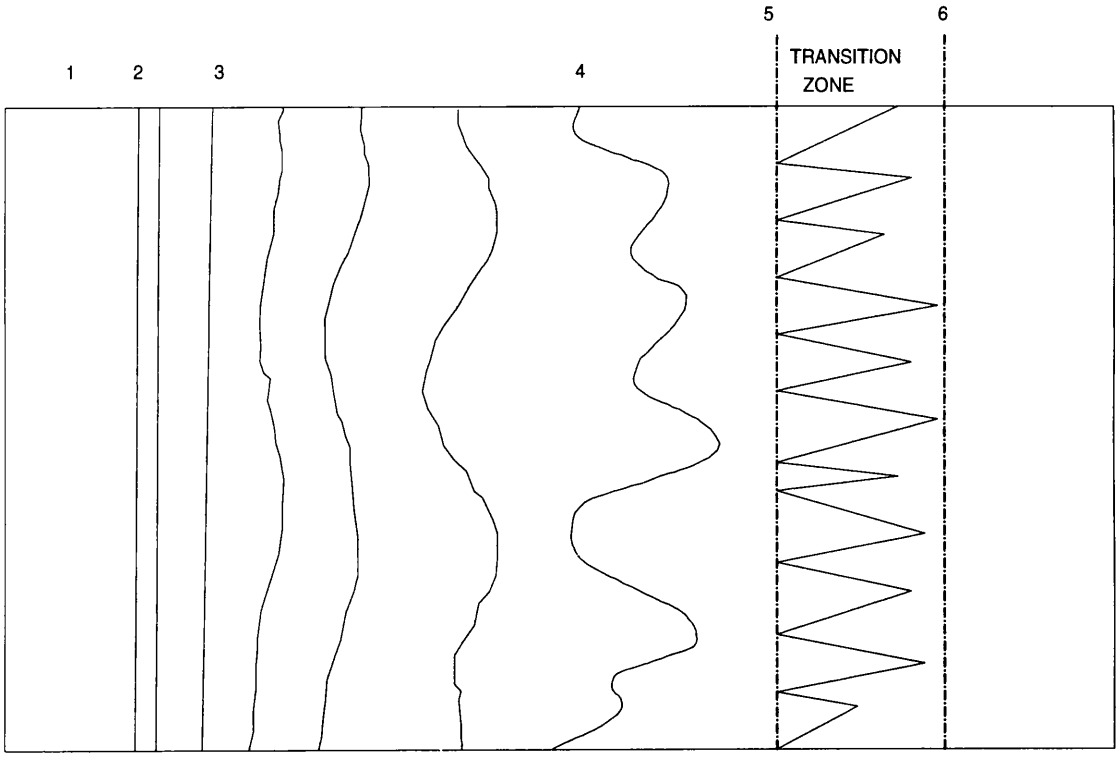

fig 1.1.2

Stages in the transition process. (1) stable laminar flow, (2) Tollmien-Schlichting waves, (3) Warping of waves, formation of vortex loops, (4) Development of nonlinear instabilities, (5) Formation and growth of turbulent spots, (6) Fully developed turbulent flow (from Young (1989)).

§1.2 DIRECT NUMERICAL SIMULATION

Here we briefly review the results obtained from certain direct numerical simulations (on spots mainly). The basic approach in all the numerical schemes that have been developed for the numerical solution of the Navier-Stokes equations for unsteady flows is to use finite differencing or spectral decomposition of the space for the numerical approximation of the spatial derivatives. From these the partial-time derivatives of u_i (the velocity components) are then found, and from them the flow field may be extrapolated to the next time interval.

Patera and Orzag (1981) performed numerical simulations of transition from the two-dimensional Tollmien-Schlichting instability wave stage to the stage of breakdown into small-scale turbulence. They were able to demonstrate that the breakdown is initiated by a secondary three-dimensional instability of the two-dimensional Tollmien-Schlichting wave. Henningson, Spalart and Kim (1989) examined computationally the evolution of a turbulent spot in a channel flow. Figure 1.2.1 shows a contour plot for the normal velocity. In figure 1.2.1 we see the appearance of oblique wave trains at the leading edges of the spot. These waves are seen in experiments, see Lindberg et al (1984); however the same characteristic waves are not found in boundary layer spots.

In a more recent study Henningson and Kim (1991) investigated the turbulence characteristics inside a turbulent spot in plane Poiseuille flow by analyzing a database obtained from a direct numerical simulation. The authors found that the spot consists of a wave area and a turbulent area, with the flow inside the turbulent area resembling a fully developed turbulent channel flow. While in the wave area they find that inflexional mean spanwise profiles cause a rapid growth of oblique waves, which break down to turbulence, see fig 1.2.2

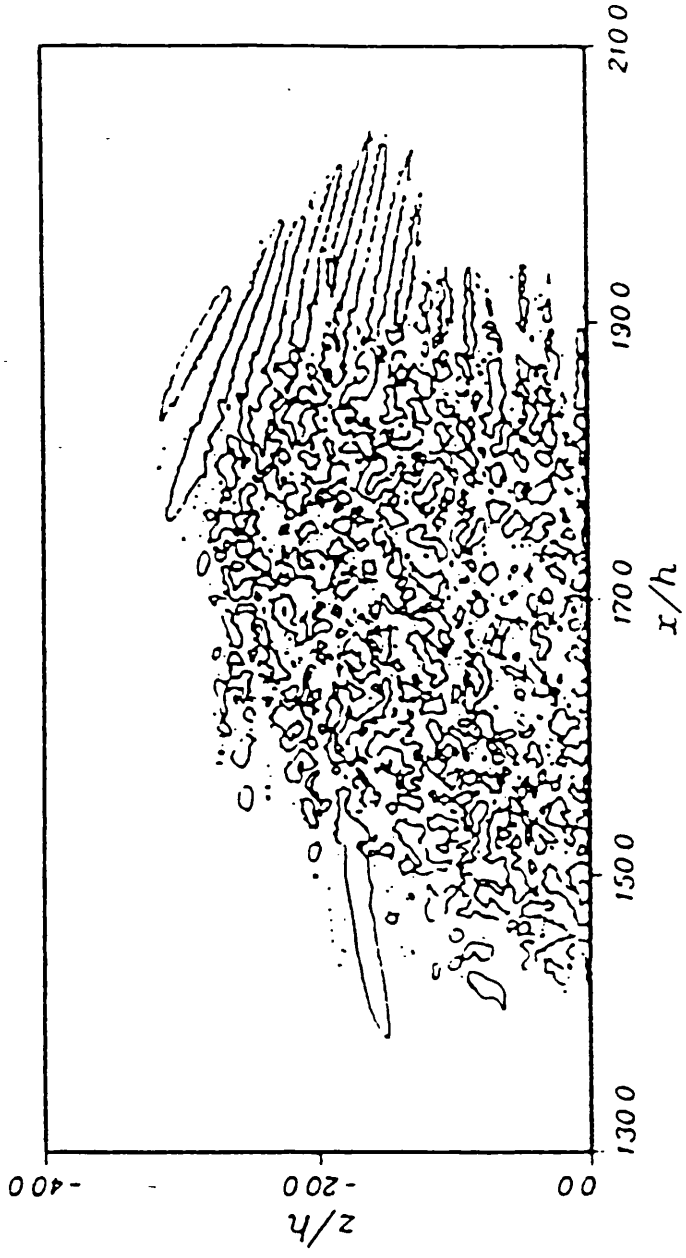

fig 1.2.1

Contours of normal velocity at centre plane of a turbulent spot in a channel for nondimensional time $t = 258$ (from Henningson, Spalart and Kim (1989)).

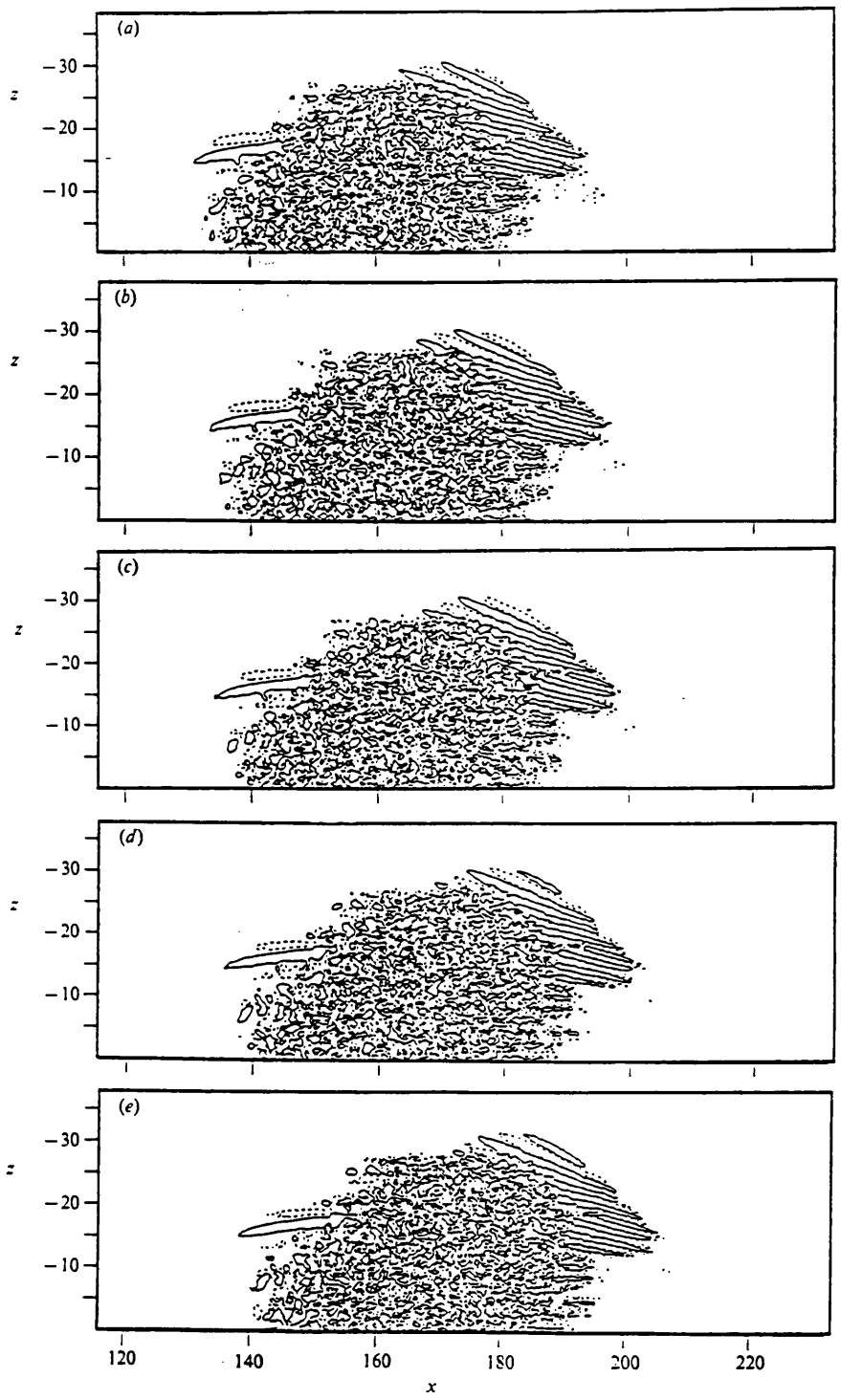

fig 1.2.2

Time development of the instantaneous normal velocity at the centreline

± 0.01 contours at (a)$t = 246$, (b)$t = 249$, (c)$t = 252$, (d)$t = 255$, (e)$t = 258$

(from Henningson and Kim (1991)).

§1.3 CHARACTERISTICS OF SPOTS IN BOUNDARY-LAYER AND CHANNEL FLOWS

In this section we review in a little more detail the results obtained from experiments on turbulent spots in boundary-layer and channel flows. Firstly for boundary-layer spots (see Wygnanski, Sokolov and Friedman (1976)):

- a typical lateral spread angle of the spots is 10° to each side of the plane of symmetry. This wedge angle which represents the spanwise growth of the spot is independent of the location of the disturbance and the free stream velocity.

- far downstream all quantities measured seem to be independent of the type of disturbance which generated the spot in the first place.

- as noted above Schubauer and Klebanoff (1956) found that the leading arrowhead shape of the boundary-layer spot propagates with about 90% of the free stream velocity and that it consists of an overhang with laminar fluid underneath, while the straight rear interface moves with about half the free-stream speed. In this way the spot entrains laminar fluid through its interfaces, resulting in its elongation as it proceeds downstream.

- the spanwise velocity component is everywhere directed outwards (i.e away from the plane of symmetry). The normal component of velocity is directed towards the surface near the leading interface and away from it in the remaining part of the spot.

- the front and the spanwise edges, or wing-tips, of the spots are notably sharp, see Smith (1992).

- the height of the overhang interface corresponds initially to the thickness of the laminar boundary layer but once the spot has developed the surrounding boundary-layer seems to have little or no effect on the spot shape. The laminar boundary layer does, however, affect the rate of growth of the spot.

- much of the dynamics in a spot resembles closely that in a fully turbulent boundary-layer.

- Wygnanski, Haritonidis and Kaplan (1979) found Tollmien-Schlichting waves trailing the spanwise wingtips of the spots, and they put forward the idea that the breakdown of these waves causes the spot(s) to spread, while Glezer, Katz and Wygnanski (1989) found that in certain instances the breakdown of the waves adds to the turbulent part of the spot. Contrary to this, Chambers and Thomas (1983) argue that these waves play no significant role in the spreading or breakdown of the spot itself, and they further argue that the trailing wave packet is only a remnant of the waves caused by the initial disturbance.

We now list some of the properties which characterize Poiseuille-flow spots in channels.

- Turbulent spots in channel flows have the arrowhead pointing in the upstream direction in contrast with the boundary-layer spot; see Carlson, Widnall and Peeters (1982). The channel geometry may be one of the factors which needs to be considered, in relation to this change in direction of the arrowhead.

- Around the spot a wave pattern occurs. Oblique waves are seen at the spanwise wingtips and trailing the turbulent region.

- Alavyoon, Henningson and Alfredsson (1986) showed that the propagation velocities vary with the Reynolds number, with typical values of 80% and 50% of the centreline velocity for the front and the trailing interface, respectively.

- The typical lateral spread-angle of the spot is found to increase with Reynolds number although the typical value is again 10°.

- Widnall (1984) found that the turbulent part of the spot acts as a partial flow blockage for the laminar fluid outside the spot.

Below we show the results of a flow-visualization study of transition in plane Poiseuille flow, by Carlson, Widnall and Peeters (1982). In all the figures $1.3.2a-f$, x/h (in the notation of the last named paper) represents the distance downstream of the generator, where h is the channel depth, and R represents the Reynolds number, see Carlson, Widnall and Peeters (1982). In figure $1.3.2e$ it is seen that the spot ultimately splits into two separate spots, a feature which has not been seen in boundary layer flows.

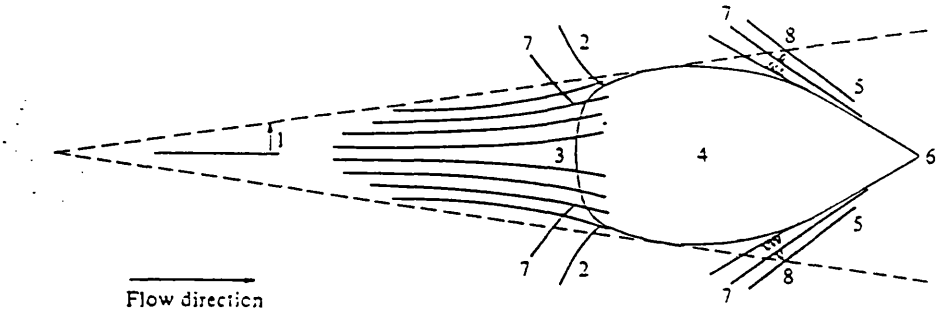

fig 1.3.1

spot nomenclature: (1) spreading half-angle; (2) spanwise tips; (3) streaks;

(4) region of small scale turbulence; (5) spot leading edge; (6) spot front;

(7) oblique waves; (8) tongues of breakdown (from Carlson, Widnall and Peeters (1982))

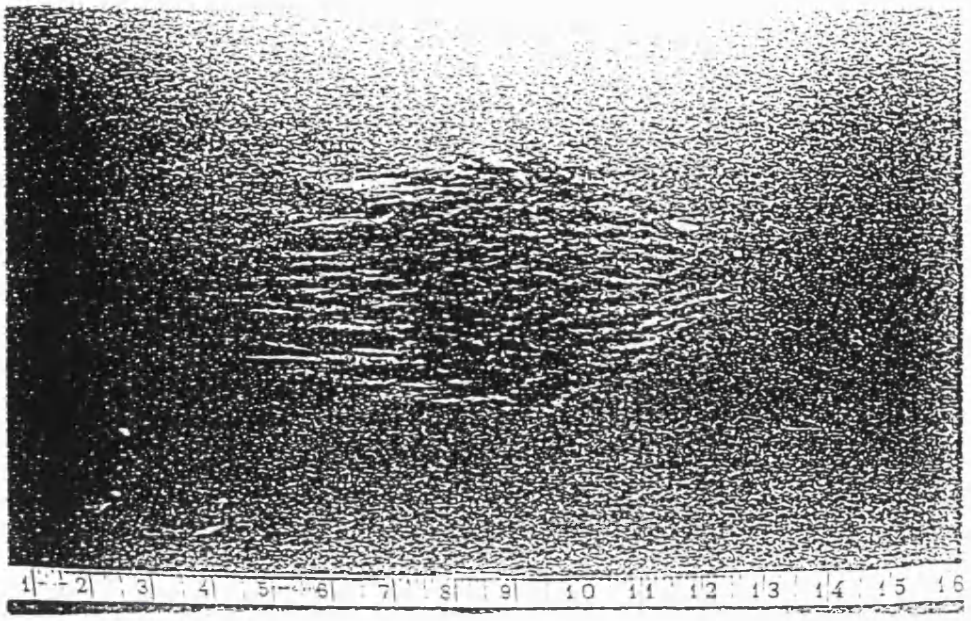

fig 1.3.2a, spot at $x/h = 50, R = 1000$.

In addition to the region of small-scale turbulence and the trailing streaks, oblique waves are visible at the sides and at the rear.

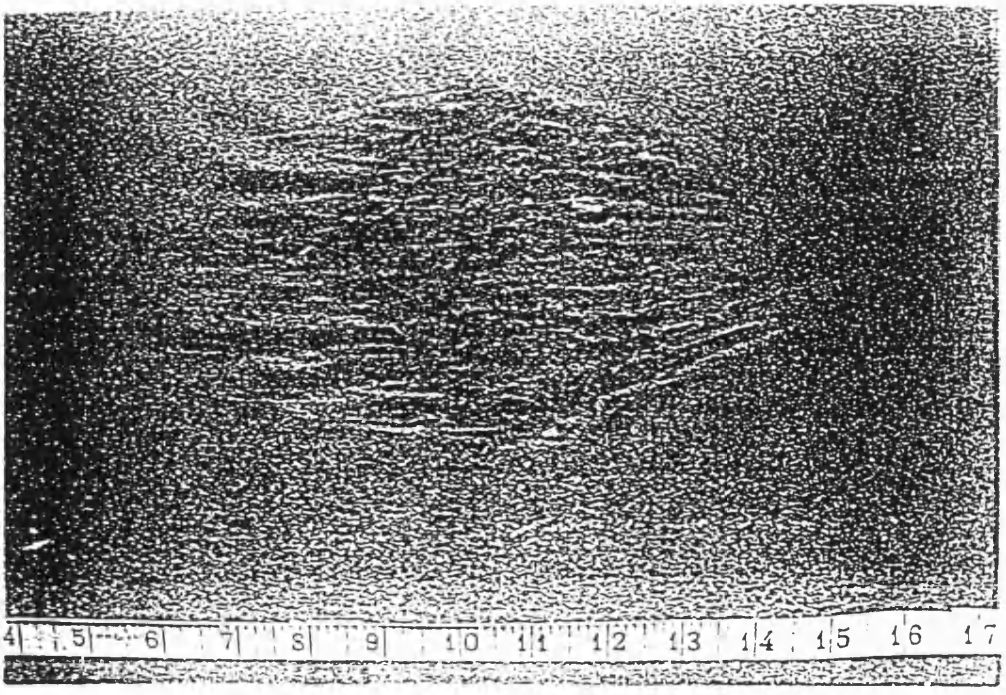

fig 1.3.2b, spot at $x/h = 64, R = 1000$.

Strong oblique waves are visible, both upstream of the leading edge of the spot and at the spanwise tips.

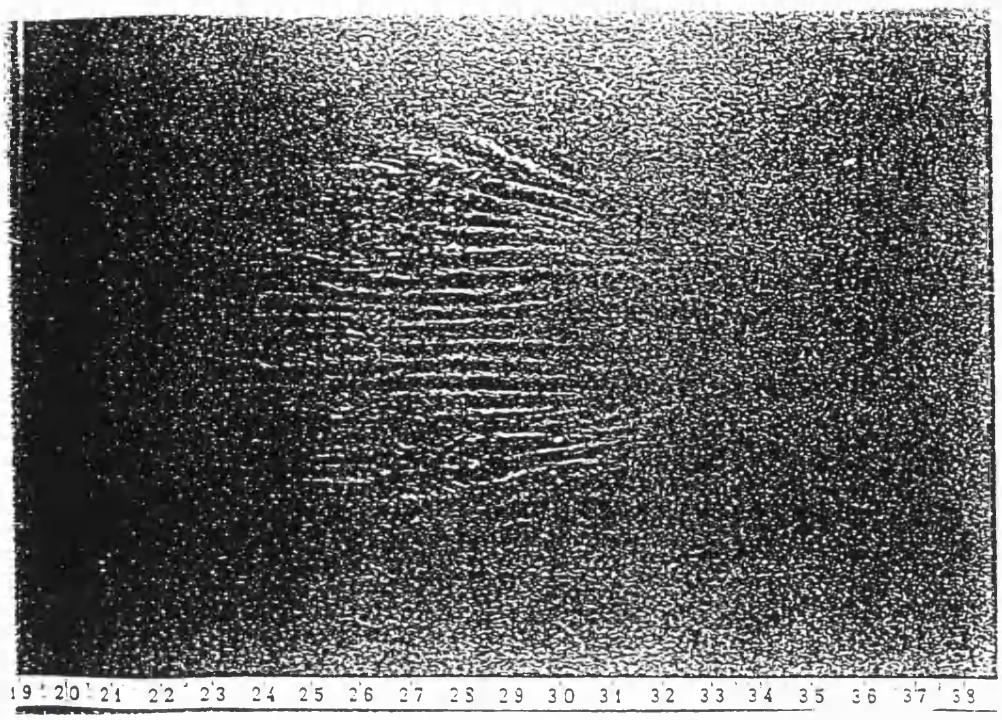

fig 1.3.2c, spot at $x/h = 132, R = 1000$.

At this stage the front tip is less well defined, and the centre region

is filled with longitudinal streaks. We observe the beginning of spot splitting.

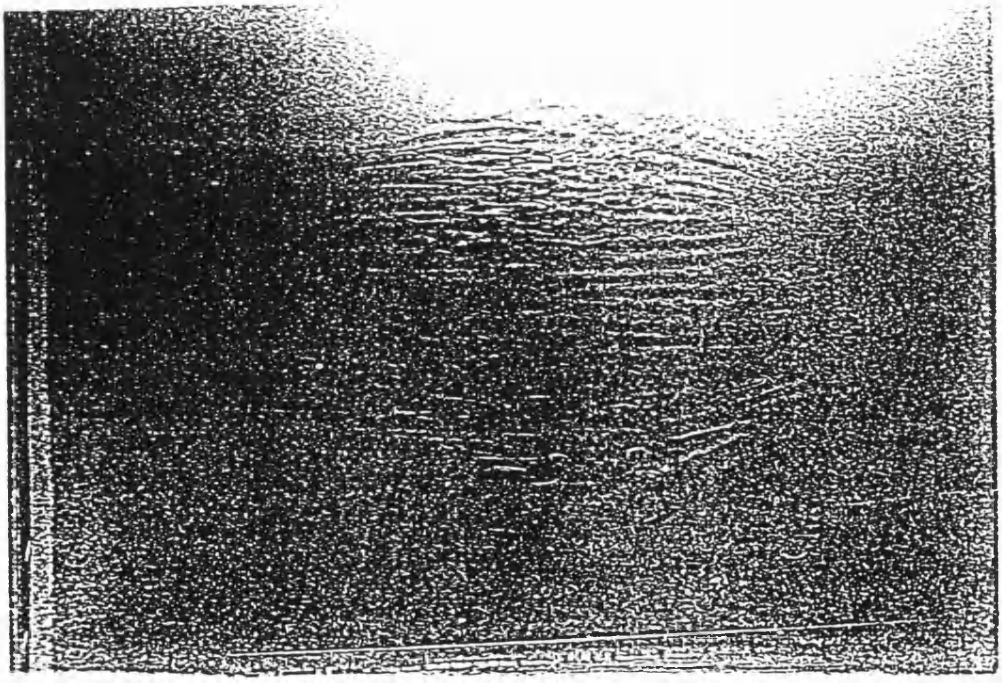

fig 1.3.2d, spot at $x/h = 132, R = 1000$.

This figure shows a spot slightly downstream of that of fig 1.3.2c.

Tongues of breakdown on the oblique waves are present.

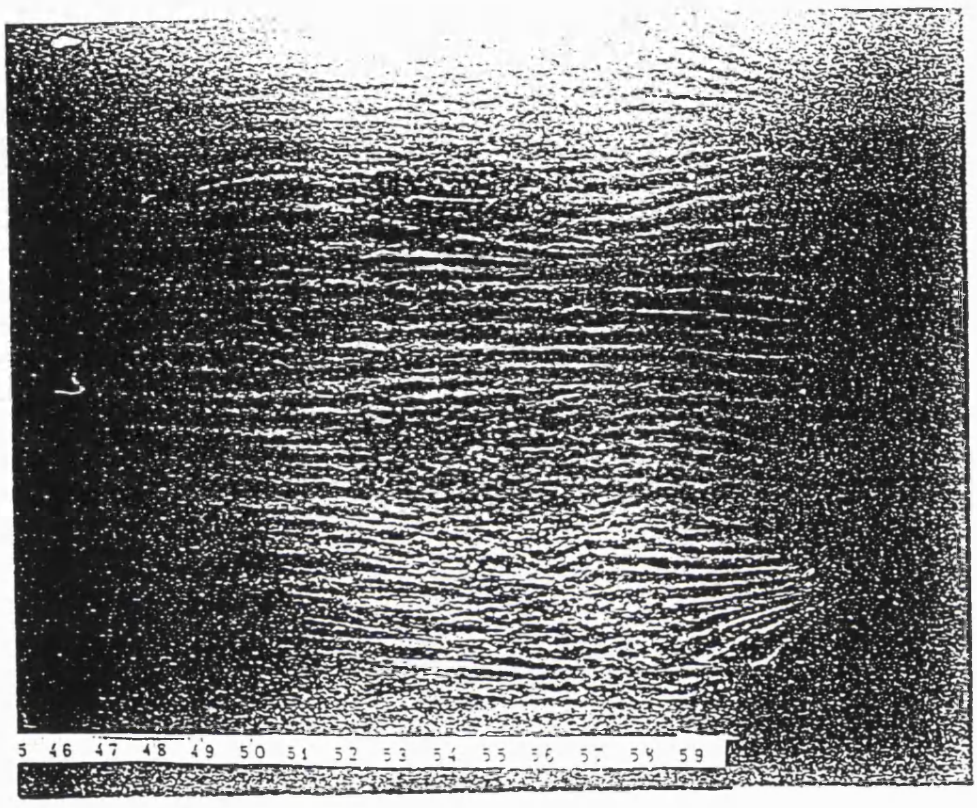

fig 1.3.2e, spot at $x/h = 260, R = 1000$.

The spot is now quite large and very flat. The channel is 6mm deep, while the diameter of the spot is 500mm. The spot has essentially become two spots separated by a region of longitudinal streaks.

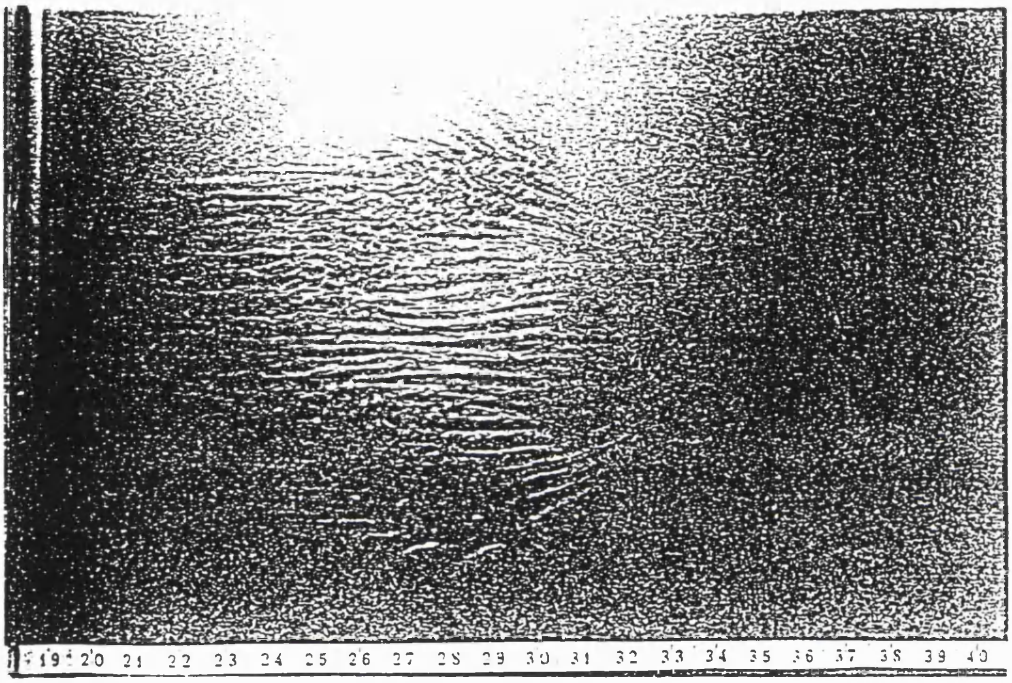

fig 1.3.2f, spot at $x/h = 132$, $R = 1100$.

At these higher Reynolds numbers, the oblique waves are less swept,

and the wake flow is more turbulent.

§1.4 THEORETICAL STUDIES ON SPOTS, AND PRESENT WORK

To date there have been numerous experimental and computational studies on turbulent spots, as described above, but little theoretical work has been done in the area. Exceptions, attempting to build up a theoretical model of such spots, are Doorly and Smith (1992), Smith (1992), Smith, Dodia and Bowles (1994), Smith, Doorly and Rothmayer (1990), Bowles and Smith (1994) (see also Gaster (1975), Gaster and Grant (1975), Gaster (1990) on laminar spots). In Doorly and Smith the authors address a linear model, as a starting point, for a transitional and/or turbulent spot in a compressible or incompressible boundary-layer. They define a spot as follows; 'a spot disturbance is the flow perturbation that develops from an initial disturbance, to a boundary-layer in the present setting, with the typical development involving mostly downstream travel, some amplitude growth, and spatial spreading of the spot'.

Their analysis concentrates on relatively long-scale disturbances in the context of the unsteady Euler equations. In the incompressible regime they find that concentrated wake activity is found downstream inside a wedge of half-angle 19.47° and that the maximum amplitude growth occurs at the edges of this wake. They note that this aspect is the same as for the Kelvin ship-wake and as studied in another context by Cheng and Johnson (1982). Their study suggests that significant effects arise mainly in two regions far downstream, the first of which has the streamwise and spanwise scaled coordinates, X, Z say, large and $O(T^{1/2})$, whereas the second region further downstream is where X, Z are $O(T)$. They draw the general conclusion that nonlinear effects need to be incorporated in order that their results match with the previous experiments and computations, since in particular the half-angle prediction is over-estimated compared with experiments and computations. However the gross features which they obtain for the spot structure match qualitatively with experiments, e.g a wedge shape with accentuated edge effects downstream at relatively large times.

In Smith (1992) a nonlinear follow-up study is presented, and in many respects it is a seminal contribution to the understanding of transitional/turbulent spots theoretically, in this author's view. The main conclusion is that as the characteristic amplitudes present in the edge-layer increase the influence of nonlinearity can spread from the edge-layer inwards towards the middle of the spot, so that the spread angle becomes reduced.

In a more recent interesting and important study by Bowles and Smith (1994), the authors analyze short-scale effects on model boundary-layer spots. They find that taking into account short scales acts to reduce the spread half-angle to approximately 11°, which is more or less the typical value obtained from experiments. Also amongst other features they find that the 'lift-up' profile and the central bulge are in agreement with experimental results and that the maximum disturbance amplitude occurs at the wingtips both in the model and in observations. The authors also suggest tentatively that the 'calm region' observed in experiments, see for instance Glezer, Katz and Wygnanski (1989) and references therein, may correspond to a linearly disturbed zone that lags behind the trailing edge of a nonlinear spot, in their study. Their main general conclusion is that both nonlinearity and short-scale effects play important roles.

The aim of the work which follows below is to model the above mentioned spot(s) in wall-jet and channel flows theoretically, although only the wall-jet case is studied in detail. A start is made by using the approach of Doorly and Smith (1992), and Smith (1992). A number of distinct regions of the spot are examined, namely the edge-layer or wing-tip region of the spot at $O(t^{1/3})$ and $O(t)$ (see chapters 2 and 4) distances in the streamwise and spanwise directions, and the middle-region of the spot covering the entire trailing-edge zone, see chapter 5. Also we investigate the influence of raised amplitudes in the $O(t^{1/3})$ zone, and establish that increased nonlinearity plays an important role. However we note that in the wall-jet case inflectional modes/disturbances are neglected by and large, in order to gain insight into nonlinear neutral

disturbances instead, although the former disturbances can be accommodated in the higher-amplitude theory.

Firstly a linear model is set-up in chapter 2, from which we obtain some important elementary properties of the spot disturbance. The half-angle prediction is found to be 30° for both the wall-jet and channel flows, which is a huge over-estimate since in experiments the typical value is approximately 10° for channel flows, as discussed above. However we show that raising the amplitude by carrying out a nonlinear study acts to reduce this angle slightly. Although as noted above short-scale effects also act to reduce this half-angle significantly, here we do not examine those effects. As in Doorly and Smith (1992) we find that increasingly concentrated waves form in the wake far downstream, but with their maximum amplitudes occurring at the edges, see chapter 2. Second a nonlinear model is presented, where we use the results from the linear theory as a starting point. At this first higher amplitude stage which we shall refer to as amplitude level I, we find as in Smith (1992), Smith, Dodia and Bowles (1994), that the main governing amplitude equation confirms the linear theory at small amplitudes, whereas the full nonlinear system which we obtain requires a computational treatment, which is shown in part 2 of chapter 2. This amplitude level I investigation in specifically centered around the $O(T^{1/3})$ scaled distance in the streamwise and spanwise directions, near the wing tips or side edges of the spot and it suggests that further higher amplitude effects need to be examined. In chapter 3 amplitude level II is analyzed. The amplitude equations that we obtain are analogous to those obtained in Smith, Dodia and Bowles (1994), Dodia, Bowles and Smith (1994/5). We find that a modified version of the governing system of equations needs to be solved initially, since the actual equations are difficult to solve at first. However when more information using a phase plane analysis on the modified equations is obtained, we are able to find suitable solutions for the actual governing equations. The main conclusion that we draw from the results is that nonlinear effects move towards the centre of the spot disturbance, at these higher am-

plitudes, i.e the spread angle is reduced. In chapter 4, we examine the edge layer further downstream at scaled distances of $O(T)$ in the streamwise and spanwise directions. As for the $O(T^{1/3})$ scaling we carry out both a linear and a nonlinear analysis. Again we find that the spread half-angle is 30°, because all along the edge layer up to $O(T)$ scaled distances the governing equations that we initially address are the thin layer Euler equations. Also as before an Airy function dependence is found in the wing tip region, with linear properties holding outside the edge layers. However we find that in this $O(t)$ zone the initial disturbance affects the amplitude at leading order, or in other words this region feels the 'footprint' of the initial disturbance. For the particular details with which we choose to work with, it is found that the amplitude is damped down exponentially. Concerning mainly higher amplitude effects again we investigate in chapter 5 (amplitude level III) strongly nonlinear effects at substantially increased amplitudes, guided by the results from chapter 3. At this level nonlinearity gradually floods into the centre of the spot, and we find Reynolds stresses and the KDV equation appearing amongst other features. The analysis in this midspot area is similar to that in Smith, Dodia and Bowles (1994), Bowles, Dodia and Smith (1994/5), for the boundary layer spot case, partly because the mean pressure-displacement law then plays only a passive role. Finally in chapter 6 we modify the analysis for the wall-jet spot case and examine a spot in a plane Poiseuille channel flow. Further details are given in the introductions to each chapter.

CHAPTER 2

PART I

LINEAR & NONLINEAR INITIAL VALUE PROBLEMS

§2.0 INTRODUCTION

This chapter concentrates upon applying, to spots in wall-jet flows, the techniques employed by Doorly and Smith (1992), Smith (1992), Smith, Dodia and Bowles (1994) in boundary layers. We start by considering the three-dimensional unsteady Euler equations which are believed to be relevant to the transitional-turbulent regime (see Smith and Burggraf (1985), Smith et al (1990), C.R.Smith et al (1991)), and to the study of spot disturbances, and so we are concerned with the inviscid dynamics of the initial-value problem for such spots. Also the entire study below is for Newtonian, incompressible-fluid flows only. In Smith, Doorly and Rothmayer (1990) the authors find agreement between the Euler-stage theory and experiments on certain of the established scales for fully turbulent flow. So the main concern here is with the three-dimensional Euler setting since we feel that the scales and speeds of real spots are captured using this setting, and attention is then focused on an unsteady thin-layer version appropriate to relatively long-scale disturbances (see also footnote 1 below).

In section 2.1 a linearized version of the thin-layer equations is examined, as a first step, permitting a relatively simple analysis which produces useful and 'universal' results at large times. In particular, concentrated wake activity is found far downstream inside a wedge of half-angle 30° in plan view (see fig 2.0.1) and the main amplitude growth occurs at the edges of this wake. Sample computational solutions of the dispersion relation obtained by Doorly and Smith (1992) from their linearized theory for a boundary layer spot are shown (see figures (2.2.1a,b), (2.2.2a,b), (2.2.3a,b)) for comparison. The corresponding wake half-angle prediction is $\sin^{-1}(1/3) = 19.47°$ for their problem. The dispersion relation obtained for the wall-jet case in the present setting is examined in section 2.2.

The linear theory just mentioned shows the emergence of two major length scales, being proportional to the scaled time and to its cube root. It is found that nonlinear effects first enter the reckoning of the large-time large-distance

behaviour in the edge layers near the spot's wing-tips (which correspond to caustics in linear theory), as the typical input amplitude is increased. In sections 2.3 and 2.4 the linear theory is used as a guide in setting up the nonlinear problem. The above-mentioned cube-root (scaled time) zone is examined. We note the interesting point that the three-dimensional Euler equations acquire a double-deck structure in this zone. In effect a similarity problem has to be solved at that stage. The amplitude equation which arises from the nonlinear study in the edge-layer region appears as a solvability condition, and is found to be an Airy equation but with an additional nonlinear contribution. The Airy dependence matches with and confirms the earlier linear study. As a check an alternative method of obtaining the linear result is also shown, using the pressure-displacement law from the linearized theory.

In section 2.6 a wall-layer study is presented, in which we establish which mixture of the two main governing mean-flow equations is needed in order to satisfy the correct wall conditions, given that the mean-flow correction velocities in the bulk of the motion outside the wall layer are singular on approach to the wall layer. There is also an internal critical layer but at the current relatively high input amplitudes it plays only a passive role, self-consistent with the analysis in Smith (1992) (see also Benney and Bergeron (1969), Bodonyi, Smith and Gajjar (1983)), as opposed to the active role for lower input amplitudes in, for example, Goldstein and Choi (1989), Smith, Brown and Brown (1993), Hall and Smith (1991) and references therein. The present wall-layer yields the appropriate mean-flow relation which is then coupled with the amplitude equation.

In part II of the present chapter we solve the above coupled system numerically using a finite-difference procedure. Sample solutions for the pressure and amplitude are presented. The solutions confirm that nonlinear effects enter the edge-layer(s) first and that at small amplitudes we obtain solutions which match with the linear theory. However as we raise the amplitude (numerically) we expect the nonlinear effects to move towards the centre of the

spot, although at the present amplitude level we are unable to obtain entirely conclusive computational evidence for this. As we shall see in chapter 3 this problem can be overcome.

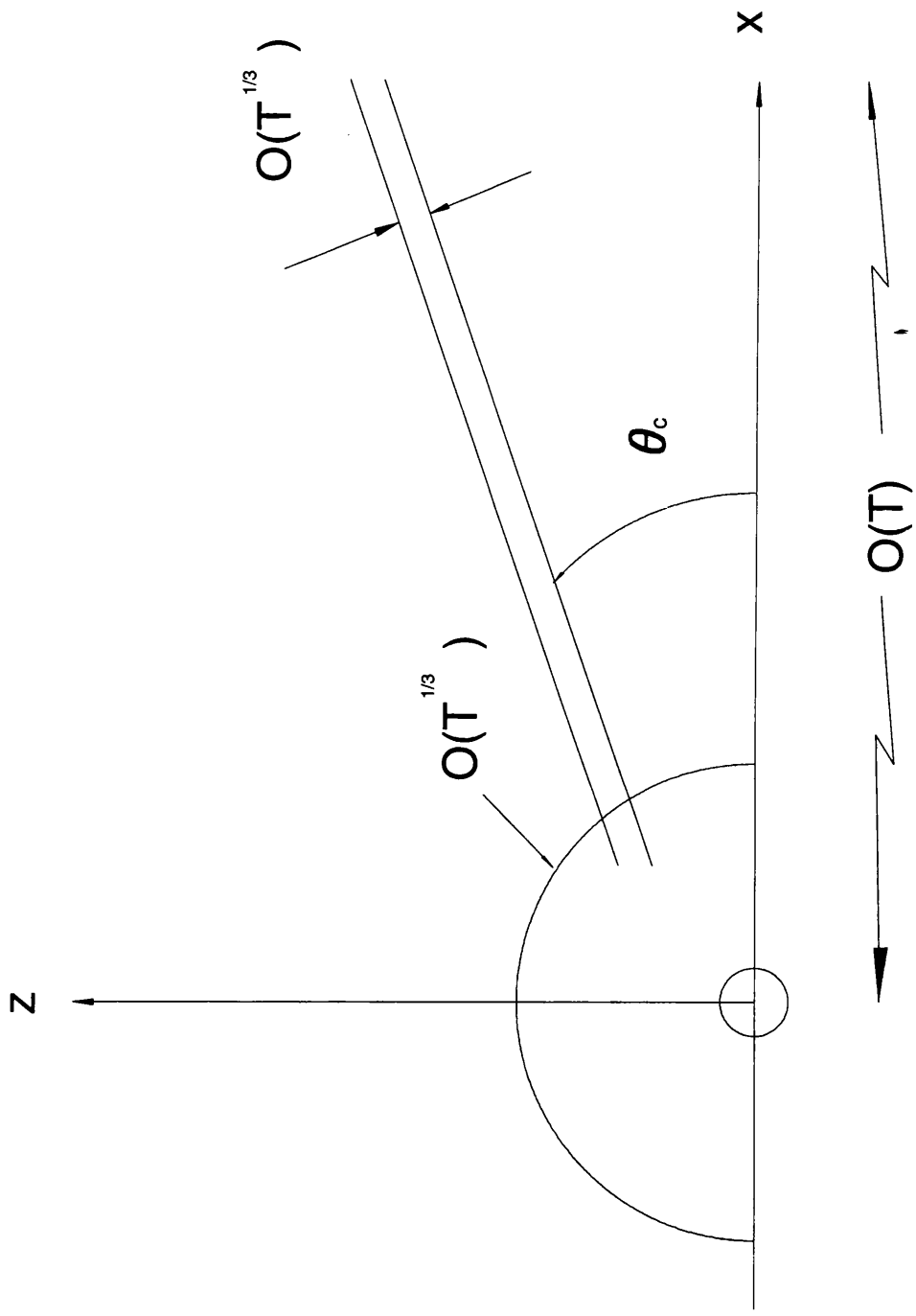

fig 2.0.1

Schematic diagram of the flow structure (in plan view, upper half only) for the large-time large-distance behaviour.

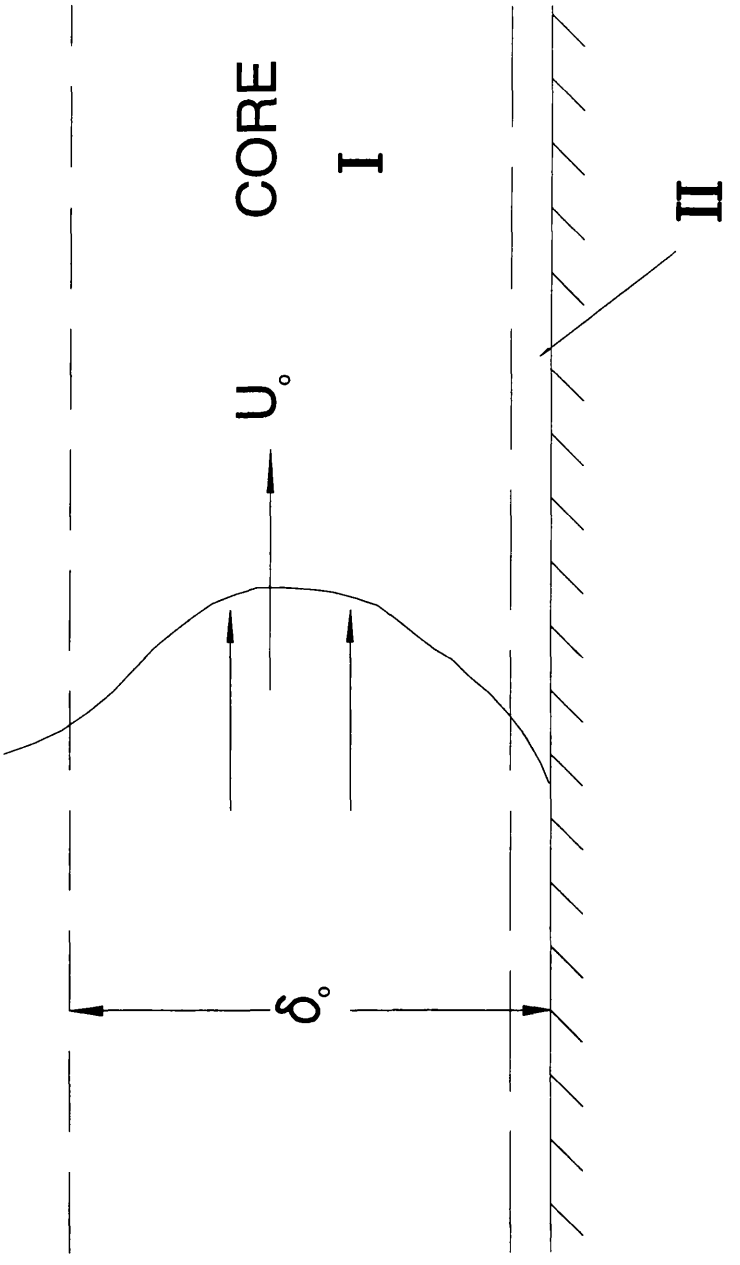

fig 2.0.2

Schematic diagram for the wall-jet flow case.

§2.1 THE ORDER $T^{1/3}$ REGION: LINEAR THEORY

We begin with the full three-dimensional Navier Stokes equations,

$$\mathbf{u_t} + (\mathbf{u}.\nabla)\mathbf{u} = -\frac{1}{\rho}\nabla p + \nu\nabla^2\mathbf{u} \quad , \quad \nabla\cdot\mathbf{u} = 0$$

where

$$\mathbf{u} \equiv (u, v, w) \text{ and } \nu = \mu/\rho,$$

μ, ρ being the viscosity and density respectively.

To non-dimensionalize the three-dimensional problem above, we make the following transformations,

$$x = \delta_0 x^*, \quad y = \delta_0 y^*, \quad z = \delta_0 z^*,$$

$$u = U_0 u^*, \quad v = U_0 v^*, \quad w = U_0 w^*,$$

$$p = \rho U_0^2 p^*, \quad t = \frac{\delta_0}{U_0} t^*,$$

in cartesian coordinates (x, y, z), where δ_0 denotes the width of the wall-jet, U_0 is the typical velocity and ρ is the density of the fluid (see figure 2.0.2). Here (x^*, y^*, z^*) are our new non-dimensional spatial coordinates and (u^*, v^*, w^*) are the new non-dimensional velocity variables in the streamwise, spanwise and normal directions respectively. Then with the Reynolds number defined by

$$Re = \frac{U_0\delta_0}{\nu} \gg 1$$

and dropping the superscript '$*$' for convenience the governing equations of continuity and momentum become

$$u_x + v_y + w_z = 0, \tag{2.1.1a}$$

$$u_t + uu_x + vu_y + wu_z = -p_x, \tag{2.1.1b}$$

$$v_t + uv_x + vv_y + wv_z = -p_y, \tag{2.1.1c}$$

$$w_t + uw_x + vw_y + ww_z = -p_z, \tag{2.1.1d}$$

i.e the unsteady, inviscid, three-dimensional Euler equations. These equations apply subject to appropriate boundedness conditions in the farfield $(x^2 + z^2 \to \infty)$ including matching to the basic wall-jet profile, $u = u_o(y)$ say, upstream and subject to the tangential flow constraint $v = 0$ at the wall.

We investigate below long-scale 3D disturbances[1]. Thus $(x, z) = \ell(X, Z)$ say, with the non-dimensional length scale ℓ being large, and the main time scale has $t = \ell^3 T$, where X, Z, T are typically $O(1)$. An order-of-magnitude argument (similar to the argument for triple-deck theory, in fact, and summarized just after (2.1.7*b*) below) suggests that in the $t = O(\ell^3)$ zone the large-time solution of the unsteady Euler problem (2.1.1a-d) takes on a double-deck structure as follows. The lower and upper deck scalings are, in turn,

$$[u, v, w, p] \sim [\ell^{-2}U, \ell^{-5}V, \ell^{-2}W, \ell^{-4}P], \quad y = \ell^{-2}Y, \tag{2.1.2a}$$

$$[u, v, w, p] \sim [u_0(y) + \ell^{-2}u_1, \ell^{-3}v_1, \ell^{-4}w_1, \ell^{-4}p_1], \quad y = O(1), \tag{2.1.2b}$$

where the profile $u_0(y)$ is supposed here to be monotonic, inflexion-free and $u_0(0) = 0$, $u_0'(0) = \lambda_0 > 0$, an example being the Blasius profile. The asymptotic expansions (2.1.2b) in the core, region I, imply the governing equations

$$u_{1X} + v_{1y} = 0, \tag{2.1.3a}$$

$$u_o u_{1X} + v_1 u_{oy} = 0, \tag{2.1.3b}$$

[1]In experiments, e.g Carlson, Widnall and Peeters (1982), the typical scalings are consistent with the assumption $X, Z \gg Y$ where X, Y, Z are the streamwise, normal and spanwise coordinates respectively.

$$u_o v_{1X} = -p_{1y}, \tag{2.1.3c}$$

$$u_o w_{1X} = -p_{1Z}, \tag{2.1.3d}$$

from the leading-order continuity, streamwise, lateral and spanwise momentum balances respectively. So solving (2.1.3a-c) we obtain

$$u_1 = u_o'(y)A(X,Z), \quad v_1 = -u_o(y)A_X(X,Z)$$

and

$$p_1 = p_1(X,0,Z) + A_{XX}(X,Z)\int_0^y u_o^2(y)dy. \tag{2.1.4}$$

Hence we may now write (2.1.2b) as

$$[u,v,w,p] \sim [u_0(y) + \ell^{-2}u_o'A, \ell^{-3}u_0A_X, \ell^{-4}w_1, \ell^{-4}p_1] \quad y = O(1). \tag{2.1.5}$$

We note that (2.1.4) gives the pressure-displacement (A) relations

$$P^+ - P^- = 2A_{XX}, \quad P = -A_{XX}, \tag{2.1.6a-b}$$

for the channel and wall-jet flows respectively, in non-dimensional form, where $+$ and $-$ correspond to the upper and lower channel walls respectively (see chapter 6 below). As $Y \to \infty$ (2.1.2a), (2.1.5) yield the matching conditions

$$U \sim \lambda_0(Y + A), \quad W \to 0, \tag{2.1.7a}$$

while the tangential-flow constraint at the wall requires that

$$V = 0 \quad \text{at} \quad Y = 0. \tag{2.1.7b}$$

Having established the pressure-amplitude law (in 2.1.6b) we can now see that the balances

$$\frac{u}{t} \sim \frac{u^2}{x} \sim \frac{p}{x},$$

$$u \sim y \sim A,$$

$$p \sim \frac{A}{x^2},$$

(from (2.1.1b), (2.1.7a) and (2.1.6b)) require the scalings in (2.1.2a) for the near-wall response. Substituting (2.1.2a) into (2.1.1$a-d$) then gives the non-linear unsteady thin-layer system

$$\nabla.\underline{U} = 0, \tag{2.1.8a}$$

$$(\partial_T + \underline{U}.\nabla)(U, W) = -(P_X, P_Z), \quad \nabla \equiv (\partial_X, \partial_Y, \partial_Z), \tag{2.1.8$b-c$}$$

subject to

$$V = 0 \text{ at } Y = 0, \quad U \sim \lambda_0(Y + A), \quad W \to 0 \text{ as } Y \to \infty \tag{2.1.8d}$$

from (2.1.7a,b). The work below concentrates mostly on the system (2.1.8$a-d$) for which we note in passing that the constant λ_0 may be normalized to unity.

§2.2 DEVELOPMENT FROM AN INITIAL SPOT DISTURBANCE

In this section, as a start, we consider small disturbances in which the basic flow $U = Y$ is slightly disturbed, to examine the linearized features. There to leading orders

$$[U - Y, V, W, A, P] = \hat{h}[\bar{U}, \bar{V}, \bar{W}, \bar{A}, \bar{P}] + \ldots,$$

say, with $\hat{h} \ll 1$. As a result (2.1.8a-d) become

$$\bar{U}_X + \bar{V}_Y + \bar{W}_Z = 0, \tag{2.2.1a}$$

$$\bar{U}_T + Y\bar{U}_X + \bar{V} = -\bar{P}_X, \tag{2.2.1b}$$

$$\bar{W}_T + Y\bar{W}_X = -\bar{P}_Z, \tag{2.2.1c}$$

with

$$\bar{V} = 0 \text{ at } Y = 0, \text{ and } \bar{U} \to \bar{A}, \bar{W} \to 0 \text{ as } Y \to \infty. \tag{2.2.1d}$$

An appropriate solution may be derived from adding together the $X-$, $Z-$ derivatives of (2.2.1b-c) respectively, which yields a quasi-2D system for $\bar{U}_X + \bar{W}_Z$, $\bar{V}_X$ whose solution subject to suitable initial conditions has $\bar{U}_X + \bar{W}_Z$ independent of Y and hence identically equal to $\bar{A}_X$. This is consistent with the momentum balances provided

$$\bar{A}_{XT} = -\nabla^2 \bar{P}, \quad \nabla^2 \equiv (\partial_X^2, \partial_Z^2).$$

Hence the function $\bar{A}(X, Z, T)$ satisfies

$$\bar{A}_{XT} = \nabla^2 \bar{A}_{XX}, \tag{2.2.2}$$

since $\bar{P} = -\bar{A}_{XX}$. We may now solve for $\bar{A}$ by taking the double Fourier transform (denoted **) in X, Z of (2.2.2) to obtain

$$i\alpha \bar{A}_T^{**} = (\alpha^2 + \beta^2)\alpha^2 \bar{A}^{**},$$

where α, β are the transform variables corresponding to X, Z respectively. Hence the displacement is given by

$$4\pi^2 \bar{A}(X, Z, T) = \int_{-\infty}^{\infty} \int_{-\infty}^{\infty} \tilde{Q}(\alpha, \beta) \exp(i\alpha X + i\beta Z - [\alpha^2 + \beta^2] i\alpha T) d\alpha d\beta \tag{2.2.3}$$

where $\tilde{Q}(\alpha, \beta)$ is the initial distribution of the negative-displacement transform $A^{**}(\alpha, \beta, 0)$.We note that the equation (2.2.3) also holds for the channel-flow case. Here (2.2.3) determines the development of the displacement in space and time, and hence the pressure from (2.1.6b), for any prescribed initial distribution. We note the broad similarities between (2.2.3) and the dispersion relation obtained by Doorly and Smith (1992), i.e.

$$4\pi^2 \bar{A}(X, Z, T) = \int_{-\infty}^{\infty} \int_{-\infty}^{\infty} \tilde{Q}(\alpha, \beta) \exp(i\alpha X + i\beta Z - i\alpha [\alpha^2 + \beta^2]^{1/2} T) d\alpha d\beta,$$

sample solutions of which are shown in figures (2.2.1a, b), (2.2.2a, b), (2.2.3a, b).

We are interested in the behaviour of the flow solution at large times, as mentioned above, from the start. From (2.2.3) we observe that X, Z are $O(T^{1/3})$ for any significant effect to be present there, provided that $X \sim \alpha^{-1}$

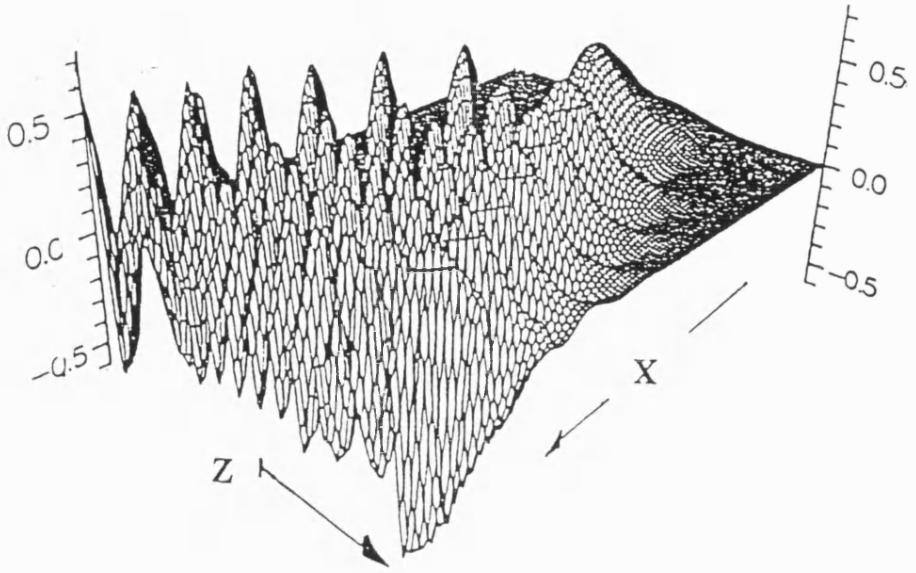

(a)

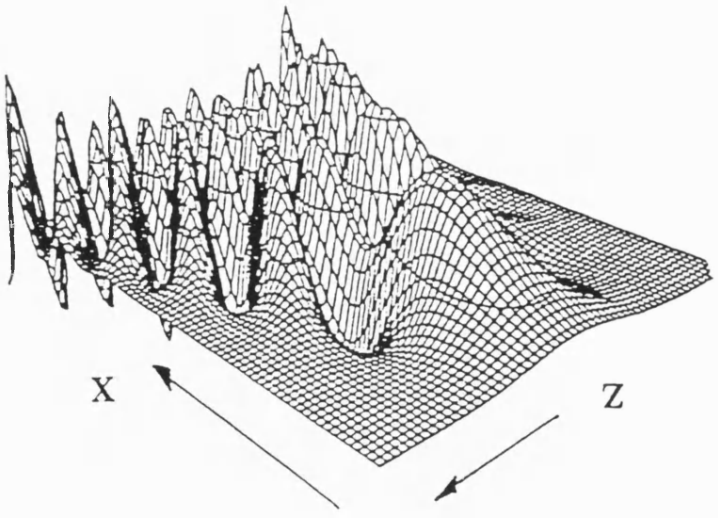

(b)

fig 2.2.1a,b

Numerical results for the incompressible boundary layer.

Surface plots of disturbance $A(\bar{X}.\bar{Z}, T)$ for very large time T. ($T = 256$)

From Doorly and Smith (1992)

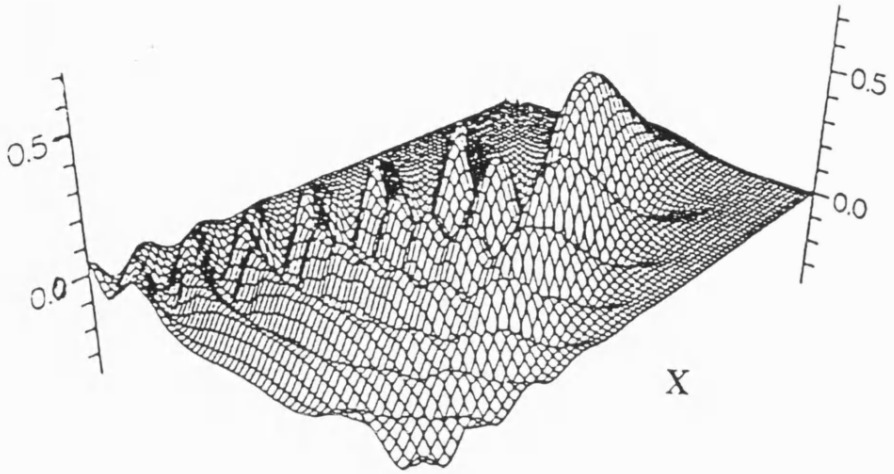

(a)

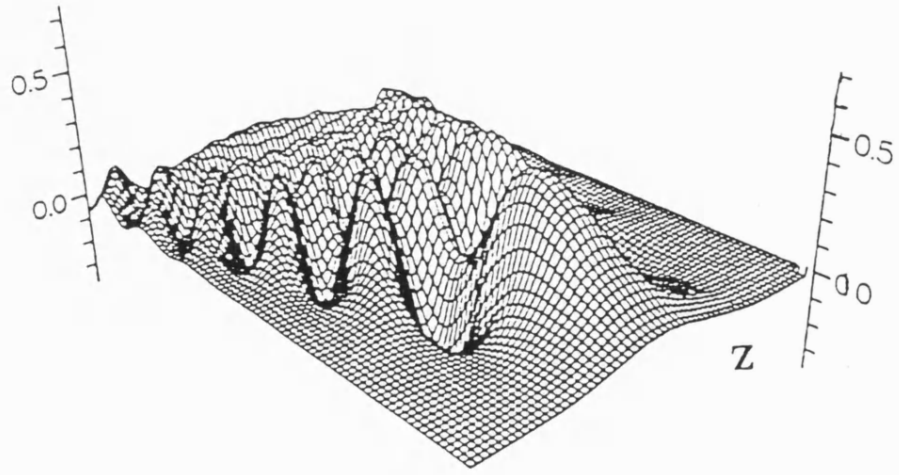

(b)

fig 2.2.2a,b

Surface plot of $A(\bar{X}, \bar{Z}, T)$ for short time T. $(T = 2)$

From Doorly and Smith (1992).

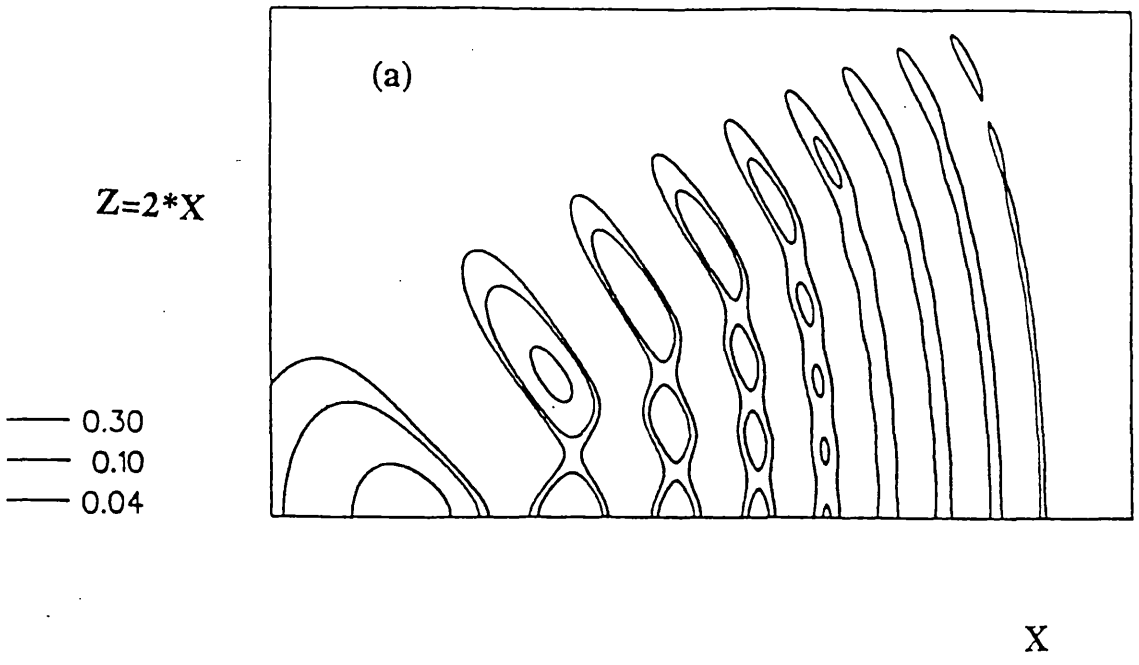

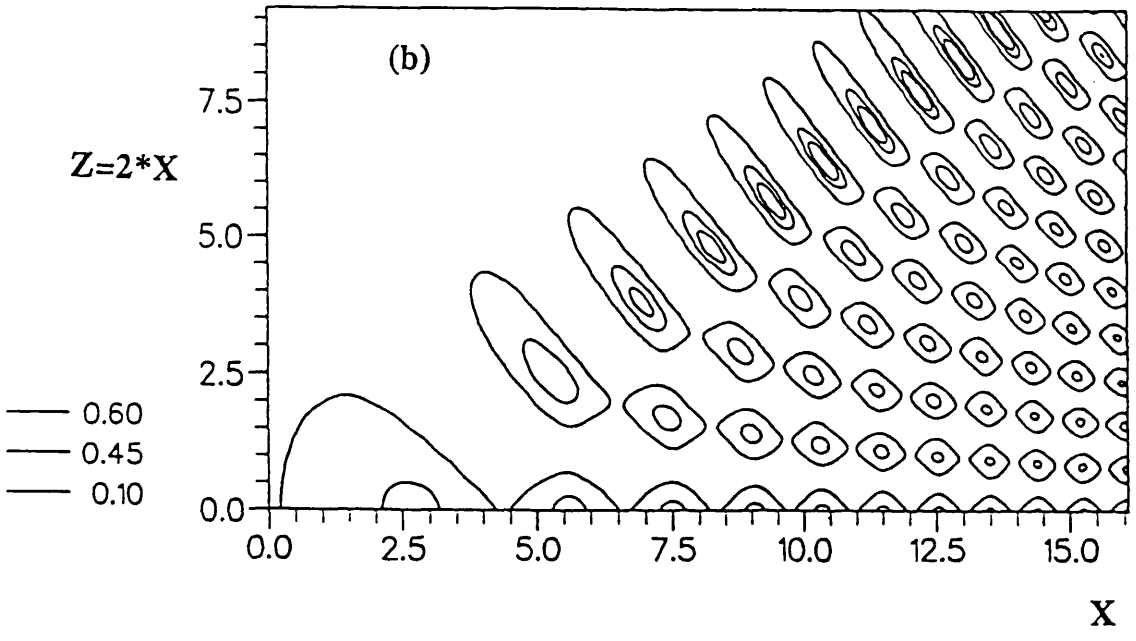

fig 2.2.3a,b

Contours of $A(\bar{X}, \bar{Z}, T)$ for short (a) and long (b) times.

At large times, the maximum amplitudes are clearly seen to lie along the caustic.

From Doorly and Smith (1992).

and $T \sim \alpha^{-3}$, where $\alpha \ll 1$ (the second region of interest further downstream, occurs when the distances are increased to $O(T)$; this is examined in chapter 4). This observation is suggested by the fact that we require x, z to be $O(\ell)$ for t of $O(\ell^3)$, from above. Therefore in (2.2.3) we write

$$(X, Z) = T^{1/3}(\bar{X}, \bar{Z}) = T^{1/3}R(\cos\theta, \sin\theta), \tag{2.2.4a}$$

$$(\alpha, \beta) = T^{-1/3}(\bar{\alpha}, \bar{\beta}) = T^{-1/3}\bar{r}(\cos\phi, \sin\phi), \tag{2.2.4b}$$

in terms of polar coordinates. Substituting these into (2.2.3) yields

$$2\pi\bar{A} \sim T^{-2/3}\tilde{Q}(0,0)\int_0^\infty \bar{r}J_o(\Phi)d\bar{r}, \tag{2.2.5}$$

after an integration with respect to ϕ . Here J_o is the standard Bessel function of zeroth order and $\tilde{Q}(0,0)$ is the double integral with respect to X, Z of the initial disturbance $A(X, Z, 0)$, while $\Phi = (\bar{r}^2R^2 - 2\bar{r}^4R\cos\theta + \bar{r}^6)^{1/2}$. Also (2.2.5) gives most of the large-time behaviour for $O(1)$ values of the scaled distance $R \equiv (X^2 + Z^2)^{1/2}T^{-1/3}$ and $O(1)$ angles θ. For large distances R the beginning of a confined 'wake' can be distinguished. For then the range $\bar{r} = (\sigma R)^{1/2} \gg 1$ is important (with σ of order unity), giving $\Phi^2 = R^3(\sigma - 2c\sigma^2 + \sigma^3) \gg 1$ (where $c \equiv \cos\theta$) and so $J_o(\Phi) \sim (2/\pi\Phi)^{1/2}\cos(\Phi - \pi/4)$. Since $R \gg 1$ the major contributions to the integral are made when $f(\sigma) = (\sigma - 2c\sigma^2 + \sigma^3)$ has a maximum, as J_o is largely oscillatory. But $f'(\sigma) = 3(\sigma - 2c/3)^2 + (1 - 4c^2/3)$ so maxima are possible only for $c^2 > 3/4$, i.e when $|\theta| < \theta_c$, where $\theta_c = 30°$ is the "spread half-angle".

For such angles 'inside the wake' we may use the method of stationary phase to deduce analytically the large-time behaviour of (2.2.5). After some working (near the stationary points of $f(\sigma)$) we obtain

$$2^{1/2}\pi\bar{A} \sim T^{-2/3}Q(0,0)R^{-1/2}[\frac{1}{(B_2^+B_1^+)^{1/2}}\cos(R^{3/2}B_1^+) +$$

$$\frac{1}{(B_2^-B_1^-)^{1/2}}\cos(R^{3/2}B_1^-)], \tag{2.2.6}$$

for $R \gg 1$ with $-\theta_c < \theta < \theta_c$, consisting of two wave forms in which

$$B_1(\theta) = (\sigma_1 - 2\sigma_1^2 c + \sigma_1^3)^{1/2},$$

$$B_2(\theta) = (3\sigma_1 - 2c)B_1^{-1},$$

$$\sigma_1^{\pm}(\theta) = (1/3)(2c \pm (4c^2 - 3)^{1/2}), \qquad c \equiv \cos\theta.$$

From this it can be seen that increasingly concentrated waves form in the wake far downstream, but with their maximum amplitudes occurring at the edges (or caustics) $\theta \sim \pm\theta_c$, since $B_2 \to 0$, $B_1 \to O(1)$ as $|\theta| \to \theta_c$. Near the caustic the two roots of $f(\sigma)$ coalesce at $\sigma = 2c/3$; therefore we introduce $\mu = \sigma - 3^{-1/2}$, and since $\tan\theta_c = 3^{-1/2} = \bar{Z}/\bar{X}$ we introduce $\lambda = \bar{Z}/\bar{X} - 3^{-1/2}$. Hence we can evaluate the integral (2.2.5) in detail by expanding Φ as

$$\Phi = \bar{X}^{3/2}\left(\frac{2}{3}\right)^{3/2}\left(1 + \frac{9}{3^{1/2}4}\lambda + \frac{9}{4}\lambda\mu + \frac{9}{3^{1/2}2}\mu^3\right) + O(\mu^4, \lambda^2).$$

This allows (2.2.5) to be evaluated near the caustic as

$$2\pi\bar{A} = T^{-2/3}\tilde{Q}(0,0)(2\pi)^{1/2}R^{-1/4}2^{1/3}3^{-5/24}\cos(B_1\bar{X}^{3/2})A_i(\eta), \qquad (2.2.7)$$

where A_i is the Airy function, while

$$\eta = (3^{1/6}/2^{2/3})\bar{X}\lambda,$$

and

$$B_1 = ((2/3)^{3/2} + (1/2^{1/2})\lambda)$$

(see Cheng and Johnson (1982), Pedlosky (1987)). Hence near each edge of the spot $\bar{A}$ acquires the form of an Airy function, matching with the wave-like behaviour (2.2.6) inside the wake and with the exponentially small response outside (for $|\theta| > \theta_c$). We note here that due to a typographical error the factor $T^{-1}\tilde{Q}(0,0)$ did not appear in the work of Doorly and Smith (1992) (page 96, equation (3.9)).

§2.3NONLINEAR THEORY: AMPLITUDE LEVEL I

We now use the linear work above as a starting point for the following nonlinear approach, as in Smith (1992), Smith, Dodia and Bowles (1994). We start by obtaining our governing equations, using the scalings $(x, z) = t^{1/3}(\hat{X}, \hat{Z})$ (see below) and appropriate expansions for the velocity , pressure and amplitude.

The aim of the present nonlinear approach is to obtain the governing nonlinear amplitude and mean-flow equations as in Smith (1992), near the spot's wing-tips in two 'edge layers', where nonlinear effects can be concentrated. These equations have solutions that match with the linear theory in a low-amplitude limit and they enable us to gauge what happens as the amplitude is increased. These aspects will be examined in more detail later.

§2.3.1SETTING-UP THE NONLINEAR PROBLEM

In section 2.1 we used the scalings (2.1.2a) which are valid for all scaled times. Then the dispersion relation (2.2.3) suggests that
$(x, z) = t^{1/3}(\hat{X}, \hat{Z})$; hence in a sense the time t replaces the length scale ℓ^3. Keeping this in mind we modify (2.1.2a) as below,

$$[u, v, w, p, A] = [t^{-2/3}\hat{U}, t^{-5/3}\hat{V}, t^{-2/3}\hat{W}, t^{-4/3}\hat{P}, t^{-2/3}\hat{A}], \qquad (2.3.1a)$$

$$[x, y, z] = [t^{1/3}\hat{X}, t^{-2/3}\hat{Y}, t^{1/3}\hat{Z}], \qquad (2.3.1b)$$

where these velocity, pressure, amplitude and spatial variables hold in the lowest layer. Substituting (2.3.1$a-b$) into the governing Euler equations (2.1.1a-d) we obtain

$$\hat{U}_{\hat{X}} + \hat{V}_{\hat{Y}} + \hat{W}_{\hat{Z}} = 0, \qquad (2.3.2a)$$

$$-\frac{2}{3}\hat{U} + \left(\hat{U} - \frac{1}{3}\hat{X}\right)\hat{U}_{\hat{X}} + \left(\hat{V} + \frac{2}{3}\hat{Y}\right)\hat{U}_{\hat{Y}} + \left(\hat{W} - \frac{1}{3}\hat{Z}\right)\hat{U}_{\hat{Z}} = -\hat{P}_{\hat{X}}, \quad (2.3.2b)$$

$$-\frac{2}{3}\hat{W}+\left(\hat{U}-\frac{1}{3}\hat{X}\right)\hat{W}_{\hat{X}}+\left(\hat{V}+\frac{2}{3}\hat{Y}\right)\hat{W}_{\hat{Y}}+\left(\hat{W}-\frac{1}{3}\hat{Z}\right)\hat{W}_{\hat{Z}}=-\hat{P}_{\hat{Z}},\ (2.3.2c)$$

with (2.1.1c) confirming that

$$\frac{\partial\hat{P}}{\partial\hat{Y}}=0.$$

The main boundary conditions are

$$\hat{V}=0\ \text{ at }\ \hat{Y}=0,\qquad(2.3.3a)$$

$$\hat{U}\sim\hat{Y}+\hat{A},\ \ \hat{W}\to 0\ \text{ as }\ \hat{Y}\to\infty,\qquad(2.3.3b)$$

from (2.1.7a-b) respectively. The pressure amplitude relation is now given by

$$\hat{P}=-\hat{A}_{\hat{X}\hat{X}}.\qquad(2.3.4)$$

Thus $(2.3.1a,b)$ represent a large-time asymptote of the three-dimensional Euler system.

§2.4 MAIN FEATURES IN THE BULK OF THE FLOW

We use the term bulk to refer to the major part of the flow structure in the normal direction. The expansion of the flow solution at relatively large distances $\hat{X}\gg 1$ is inferred from above and takes the form,

$$\hat{U}=\hat{X}s+(Eu_0+E^{-1}u_0^*)\hat{X}^{-1/4}+\ldots+(E^2u_{12}\hat{X}^{-3/2}+Eu_{11}\hat{X}^{-3/4}+\hat{X}^{-1/2}u_{10}+c.c)$$

$$+\hat{X}^{-1/2}(E^3u_{23}\hat{X}^{-9/4}+\ldots+Eu_{21}\hat{X}^{-3/4}+\ldots)+\ldots,\qquad(2.4.1a)$$

$$\hat{V}=\hat{X}^{5/4}(Ev_0+E^{-1}v_0^*)+\ldots+\hat{X}^{3/2}(E^2v_{12}\hat{X}^{-3/2}+Ev_{11}\hat{X}^{-3/4}+\hat{X}^{-1/2}v_{10}+c.c)+$$

$$\ldots+\hat{X}(E^3v_{23}\hat{X}^{-9/4}+\ldots+Ev_{21}\hat{X}^{-3/4}+\ldots)+\ldots,\qquad(2.4.1b)$$

$$\hat{W}=(Ew_0+E^{-1}w_0^*)\hat{X}^{-1/4}+\ldots+(E^2w_{12}\hat{X}^{-3/2}+Ew_{11}\hat{X}^{-3/4}+\hat{X}^{-1/2}w_{10}+c.c)$$

$$+\hat{X}^{-1/2}(E^3 w_{23}\hat{X}^{-9/4}+\ldots+Ew_{21}\hat{X}^{-3/4}+\ldots)+\ldots, \qquad (2.4.1c)$$

for the velocity components, and

$$\hat{P}=(Eg_0+E^{-1}g_0^*)\hat{X}^{3/4}+\ldots+\hat{X}(E^2 g_{12}\hat{X}^{-3/2}+Eg_{11}\hat{X}^{-3/4}+\hat{X}^{-3/2}g_{10}+c.c)$$
$$+\hat{X}^{1/2}(E^3 g_{23}\hat{X}^{-9/4}+\ldots)+\ldots, \qquad (2.4.1d)$$

$$\hat{A}=(EA_0+E^{-1}A_0^*)\hat{X}^{-1/4}+\ldots+(E^2 A_{12}\hat{X}^{-3/2}+EA_{11}\hat{X}^{-3/4}+\hat{X}^{-1/2}A_{10}+c.c)$$
$$+\hat{X}^{-1/2}(E^3 A_{23}\hat{X}^{-9/4}+\ldots+EA_{21}\hat{X}^{-3/4}+\ldots)+\ldots, \qquad (2.4.1e)$$

for the pressure and displacement respectively. We justify using these particular expansions later in section 2.9. The unknown velocity coefficients u_n, v_n, w_n depend only on $s, \hat{\eta}$ while g_n, A_n are unknown functions of $\hat{\eta}$ alone, with the explicit $E-$ dependence shown. Here $c.c$ denotes the complex conjugate and the wave contribution is

$$E \equiv \exp[i(b_1\hat{X}^{3/2}+a_1\hat{X}^{1/2}\hat{\eta})], \qquad (2.4.2)$$

where b_1, a_1 are constants. Also

$$\hat{Y}=\hat{X}s, \quad \hat{\eta}=\hat{Z}-\bar{q}\hat{X}, \qquad (2.4.3a,b)$$

where the constant $\bar{q}$ is equal to $1/3^{1/2}$, corresponding to the wake half-angle of 30°, in view of the linearity holding outside and in-between the two edge layers, and s, $\hat{\eta}$ are $O(1)$. The expressions for the wave contribution and edge layer follow from (2.2.7), while in order to obtain (2.4.3a) we need to take the balances

$$\hat{U}\sim\frac{\hat{U}\hat{U}}{\hat{X}}, \quad \hat{U}\sim\hat{Y},$$

from (2.3.2b) and (2.3.3b) respectively; the result (2.4.3a) follows. So (2.4.1$a-e$), (2.4.2) and (2.4.3a,b) form the basis for the nonlinear theory, with the transformations

$$\partial_{\hat{X}}\to\partial_{\hat{X}}-\bar{q}\partial_{\hat{\eta}}-\hat{X}^{-1}s\partial_s, \quad \partial_{\hat{Y}}\to\hat{X}^{-1}\partial_s, \quad \partial_{\hat{Z}}\to\partial_{\hat{\eta}},$$

and

$$E_{\hat{X}} = \left(\frac{3}{2}b_1\hat{X}^{1/2} + \frac{1}{2}a_1\hat{X}^{-1/2}\hat{\eta}\right)iE, \quad E_{\hat{\eta}} = a_1\hat{X}^{1/2}iE,$$

from above.

Substituting (2.4.1a-d) into the large-time equations (2.3.2a-c) yields the successive controlling equations as follows. At first order (E terms only) the continuity, streamwise and spanwise momentum balances give

$$iBu_0 + v_{0s} + ia_1w_0 = 0, \tag{2.4.4a}$$

$$v_0 + i\delta u_0 = -ig_0B, \tag{2.4.4b}$$

$$i\delta w_0 = -ia_1g_0, \tag{2.4.4c}$$

respectively, where $B = \frac{3}{2}b_1 - \bar{q}a_1$ and $\delta = Bs - b_1/2$. These controlling equations apply subject to the constraints

$$v_0 = 0 \text{ at } s = 0, \quad u_0 \to A_0 \text{ as } s \to \infty,$$

from (2.3.3a,b). The solutions for u_0, v_0, w_0 hence obtained are

$$u_0 = A_0 + \frac{a_1^2g_0}{B\delta}, \tag{2.4.5a}$$

$$v_0 = -iBA_0s, \tag{2.4.5b}$$

$$w_0 = -\delta^{-1}g_0a_1, \tag{2.4.5c}$$

with the resulting 'internal' pressure-displacement relation being

$$A_0 = \kappa g_0 \text{ where } \kappa \equiv 2b_1^{-1}B^{-1}(a_1^2 + B^2). \tag{2.4.6}$$

The results here and in the remainder of this section hold strictly for $\delta \neq 0$, i.e for $s \neq b_1/2B$, outside a critical layer. At second order (E terms only) the continuity, streamwise and spanwise momentum balances yield

$$iBu_{11} + ia_1w_{11} + v_{11s} - \bar{q}u_{0\hat{\eta}} + w_{0\hat{\eta}} = 0, \tag{2.4.7a}$$

$$i\delta u_{11} + v_{11} - s\bar{q}u_{0\hat{\eta}} = -iBg_{11} + \bar{q}g_{0\hat{\eta}}, \tag{2.4.7b}$$

$$i\delta w_{11} - s\bar{q}w_{0\hat{\eta}} = -g_{0\hat{\eta}} - ia_1 g_{11}, \tag{2.4.7c}$$

respectively. The solutions for (u_{11}, v_{11}, w_{11}) subject to the constraints

$$v_{11} = 0 \ \text{ at } \ s = 0, \ \ u_{11} \to A_{11} \ \text{ as } \ s \to \infty,$$

are

$$u_{11} = \frac{i}{B}\left\{\frac{\alpha}{\delta} + \frac{\beta}{2\delta^2}\right\} + A_{11}, \tag{2.4.8a}$$

$$v_{11} = \bar{q}s\left\{\frac{a_1^2 g_{0\hat{\eta}}}{B\delta} + A_{0\hat{\eta}}\right\} - iBg_{11} + \bar{q}g_{0\hat{\eta}} - i\delta u_{11}, \tag{2.4.8b}$$

$$w_{11} = -\left\{\frac{a_1 g_{11} - ig_{0\hat{\eta}}}{\delta}\right\} + \frac{is\bar{q}g_{0\hat{\eta}}a_1}{\delta^2}, \tag{2.4.8c}$$

where

$$\alpha = -ia_1^2 g_{11} - 2a_1(1 + \bar{q}a_1 B^{-1})g_{0\hat{\eta}},$$

$$\beta = -\bar{q}a_1^2 b_1 B^{-1} g_{0\hat{\eta}}.$$

The internal pressure-displacement relation between g_{11}, A_{11} here takes the form

$$ib_1\kappa g_{11} = ib_1 A_{11} + 2g_{0\hat{\eta}}B^{-1}[\frac{3}{2}b_1\bar{q} - \bar{q}^2 a_1 - 2a_1 - a_1^2\bar{q}B^{-1}]. \tag{2.4.9}$$

Similarly at third order (E terms only) the controlling equations are

$$iBu_{21} + v_{21s} + ia_1 w_{21} + \frac{1}{2}a_1\hat{\eta}iu_0 - \bar{q}u_{11\hat{\eta}} + w_{11\hat{\eta}} = 0, \tag{2.4.10a}$$

$$i\delta u_{21} - s\bar{q}u_{11\hat{\eta}} + v_{21} + \frac{1}{2}(s-1)a_1\hat{\eta}iu_0 = -iBg_{21} + \bar{q}g_{11\hat{\eta}} - \frac{1}{2}a_1\hat{\eta}ig_0, \tag{2.4.10b}$$

$$\frac{1}{2}i(s-1)a_1\hat{\eta}w_0 - s\bar{q}w_{11\hat{\eta}} + i\delta w_{21} = -g_{11\hat{\eta}} - ia_1 g_{21}, \tag{2.4.10c}$$

from the continuity, streamwise and spanwise momentum balances respectively. We can rewrite these for u_{21}, v_{21}, w_{21} as

$$u_{21} = A_{21} - i\int_{\infty}^{s}[-2g_{11\hat{\eta}}\bar{q}a_1^2\frac{s}{\delta^3} + i\bar{q}2a_1(2+\bar{q}a_1B^{-1})g_{0\hat{\eta}\hat{\eta}}\frac{s}{\delta^3}$$
$$+ia_1^3\hat{\eta}g_0\frac{s}{\delta^3} - ia_1^3\hat{\eta}g_0\frac{1}{\delta^3} - (2a_1g_{11\hat{\eta}} - ig_{0\hat{\eta}\hat{\eta}})\frac{1}{\delta^2}$$
$$-ia_1^2g_{21}\frac{1}{\delta^2} + i\bar{q}^2a_1^2b_1g_{0\hat{\eta}\hat{\eta}}\frac{s}{B\delta^4} + ia_1^2\bar{q}^2g_{0\hat{\eta}\hat{\eta}}\frac{s^2}{\delta^4}]\,ds, \qquad (2.4.11a)$$

$$v_{21} = -iBg_{21} + \bar{q}g_{11\hat{\eta}} - \frac{1}{2}a_1\hat{\eta}ig_0 - \frac{1}{2}(s-1)a_1\hat{\eta}iu_0 + s\bar{q}u_{11\hat{\eta}} - i\delta u_{21}, \quad (2.4.11b)$$

$$w_{21} = -i\delta^{-1}[s\bar{q}w_{11\hat{\eta}} - \frac{1}{2}i(s-1)a_1\hat{\eta}w_0 - g_{11\hat{\eta}} - ia_1g_{21}], \qquad (2.4.11c)$$

subject to

$$v_{21} = 0 \ \text{ at } \ s = 0, \ \ u_{21} \to A_{21} \ \text{ as } \ s \to \infty.$$

Now the fourth-order E balances give

$$iBu_{31} + v_{31s} + ia_1w_{31} - \bar{q}u_{21\hat{\eta}} + w_{21\hat{\eta}} + a_1\hat{\eta}iu_{11}/2 - su_{0s} - u_0/4 = 0, \quad (2.4.12a)$$

$$i\delta u_{31} + v_{31} + (s-1)a_1\hat{\eta}iu_{11}/2 + iBu_{10}u_0 + v_{10}u_{0s} + v_0u_{10s} + w_{10}u_0a_1i$$
$$-s\bar{q}u_{21\hat{\eta}} - (s-1)su_{0s} - \left(\frac{s}{4} + \frac{7}{12}\right)u_0 - \hat{\eta}u_{0\hat{\eta}}/3$$
$$= -Big_{31} + \bar{q}g_{21\hat{\eta}} - a_1ig_{11}\hat{\eta}/2 - 3g_0/4, \qquad (2.4.12b)$$

$$i\delta w_{31} - s\bar{q}w_{21\hat{\eta}} + i(s-1)a_1\hat{\eta}w_{11}/2 - \left(\frac{s}{4} + \frac{7}{12}\right)w_0 - (s-1)sw_{0s} -$$
$$\hat{\eta}w_{0\hat{\eta}}/3 + v_0w_{10s} + v_{10}w_{0s} + iBu_{10}w_0 + ia_1w_{10}w_0$$
$$= -g_{21\hat{\eta}} - ia_1g_{31}, \qquad (2.4.12c)$$

from the continuity, streamwise and spanwise momentum balances respectively. Further work on these controlling equations is shown in section 2.7.

We now need to consider the leading order mean-flow responses (E^0 contributions), at various orders. These arise mainly at two levels as follows. At third order we obtain

$$-\bar{q}u_{10\hat{\eta}} + v_{20s} + w_{10\hat{\eta}} = 0, \tag{2.4.13a}$$

$$v_{20} - s\bar{q}u_{10\hat{\eta}} = 0, \tag{2.4.13b}$$

$$-s\bar{q}w_{10\hat{\eta}} = 0, \tag{2.4.13c}$$

from the continuity, streamwise and spanwise balances respectively, hence

$$w_{10} = 0, \quad v_{20} = s\bar{q}A_{10\hat{\eta}}, \quad u_{10} = A_{10}.$$

The next level leads to the controlling equations for (u_{30}, v_{40}, w_{30}), as below,

$$(-1/2)u_{10} - \bar{q}u_{30\hat{\eta}} - su_{10s} + v_{40s} + w_{30\hat{\eta}} = 0, \tag{2.4.14a}$$

from the continuity balance, and

$$(2/3)su_{10s} - (1/3)\hat{\eta}u_{10\hat{\eta}} - (1/2)su_{10} - (1/2)u_{10} + v_{40} - s\bar{q}u_{30\hat{\eta}}$$

$$+v_{10}u_{10s} - (s - (1/3))su_{10s} + f_1 = \bar{q}g_{10\hat{\eta}}, \tag{2.4.14b}$$

where

$$f_1 = [v_0u^*_{11s} + v_{11}u^*_{0s} - w_0a_1iu^*_{11} - w_{11}a_1iu^*_0 + w_0u^*_{0\hat{\eta}} - u_0\bar{q}u^*_{0\hat{\eta}} + c.c]$$

$$sw_{10s} - s^2w_{10s} - (1/3)\hat{\eta}w_{10\hat{\eta}} - (1/2)w_{10} - (1/2)sw_{10}$$

$$-s\bar{q}w_{30\hat{\eta}} + v_{10}w_{10s} + f_2 = -g_{10\hat{\eta}}, \tag{2.4.14c}$$

where

$$f_2 = [v_0w^*_{11s} + v_{11}w^*_{0s} + w_0w^*_{0\hat{\eta}} - iBu_0w^*_{11} - iBu_{11}w^*_0 - u_0\bar{q}w^*_{0\hat{\eta}} + c.c],$$

from the streamwise and spanwise momentum responses respectively. The tangential flow condition as $s \to 0$ therefore yields the mean-flow results,

$$\bar{q}g_{10\hat{\eta}} = -\frac{1}{3}\hat{\eta}A_{10\hat{\eta}} - \frac{1}{2}A_{10} - 4\bar{q}b_1^{-2}(B^2 + a_1^2)(|g_0|^2)_{\hat{\eta}}, \qquad (2.4.15a)$$

$$g_{10\hat{\eta}} = -\frac{4}{b_1^2}(B^2 + a_1^2)(|g_0|^2)_{\hat{\eta}}, \qquad (2.4.15b)$$

for (2.4.14b,c) respectively. Here we have made use of the solutions for $(u_0, u_{11}, w_0, w_{11})$ from earlier in this section.

At first sight (2.4.15a,b) seem to contradict each other, since in equation (2.4.15a) we have extra mean-flow momentum contributions present through the terms proportional to A_{10}, but a resolution is provided by examining a thin wall-layer present close to the surface, between the current $s \sim O(1)$ zone and the surface. Further details on this wall-layer are provided in section 2.6. Finally in this section we note that the second-order (E^0) balance from the continuity equation reveals

$$v_{10s} = 0,$$

which is consistent with the result $v_{10} \equiv 0$ from the streamwise momentum equation (second order E^0 balance).

§2.5 EXTERNAL RELATIONS

From section 2.3 we have the pressure-displacement relation

$$\hat{P} = -\hat{A}_{\hat{X}\hat{X}},$$

for the wall-jet study. We can substitute the expansions (2.4.1d,e) into this law to obtain 'external' relations between $(g_0, g_{11}, g_{21}, g_{31}, g_{10})$ and $(A_0, A_{11}, A_{21}, A_{31}, A_{10})$, which may then be coupled with the internal relations of the previous section. This process is described below. We proceed as before and derive the controlling equations at various orders.

At first order

$$g_0 = A_0 B^2, \qquad (2.5.1a)$$

at second order

$$g_{11} = A_{11}B^2 + 2\bar{q}iA_{0\hat{\eta}}B, \tag{2.5.1b}$$

at third order

$$g_{21} = -\bar{q}^2 A_{0\hat{\eta}\hat{\eta}} + a_1\hat{\eta}A_0B + A_{21}B^2 + 2\bar{q}iBA_{11\hat{\eta}}, \tag{2.5.1c}$$

at fourth order

$$g_{31} = A_{31}B^2 + 2\bar{q}iA_{21\hat{\eta}}B - \bar{q}^2A_{11\hat{\eta}\hat{\eta}} + a_1\hat{\eta}A_{11}B + i\bar{q}a_1\hat{\eta}A_{0\hat{\eta}} + ia_1\bar{q}A_0/2, \tag{2.5.1d}$$

where all of these relations come from balancing terms proportional to E. From the E^0 terms at leading order we have the equation

$$-g_{10} = \bar{q}^2 A_{10\hat{\eta}\hat{\eta}}. \tag{2.5.2}$$

Coupling the external relation (2.5.1a) and the internal relation (2.4.6) gives

$$b_1 = 2B(a_1^2 + B^2),$$

which is the dominant eigenrelation, leaving the amplitude function g_0 still arbitrary. Coupling (2.5.1b) with (2.4.9) gives

$$2a_1B^2 - \bar{q}b_1 = \bar{q}B(B^2 - a_1^2),$$

the eigenrelation leaving g_0, g_{11} arbitrary. Given that we know $\bar{q} = 1/3^{1/2}$ we can use these eigenrelations to determine the other constants B, a_1, and b_1. For the half-angle $\theta_c = 30°$ the constants are found to be

$$a_1 = \frac{1}{2^{1/2}}, \quad b_1 = \left(\frac{2}{3}\right)^{3/2}, \quad B = \bar{q}a_1,$$

consistent with the linear work above.

§2.6 THE WALL LAYER

As mentioned in section (2.4) a thin wall-layer, close to the surface, helps us to decide on which mixture of equations $(2.4.15a, b)$ we need. This extra layer arises because of the singular response $O(s^{-1})$ of the mean-correction

velocities u_{30}, w_{30} as $s \to 0$ (see below), while $v_{40} \to 0$ as $s \to 0$. We start with our mean-flow equations (subject to the tangential flow constraint as $s \to 0+$) from the continuity, streamwise and spanwise equations respectively , i.e

$$-\frac{1}{2}A_{10} + v_{40s} - \bar{q}u_{30\hat{\eta}} + w_{30\hat{\eta}} = 0 \qquad , \quad . \tag{2.6.1a}$$

$$-s\bar{q}u_{30\hat{\eta}} + v_{40} + B_{10} - \frac{4\bar{q}}{b_1^2}(B^2 + a_1^2)(|g_0|^2)_{\hat{\eta}} - \frac{1}{2}sA_{10} = \bar{q}g_{10\hat{\eta}} \qquad , \tag{2.6.1b}$$

where

$$B_{10} = -\frac{1}{3}\hat{\eta}A_{10\hat{\eta}} - \frac{1}{2}A_{10},$$

$$-s\bar{q}w_{30\hat{\eta}} + \frac{4}{b_1^2}(B^2 + a_1^2)(|g_0|^2)_{\hat{\eta}} = -g_{10\hat{\eta}} \qquad . \tag{2.6.1c}$$

Taking the combination (2.6.1b) + $\bar{q} *$ (2.6.1c) yields

$$-\bar{q}s[u_{30\hat{\eta}} + \bar{q}w_{30\hat{\eta}}] + v_{40} + B_{10} - \frac{1}{2}sA_{10} = 0, \tag{2.6.2}$$

and equation (2.6.1c) gives the asymptote

$$w_{30} \sim \lambda_{30}s^{-1} + P_{30} + \ldots, \tag{2.6.3a}$$

where

$$\lambda_{30} = \bar{q}^{-1}[g_{10} + \frac{4}{b_1^2}(B^2 + a_1^2)(|g_0|^2)].$$

Also the partial derivative of (2.6.1b) with respect to s implies

$$-\bar{q}u_{30\hat{\eta}} - s\bar{q}u_{30\hat{\eta}s} + v_{40s} - \frac{1}{2}A_{10} = 0,$$

i.e

$$-\bar{q}su_{30\hat{\eta}s} - w_{30\hat{\eta}} = 0.$$

So the asymptote for u_{30} is

$$u_{30} \sim \frac{\alpha_{30}}{s} + \tilde{\beta}_{30}\ln|s| + \beta_{30} + \ldots, \tag{2.6.3b}$$

with

$$\alpha_{30} = \frac{\lambda_{30}}{\bar{q}}, \qquad \tilde{\beta}_{30} = -\frac{P_{30}}{\bar{q}}.$$

Then combining (2.6.2),(2.6.3a) and (2.6.3b) we obtain after some working

$$v_{40} \sim [-B_{10} + \lambda_{30\hat{\eta}}(\bar{q}^2 + 1)] + \bar{q}\tilde{\beta}_{30\hat{\eta}} s \ln|s| + \frac{1}{2} s A_{10} + \ldots .$$

Now the tangential flow constraint as $s \to 0$ means that

$$v_{40} \to 0 \Rightarrow \lambda_{30\hat{\eta}} = B_{10}(1 + \bar{q}^2)^{-1} \neq 0;$$

this result implies that

$$w_{30} \sim s^{-1}, \quad u_{30} \sim s^{-1},$$

i.e as $s \to 0$ and $v_{40} \to 0$, u_{30} and w_{30} become singular as $O(s^{-1})$. To incorporate the singular behaviour of u_{30}, w_{30} into the wall-layer we need to adopt the new scaling $\hat{Y} = \hat{X}^{-1/4}\hat{y}$. This scaling for the thickness of the wall-layer is deduced from comparison of the basic mean-flow term $\hat{X}s$ in (2.4.1a), and the corrective term $O(\hat{X}^{-3/2}s^{-1})$ due to u_{30}, giving the scaling as $s \sim \hat{X}^{-5/4}$, i.e $\hat{Y} \sim \hat{X}^{-1/4}$. The implied expression for the wall-layer solution is therefore

$$\hat{U} = \hat{X}^{-1/4}\bar{u}_{00} + \hat{X}^{-1/2}A_{10} + \hat{X}^{-1/4}(E\bar{u}_{01} + c.c) + (E^2\bar{u}_{12}\hat{X}^{-3/2} + E\bar{u}_{11}\hat{X}^{-3/4} + c.c)$$

$$+\hat{X}^{-1/2}(E^2\bar{u}_{23}\hat{X}^{-9/4} + \ldots + E\bar{u}_{21}\hat{X}^{-3/4} + \ldots) + \hat{X}^{-1}(\ldots + \hat{X}^{-3/2}E^2\bar{u}_{32} +$$

$$\hat{X}^{-3/4}E\bar{u}_{31} + \hat{X}^{-1/2}\beta_{30} + \ldots) + c.c) + \ldots, \qquad (2.6.4a)$$

$$\hat{V} = (E\bar{v}_{01} + c.c) + \hat{X}^{3/2}(E\bar{v}_{11}\frac{\hat{X}^{-3/4}}{\hat{X}^{5/4}} + c.c + \ldots) + \hat{X}^{-1/2}\bar{v}_{00} +$$

$$\hat{X}(E\bar{v}_{21}\frac{\hat{X}^{-3/4}}{\hat{X}^{5/4}} + c.c + \bar{v}_{20}\frac{\hat{X}^{-1/2}}{\hat{X}^{5/4}}) + \hat{X}^{1/2}(\ldots + \bar{v}_{30}\frac{\hat{X}^{-1/2}}{\hat{X}^{5/4}} + \ldots) + \ldots$$

$$\ldots + \hat{X}^{0}(\hat{X}^{-1/2}[\tau_{40}\frac{\hat{y}}{\hat{X}^{5/4}} + \bar{q}\tilde{\beta}_{30\hat{\eta}}\frac{\hat{y}}{\hat{X}^{5/4}}(\ln\hat{y} - \ln\hat{X}^{5/4})] + \ldots) + \ldots, \qquad (2.6.4b)$$

$$\hat{W} = \hat{X}^{-1/4}\bar{w}_{00} + \hat{X}^{-1/4}(E\bar{w}_{01} + c.c) + \ldots + (E^2\bar{w}_{12}\hat{X}^{-3/2} + \ldots + c.c) +$$

$$\hat{X}^{-1/2}(E\bar{w}_{21}\hat{X}^{-3/4} + \ldots + c.c) + \hat{X}^{-1}(\ldots + \hat{X}^{-1/2}P_{30} + \ldots) + \ldots, \qquad (2.6.4c)$$

as suggested by the behaviour of the bulk-flow components $(2.4.1a-c)$. Here the boundary conditions are such that, as $\hat{y} \to \infty$

$$\bar{u}_{00} \sim \hat{y} + \alpha_{30}\hat{y}^{-1},$$

$$\bar{v}_{00} \sim \kappa_{40}, \quad \text{where} \quad \kappa_{40} = \lambda_{30\hat{\eta}}(\bar{q}^2 + 1) - B_{10},$$

$$\tau_{40} \sim A_{10}/2,$$

$$\bar{w}_{00} \sim \lambda_{30}\hat{y}^{-1}$$

to match with the previous solutions from the bulk. Also

$$\bar{u}_{01} \sim 2Bg_0b_1^{-1} \qquad \bar{u}_{11} \sim O(1),$$

$$\bar{v}_{01} \sim -iB\kappa g_0\hat{y} \qquad \bar{v}_{11} \sim O(\hat{y}),$$

$$\bar{w}_{01} \sim 2a_1g_0b_1^{-1} \qquad \bar{w}_{11} \sim O(1).$$

The modified transformations are

$$\partial_{\hat{Y}} \to \hat{X}^{1/4}\partial_{\hat{y}},$$

$$\partial_{\hat{Z}} \to \partial_{\hat{\eta}},$$

$$\partial_{\hat{X}} \to \partial_{\hat{X}} - \bar{q}\partial_{\hat{\eta}} + \frac{1}{4}\hat{y}\hat{X}^{-1}\partial_{\hat{y}},$$

and the dependence on the fast variable E is as before. From here a process similar to that in section 2.4 is used where the leading-order controlling equations are obtained. From substituting (2.6.4a-c) into the continuity equation $(2.3.2a)$, the leading order balances for terms in E are

$$iB\bar{u}_{01} + \bar{v}_{01\hat{y}} + ia_1\bar{w}_{01} = 0, \qquad (2.6.5a)$$

$$iB\bar{u}_{11} - \bar{q}\bar{u}_{01\hat{\eta}} + \bar{v}_{11\hat{y}} + ia_1\bar{w}_{11} + \bar{w}_{01\hat{\eta}} = 0, \qquad (2.6.5b)$$

where again $B = (3/2)b_1 - \bar{q}a_1$, and the leading-order balances for terms in E^0 are

$$-\bar{q}\bar{u}_{00\hat{\eta}} + \bar{v}_{00\hat{y}} + \bar{w}_{00\hat{\eta}} = 0, \qquad (2.6.6a)$$

$$-\bar{q}A_{10\hat{\eta}} + \bar{v}_{20\hat{y}} = 0. \qquad (2.6.6b)$$

The streamwise momentum equation yields

$$\frac{b_1}{2}\bar{u}_{01} = g_0 B, \qquad (2.6.7a)$$

$$-\frac{1}{2}b_1 i\bar{u}_{11} = -Big_{11} + \bar{q}g_{0\hat{\eta}}, \qquad (2.6.7b)$$

at first and second order (E terms only) respectively, and

$$\bar{q}g_{10\hat{\eta}} = -\frac{1}{2}A_{10} - \frac{1}{3}\hat{\eta}A_{10\hat{\eta}} + \bar{v}_{00}\bar{u}_{00\hat{y}} + \bar{w}_{00}\bar{u}_{00\hat{\eta}} - \bar{q}\bar{u}_{00}\bar{u}_{00\hat{\eta}} + \bar{F}_1, \qquad (2.6.7c)$$

as the leading-order mean-flow term balance (E^0 terms only) where

$$\bar{F}_1 = -\bar{q}\frac{4}{b_1^2}(B^2 + a_1^2)(|g_0|^2)_{\hat{\eta}} \quad \text{at} \quad \hat{y} = 0.$$

The spanwise momentum balance yields

$$\frac{1}{2}b_1\bar{w}_{01} = a_1 g_0, \qquad (2.6.8a)$$

at first order (E terms only)

$$-\frac{1}{2}b_1 i\bar{w}_{11} = -g_{0\hat{\eta}} - g_{11}a_1 i, \qquad (2.6.8b)$$

at second order (E terms only), and

$$-g_{10\hat{\eta}} = \bar{v}_{00}\bar{w}_{00\hat{y}} + \bar{w}_{00}\bar{w}_{00\hat{\eta}} - \bar{q}\bar{w}_{00\hat{\eta}}\bar{u}_{00} + \bar{F}_2, \qquad (2.6.8c)$$

where

$$\bar{F}_2 = -\frac{\bar{F}_1}{\bar{q}} \quad \text{at} \quad \hat{y} = 0,$$

as the leading-order mean-flow balance. Equations (2.6.6a), (2.6.7c) and (2.6.8c) now need to be combined to give a single equation linking (g_{10}, g_0, A_{10}). So taking the combination $-\bar{q} * (2.6.7c) + (2.6.8c)$ we obtain

$$\frac{1}{2}\bar{q}A_{10} + \frac{1}{3}\bar{q}\hat{\eta}A_{10\hat{\eta}} + Q_{00\hat{y}}\bar{v}_{00} + Q_{00\hat{\eta}}\bar{w}_{00} - Q_{00\hat{\eta}}\bar{q}\bar{u}_{00} =$$

$$-(\bar{q}^2 + 1)g_{10\hat{\eta}} + (\bar{q}\bar{F}_1 - \bar{F}_2),$$

where $Q_{00} = (-\bar{q}\bar{u}_{00} + \bar{w}_{00})$, so (2.6.6$a$) becomes

$$Q_{00\hat{\eta}} + \bar{v}_{00\hat{y}} = 0.$$

The boundary conditions are now

$$Q_{00} \sim -\bar{q}(\hat{y} + \alpha_{30}\hat{y}^{-1} + \ldots) + \lambda_{30}\hat{y}^{-1} + \ldots,$$

i.e

$$Q_{00} \sim -\bar{q}\hat{y} + O(\hat{y}^{-2}) \quad \text{and} \quad \bar{v}_{00} \sim \kappa_{40} + \ldots, \quad \text{as} \quad \hat{y} \to \infty,$$

and

$$\bar{v}_{00} = 0 \quad \text{at} \quad \hat{y} = 0.$$

Therefore a particular solution is

$$Q_{00} = -\bar{q}\hat{y} \quad \bar{v}_{00} = \kappa_{40},$$

provided

$$(-\bar{q}\hat{y})_{\hat{\eta}} + (\kappa_{40})_{\hat{y}} = 0,$$

which holds true, and provided

$$\frac{1}{2}\bar{q}A_{10} + \frac{1}{3}\bar{q}\hat{\eta}A_{10\hat{\eta}} - \bar{q}\kappa_{40} = -(\bar{q}^2 + 1)g_{10\hat{\eta}} + (\bar{q}\bar{F}_1 - \bar{F}_2),$$

which also holds true, but to satisfy the condition at $\hat{y} = 0$ we need $\kappa_{40} = 0$. This corresponds to adding $\bar{q}$ times the momentum equation (2.6.1b) to (-1) times (2.6.1c) and then setting $s = 0$ in the resulting combined momentum equation. Also that confirms that both of the tangential velocities u_{30}, w_{30}

are singular of order s^{-1} as $s \to 0+$ in the bulk flow, these singularities being smoothed out in the wall layer. So finally we have

$$g_{10\hat{\eta}} = -\frac{4}{b_1^2}(B^2 + a_1^2)(|g_0|^2)_{\hat{\eta}} - \frac{\bar{q}}{\bar{q}^2+1}\left(\frac{1}{2}A_{10} + \frac{1}{3}\hat{\eta}A_{10\hat{\eta}}\right), \tag{2.6.9}$$

the main mean-flow equation linking (g_{10}, g_0, A_{10}).

§2.7 GOVERNING AMPLITUDE EQUATION

In this section the governing amplitude equation for the current amplitude level I is derived.

From equation (2.4.12c) we have

$$w_{31} = -i\delta^{-1}(s\bar{q}w_{21\hat{\eta}} - i(s-1)a_1\hat{\eta}w_{11}/2 + \left(\frac{s}{4} + \frac{7}{12}\right)w_0 + (s-1)sw_{0s} +$$

$$\hat{\eta}w_{0\hat{\eta}}/3 - v_0w_{10s} - v_{10}w_{0s} - iBu_{10}w_0 - ia_1w_{10}w_0$$

$$-g_{21\hat{\eta}} - ia_1g_{31}).$$

Now taking the derivative of (2.4.12b) with respect to s and substituting for w_{31} and v_{31} gives

$$u_{31} = A_{31} - i\int_{\infty}^{s} \delta^{-1}\tilde{B}_{31}ds, \tag{2.7.1}$$

subject to $u_{31} \to A_{31}$ as $s \to \infty$ after some manipulation. Here

$$\tilde{B}_{31} = \bar{Q}_1 + Q_2,$$

where

$$\bar{Q}_1 = a_1\delta^{-1}(-v_0w_{10s} - v_{10}w_{0s} - iBu_{10}w_0 - ia_1w_{10}w_0)$$

$$-(iBu_{10}u_0 + v_{10}u_{0s} + v_0u_{10s} + w_{10}u_0a_1i)_s,$$

$$Q_2 = w_{21\hat{\eta}} - (s-1)a_1\hat{\eta}iu_{11s}/2 + s\bar{q}u_{21\hat{\eta}s} + (s^2-s)u_{0ss} +$$

$$\frac{5}{4}\left(s - \frac{1}{3}\right)u_{0s} + \hat{\eta}u_{0\hat{\eta}s}/3 + a_1\delta^{-1}(s\bar{q}w_{21\hat{\eta}} - i(s-1)a_1\hat{\eta}w_{11}/2$$

$$-g_{21\hat{\eta}} - ia_1g_{31} + \left(\frac{s}{4} + \frac{7}{12}\right)w_0 + (s-1)sw_{0s} + \hat{\eta}w_{0\hat{\eta}}/3).$$

Therefore substituting this expression for u_{31} into (2.4.12b) and taking the limit $s \to 0$ establishes the internal relation at forth order as

$$\frac{b_1}{2}\left[\int_s^\infty \delta^{-1}\tilde{B}_{31}ds - iA_{31}\right] - \frac{1}{2}a_1\hat{\eta}iu_{11} + iBA_{10}u_0 - \frac{7}{12}u_0 - \frac{1}{3}\hat{\eta}u_{0\hat{\eta}} =$$

$$-Big_{31} + \bar{q}g_{21\hat{\eta}} - \frac{1}{2}a_1\hat{\eta}ig_{11} - \frac{3}{4}g_0. \qquad (2.7.2)$$

Simplifying (2.7.2) using the external relations (2.5.1$b-d$), i.e eliminating the g_{31}, g_{21}, $g_{11\hat{\eta}}$, g_{11} terms leaves as a solvability condition the amplitude equation

$$\left(\frac{4}{3^{1/2}}g_{0\hat{\eta}\hat{\eta}} - \hat{\eta}g_0\right)_{\hat{\eta}} = -iA_{10}g_0b_1^{-1}(B^2 + a_1^2), \qquad (2.7.3)$$

for g_0. The right-hand-side of (2.7.3) contains all the nonlinear effects therefore for a linear disturbance the amplitude equation reduces to Airy's equation for $g_0(\hat{\eta})$, giving the solution

$$g_0 \propto A_i(3^{1/6}4^{-1/3}\hat{\eta}), \qquad (2.7.4)$$

in terms of the Airy function A_i, which agrees with the linear theory as required (the constant of integration is zero since linear theory holds outside the edge layer).

We now have two main governing equations (2.6.9), (2.7.3) for (A_{10}, g_0), where g_{10} in (2.6.9) is replaced by (2.5.2). These equations in normalized form are

$$g_{\tilde{\eta}\tilde{\eta}} - \tilde{\eta}g = D \quad \text{where} \quad D_{\tilde{\eta}} = -iAg, \qquad (2.7.5a)$$

$$A_{\tilde{\eta}\tilde{\eta}\tilde{\eta}} - 3\left(\frac{A}{2} + \frac{\tilde{\eta}A_{\tilde{\eta}}}{3}\right) = (|g|^2)_{\tilde{\eta}}, \qquad (2.7.5b)$$

after setting

$$\hat{\eta} = \left(\frac{4}{3^{1/2}}\right)^{1/3}\tilde{\eta}, \quad A_{10} = \Omega A, \quad g_0 = \gamma g,$$

$$\text{where} \quad \Omega = b_1(B^2 + a_1^2)^{-1}, \quad \gamma = \frac{b_1^{3/2}}{2}\bar{q}(B^2 + a_1^2)^{-1}\left(\frac{3^{1/2}}{4}\right)^{1/3}.$$

At low amplitudes the equivalent of the Airy function (2.7.4) applies, whereas at most amplitudes (2.7.5a,b) require a computational treatment. The latter is addressed in part II of chapter 2.

§2.8 ALTERNATIVE APPROACH

Here we show an alternative method by which the linear result (2.7.4) and the linear portion of (2.7.3) may be obtained. From section 2.2 we have the relation

$$A_{xt} = -\nabla_{2D}^2 p.$$

Rescaling this pressure-amplitude law, using the scalings in section 2.3, namely

$$(x, z, A, p) = (t^{1/3}\hat{X}, t^{1/3}\hat{Z}, t^{-2/3}\hat{A}, t^{-4/3}\hat{P}),$$

gives

$$\hat{A}_{\hat{X}} + \frac{1}{3}\hat{X}\hat{A}_{\hat{X}\hat{X}} + \frac{1}{3}\hat{Z}\hat{A}_{\hat{X}\hat{Z}} = \hat{P}_{\hat{X}\hat{X}} + \hat{P}_{\hat{Z}\hat{Z}}. \tag{2.8.1}$$

Substituting the large-time expansions for $\hat{A}$, $\hat{P}$ into this relation yields the leading order controlling equations between $(g_0, g_{11}, g_{21}, g_{31})$ and $(A_0, A_{11}, A_{21}, A_{31})$ as shown below.

$$\frac{1}{3}A_0(B + \bar{q}a_1)B = g_0(B^2 + a_1^2), \tag{2.8.2a}$$

$$-\frac{1}{2}b_1 A_{11} B - i\bar{q}A_{0\hat{\eta}}\frac{b_1}{2} = -g_{11}(B^2 + a_1^2) - 2ig_{0\hat{\eta}}(\bar{q}B - a_1), \tag{2.8.2b}$$

$$-\frac{1}{2}A_{21}b_1 B - \frac{2}{3}A_0 a_1\hat{\eta}B - \frac{1}{2}\bar{q}b_1 A_{11\hat{\eta}}i - \frac{1}{6}\bar{q}a_1^2\hat{\eta}A_0 = -\frac{3}{2}b_1 B g_{21} + \bar{q}a_1 B g_{21}$$
$$-a_1^2 g_{21} - 2\bar{q}iBg_{11\hat{\eta}} + 2a_1 i g_{11\hat{\eta}} - g_0 a_1\hat{\eta}B + (\bar{q}^2 + 1)g_{0\hat{\eta}\hat{\eta}}, \tag{2.8.2c}$$

$$-a_1^2 g_{31} - B^2 g_{31} - 2\bar{q}iBg_{21\hat{\eta}} + 2ia_1 g_{21\hat{\eta}} - a_1\hat{\eta}Bg_{11} + \bar{q}^2 g_{11\hat{\eta}\hat{\eta}} + g_{11\hat{\eta}\hat{\eta}}$$
$$-i\bar{q}a_1\hat{\eta}g_{0\hat{\eta}} + \frac{3}{4}iBg_0 + \frac{5}{4}iBg_0 - \frac{1}{2}ig_0 a_1\bar{q} =$$
$$-\frac{1}{2}b_1 B A_{31} - \frac{1}{2}i\bar{q}b_1 A_{21\hat{\eta}} - \frac{2}{3}a_1\hat{\eta}BA_{11} - \frac{1}{6}\bar{q}a_1^2\hat{\eta}A_{11} + \frac{1}{3}i\hat{\eta}BA_{0\hat{\eta}}$$
$$-\frac{2}{3}i\bar{q}a_1\hat{\eta}A_{0\hat{\eta}} + \frac{1}{6}ia_1\hat{\eta}\bar{q}A_{0\hat{\eta}} + iBA_0 - \frac{1}{12}i\bar{q}a_1 A_0, \tag{2.8.2d}$$

from the first, second, third and fourth order E term balances respectively. We now couple $(2.8.2a-d)$ with the external pressure-displacement relations $(2.5.1a-d)$. Coupling the first-and second-order balances fixes the constants a_1, b_1 and B. At fourth order however we obtain the linear Airy equation, i.e

$$\frac{4}{3^2 2^{1/2}} g_{0\hat{\eta}\hat{\eta}\hat{\eta}} - \frac{1}{3^{3/2}2^{1/2}}\hat{\eta} g_{0\hat{\eta}} - \frac{1}{3^{3/2}2^{1/2}} g_0 = 0,$$

for g_0. Making the transformation $\hat{\eta} = 2^{2/3}\tilde{\eta}/3^{1/6}$ gives

$$(g_{0\tilde{\eta}\tilde{\eta}} - \tilde{\eta} g_0)_{\tilde{\eta}} = 0,$$

confirming the linear contribution above, e.g compare with $(2.7.5a)$. The same method can be adapted to verify the nonlinear portion on the right-hand side of (2.7.3) or $(2.7.5a)$

§2.9 APPENDIX

Before moving on to solving the governing equations numerically, we present here the argument for using the particular form of the large-time expansions $(2.4.1a-e)$.

Consider the form

$$\hat{A} = \hat{X}^{m-1}(EA_0 + c.c) + \ldots, \tag{2.9.1}$$

for the amplitude, where the notation is as before and m is a constant to be fixed. The relative effect of the typical amplitude-squared nonlinearity is of the order $\hat{X}^{2m-4}$ since $\hat{U}$ is equal to $\hat{X}s$ with an $O(\hat{X}^{m-1})$ correction due to $(2.3.3b)$. This is to be compared with the relative effect in (2.4.2) of order $\hat{X}^{-1}$. The two effects are comparable when $2m-4=-1$; giving $m=3/2$. So at this stage the streamwise momentum, amplitude and pressure expansions are

$$\hat{U} = \hat{X}s + \hat{X}^{1/2}(Eu_0 + c.c)k + \ldots + \hat{X}^0(E^2u_{12}k^2 + Eu_{11}k + u_{10} + c.c) + \ldots,$$

$$\hat{A} = \hat{X}^{1/2}(EA_0 + c.c)k + \ldots + \hat{X}^0(E^2A_{12}k^2 + EA_{11}k + A_{10} + c.c) + \ldots,$$

$$\hat{P} = \hat{X}^{3/2}(Eg_0 + c.c)k + \ldots + \hat{X}(E^2 g_{12}k^2 + Eg_{11}k + g_{10}k^2 + c.c) + \ldots,$$

where $k = \hat{X}^{m-3/2} = 1$ for $m = 3/2$, but we also need to consider the mean-flow balance between g_{10}, A_{10}. In particular

$$\hat{X}k^2 g_{10} \sim \hat{X}^0 A_{10},$$

because of the pressure-amplitude law (essentially this is comparing the relative effect in (2.4.2) with [mean-flow correction due to the pressure-amplitude law '$\hat{X}$']* $\hat{X}^{2m-4}$). Hence $k = \hat{X}^{-1/2}$ and this yields another value $m = 1$ for the index. This value gives

$$\hat{U} = \hat{X}s + \hat{X}^0(Eu_0 + c.c) + \ldots,$$

$$\hat{A} = \hat{X}^0(EA_0 + c.c) + \ldots + \hat{X}^0(E^2 A_{12}\hat{X}^{-1} + \ldots + A_{10} + c.c) + \ldots,$$

$$\hat{P} = \hat{X}(Eg_0 + c.c) + \ldots + \hat{X}(E^2 g_{12}\hat{X}^{-1} + Eg_{11}\hat{X}^{-1/2} + \hat{X}^{-1}g_{10} + c.c) + \ldots.$$

Initially these expansions seemed appropriate but further points need consideration. Firstly to match the nonlinear theory to the linear we need to go to fourth order in our expansions (see above); and secondly the pressure-displacement relation is special for the mean-flow-corrective terms, in that we require the mean-flow amplitude $A_{10} \sim \hat{\eta}$ and for $A_{10\hat{\eta}\hat{\eta}} \propto |g_0|^2$ (using the notation of section 2.4) for the nonlinear theory to connect with the linear theory. To clarify the second point we note that g_0 (from expansion (2.4.1*d*)) satisfies the Airy equation; this yields the asymptote $g_0 \propto |\hat{\eta}|^{-1/4}\sin(\frac{2}{3}|\hat{\eta}|^{3/2} + const.)$ (see (2.7.5a) above), and $A_{10} \sim g_0^2$ follows form the pressure-displacement relation (2.7.5*b*). Hence $A_{10} \sim \hat{\eta}^{3/2}$ i.e A_{10} "grows and overwhelms" $\hat{\eta}$. Therefore we reduce the order of g_0 by ϵ say. After some working it is found that $\epsilon = |\hat{\eta}|^{-1/4}$, so we still have the relation $A_{10} \sim |g_0|^2$ but now $A_{10} \sim \hat{\eta}$. These above mentioned points suggest after some working, the expansions (2.4.1*a*−*e*).

§2.10 SUMMARY

In the above part of chapter 2 we have presented first a linear model for a spot disturbance in a wall-jet or channel flow, and second a nonlinear model based on this for a spot in a wall-jet flow only. The emphasis has been on long-scale disturbances throughout, partly because experiments suggest that the streamwise and spanwise length-scales can be typically larger than the normal scale for part of the spot development.

The linear theory suggests that increasingly concentrated waves form far downstream within a wedge of semi-angle 30°, although the maximum amplitudes occur at the edges or caustics of this wedge; also linear properties hold outside the edge layer(s). In practice this 30° prediction is however an overestimate for spots in channel flows, since the typical angle is 10° from experiments. Also we find that significant effects arise in two main regions far downstream at distances of order $(time)^{1/3}$ and $(time)$.

The nonlinear theory is based around the $(time)^{1/3}$ streamwise and spanwise scales. The governing amplitude equations that we obtain match with the linear theory at low amplitudes, whereas at higher amplitudes the full set of nonlinear equations needs a computational treatment. We note that the nonlinear interaction at this amplitude level is dominated by interplay between the fundamental fluctuations $E^{\pm 1}$ and the mean-flow correction E^0.

CHAPTER 2

PART II

NUMERICAL METHOD & SOLUTIONS

§2.11 NUMERICAL METHOD & SOLUTIONS

In this part we describe a numerical scheme used to solve equations (2.7.5a, b), involving a finite difference procedure. The following discretizations were used:

$$\frac{B_{j+1} - 2B_j + B_{j-1}}{\triangle^2} - \frac{3}{2}A_j - \tilde{\eta}_j B_j = \frac{g_j(g^*_{j+1} - g^*_{j-1})}{2\triangle} + \frac{g^*_j(g_{j+1} - g_{j-1})}{2\triangle}, \tag{2.11.1a}$$

for (2.7.5b), where $B = A_{\tilde{\eta}}$ and is discretized as

$$\frac{1}{2}(B_j + B_{j-1}) = \frac{A_j - A_{j-1}}{\triangle}, \tag{2.11.1b}$$

$$\frac{g_{j+1} - 2g_j + g_{j-1}}{\triangle^2} - \tilde{\eta}_j g_j + iA_j g_j \triangle = D_j, \tag{2.11.1c}$$

where

$$D_j = -\sum^{k=j} iA_k g_k \triangle + iA_j g_j \triangle, \tag{2.11.1d}$$

for (2.7.5a). Second order accuracy is maintained throughout. The $\tilde{\eta}$ variable is given by $\tilde{\eta}_{-\infty} + (j-1)\triangle = \tilde{\eta}_j$, with $1 \leq j \leq J$, where $\tilde{\eta}_\infty = \tilde{\eta}_{-\infty} + (J-1)\triangle$ and $\tilde{\eta}_\infty$, $\tilde{\eta}_{-\infty}$ are chosen to be suitably large, with the step size $\triangle$ being small. The system (2.11.1a – d) is then solved using an iterative process, where the g_j's obtained from (2.11.1c) by inversion of a tridiagonal system, are substituted into (2.11.1a) to obtain the A_j's by inversion of a multi-diagonal system (Guassian elimination is used to invert the matrices). The g's and A's are then substituted into (2.11.1d) to establish what the new D's are and so on. This process is repeated until a converged solution is obtained. We note that the 'theoretical' boundary conditions (cf. next paragraph) on g are $g(\mp\infty) = 0$, since we require g to satisfy Airy's equation. Also the left-hand-side of equation (2.11.1a) is 'Airy-like', hence we expect $A(\mp\infty) = 0$ as theoretical boundary conditions.

In practice the linear version of (2.11.1c) is solved numerically with a non-zero input amplitude (I.A) at $\tilde{\eta}_{-\infty}$, i.e $g_1(-\infty) = I.A$, and this produces the expected Airy function for g. This is used as an initial guess for g to start up the iterative process. Typical converged results are shown below.

We note here that relaxation is used to encourage convergence. Also we expect the nonlinearity to reduce the spread half-angle, i.e we want the maximum amplitude to move towards the centre of the spot, but this is as yet not clearly visible from the numerical plots shown in the figures, although as we shall see in chapter 3, as the amplitude is raised even further, we do find a definite inward trend towards the centre. However in general the results are encouraging since the amplitude decays exponentially away from the centre and algebraically towards the centre.

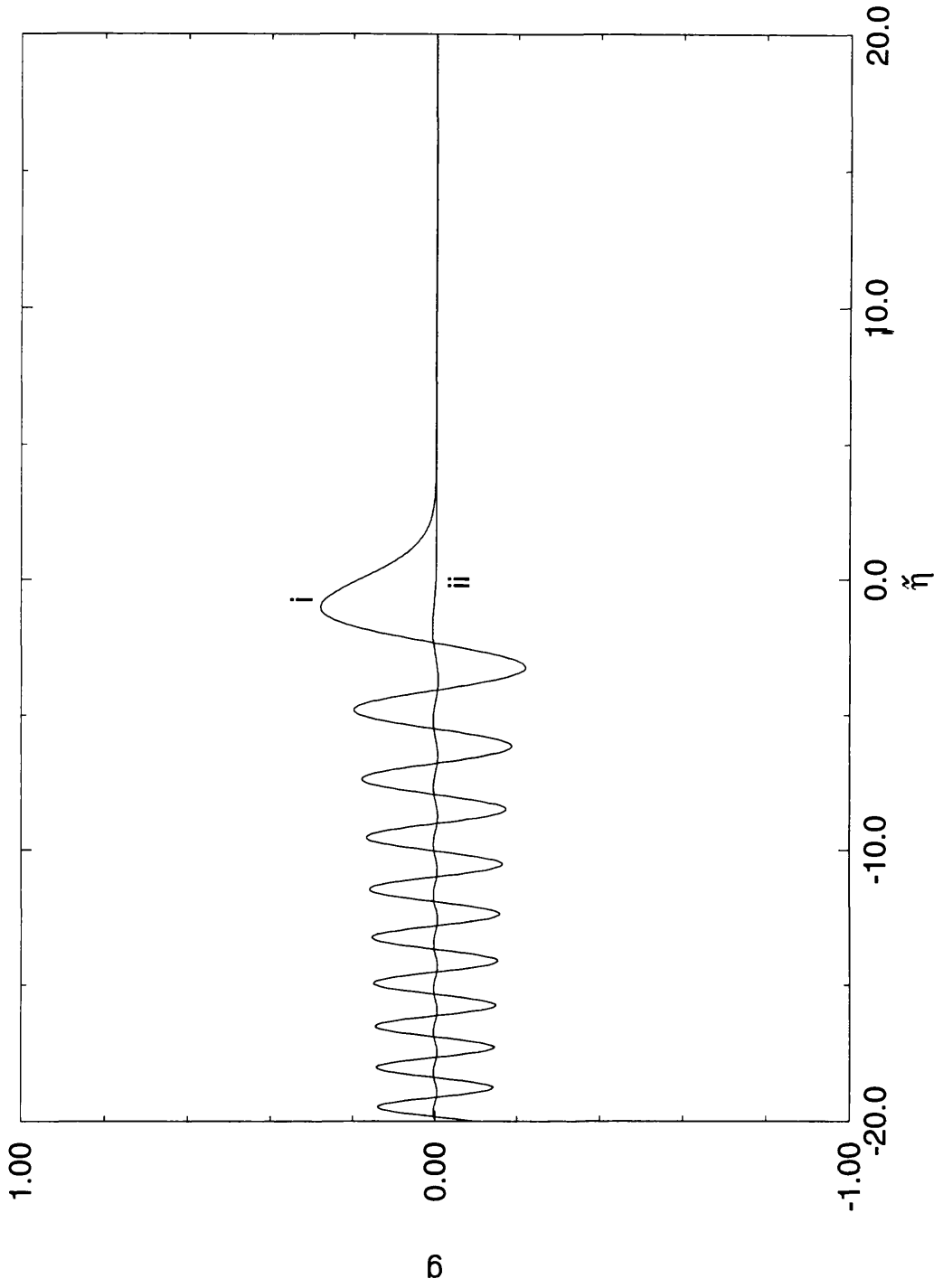

fig 2.11.1a

Solution computed for the wave contribution g (i real part, ii imaginary part),

for the small amplitude solution in fig 2.11.1*b*.

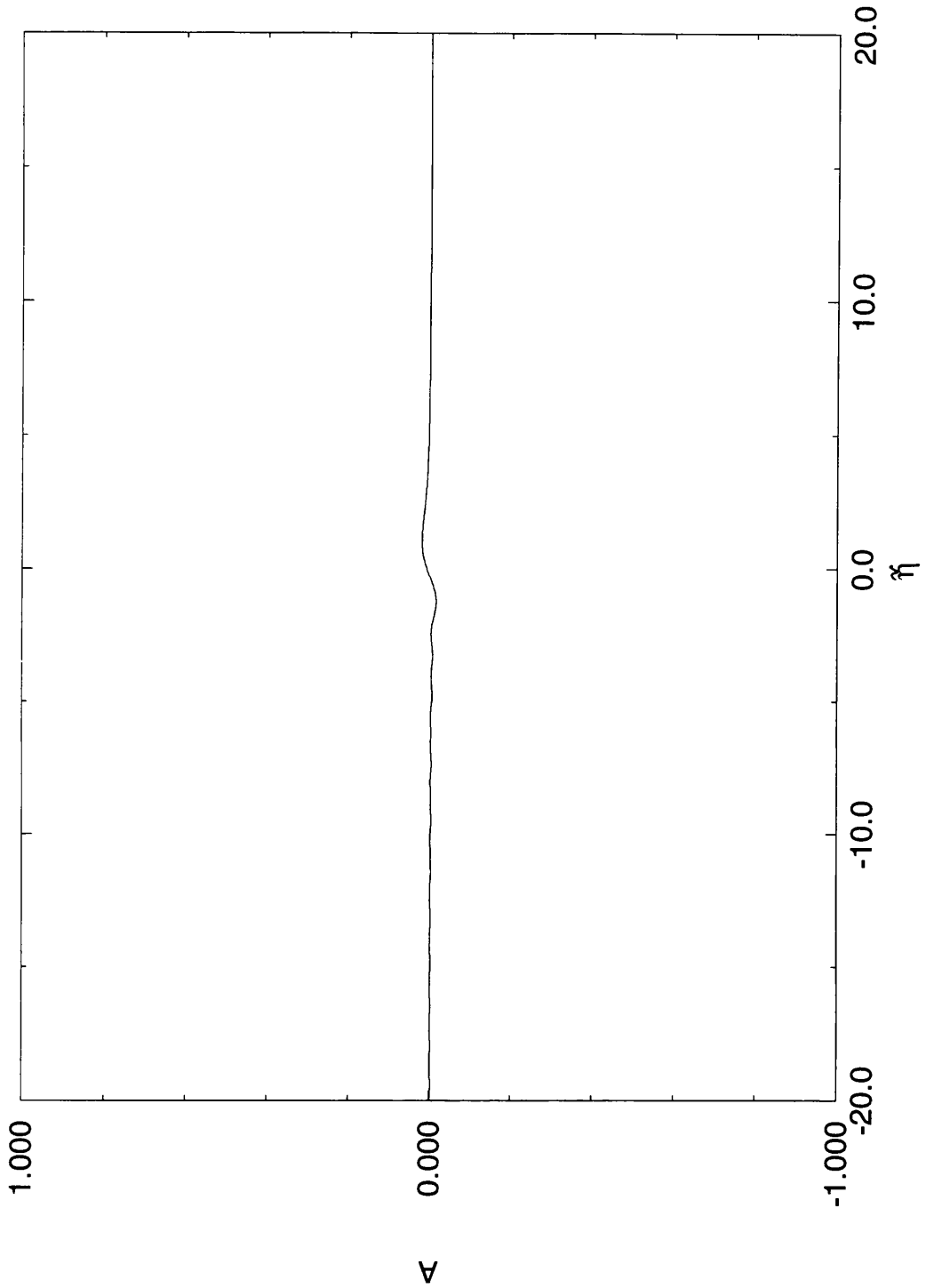

fig 2.11.1b

Solution computed for the mean amplitude A.

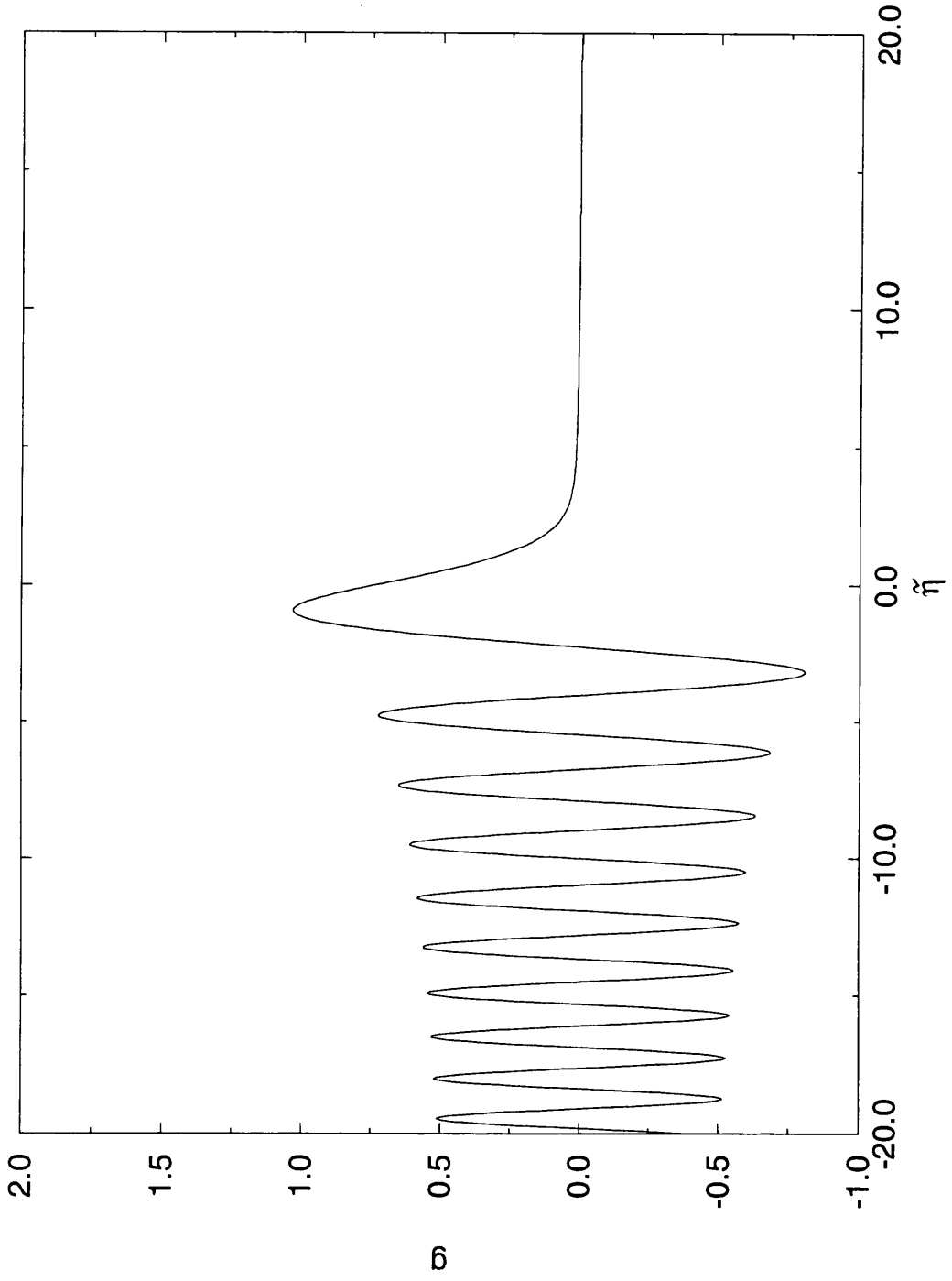

fig 2.11.2a

Solution computed for the wave contribution g (real part).

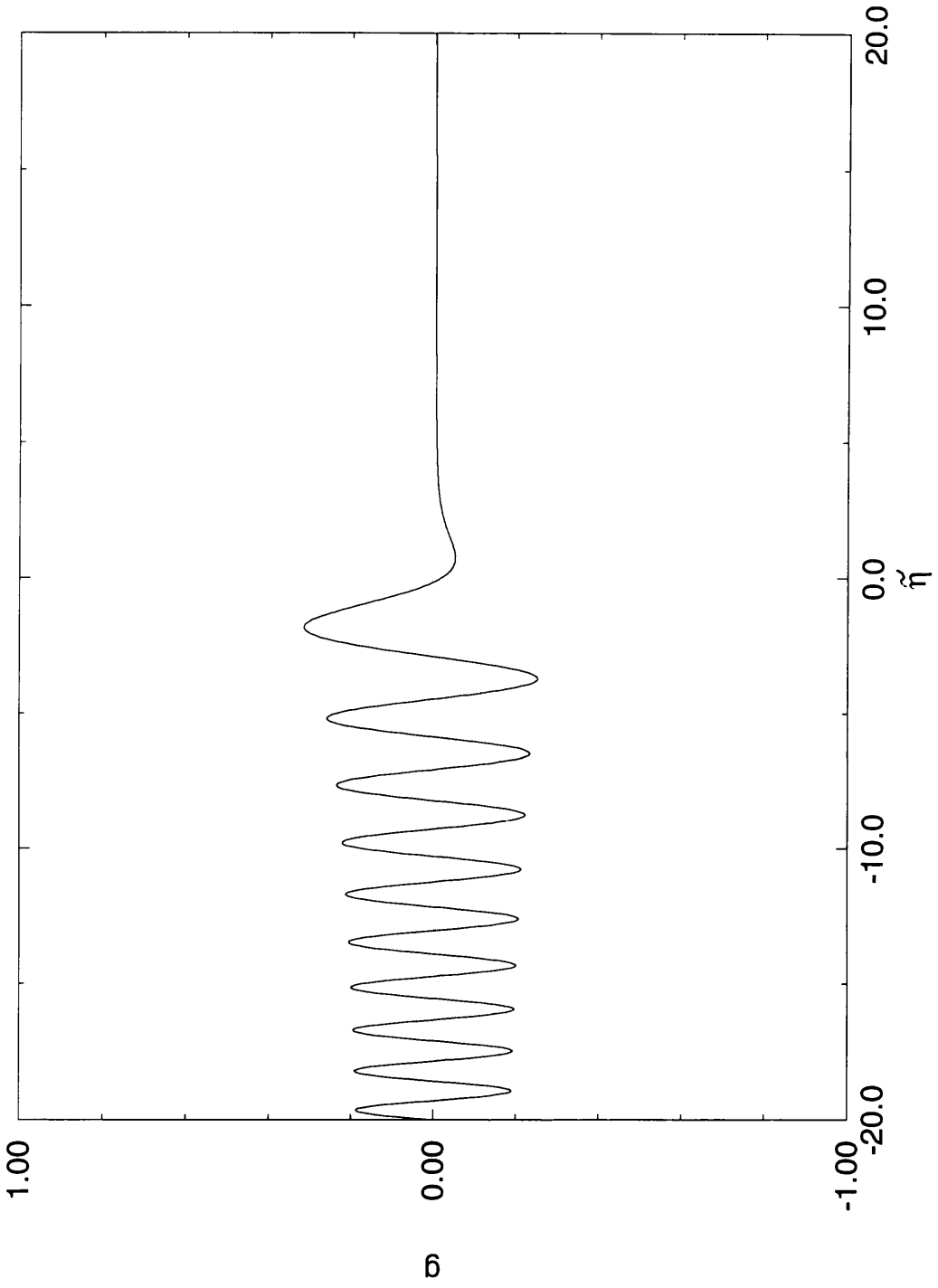

fig 2.11.2b

Solution computed for the wave contribution g (imaginary part).

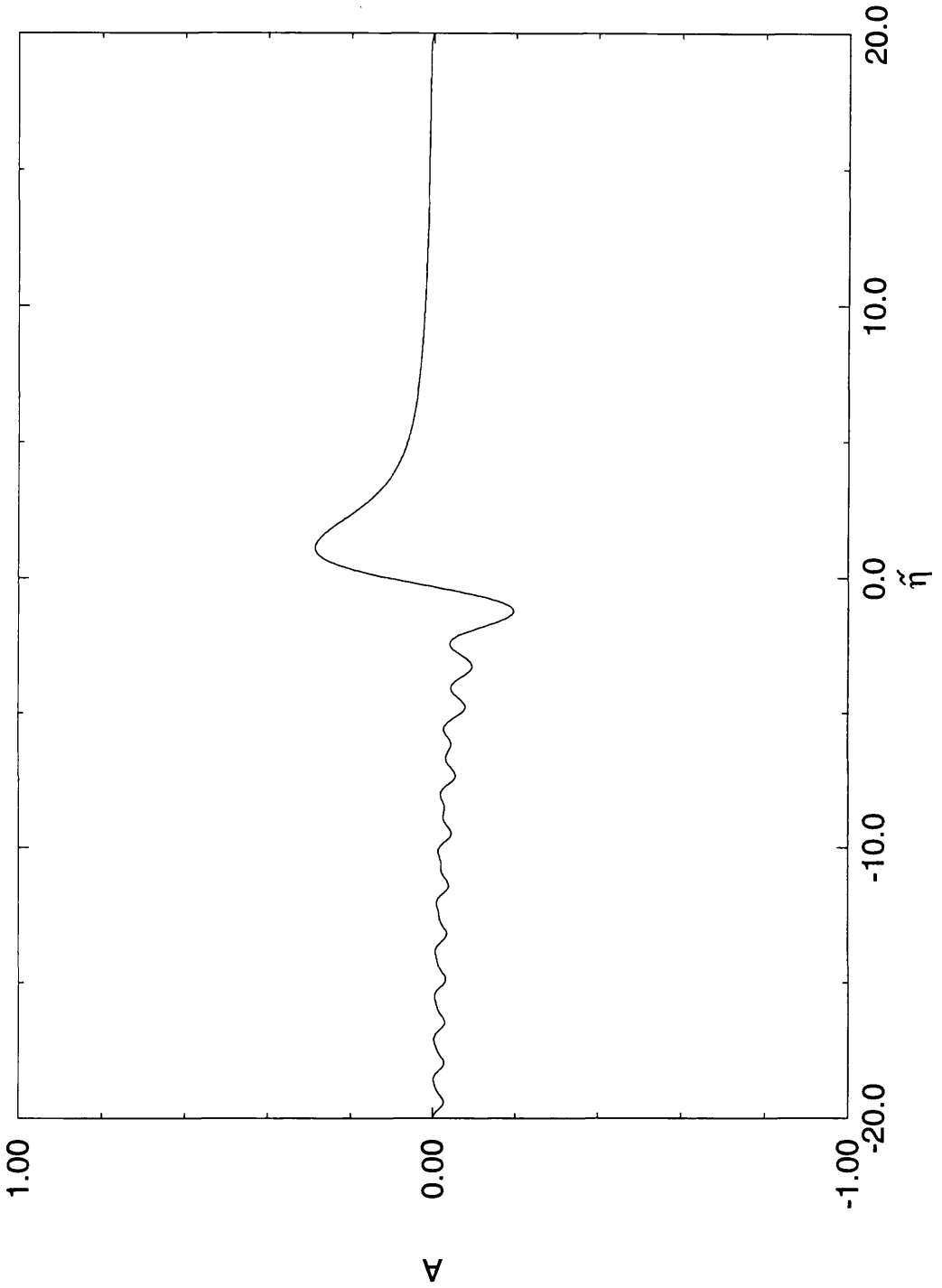

fig 2.11.2c

Solution computed for the mean amplitude A corresponding

to the wave contribution g in figs 2.11.2a, b.

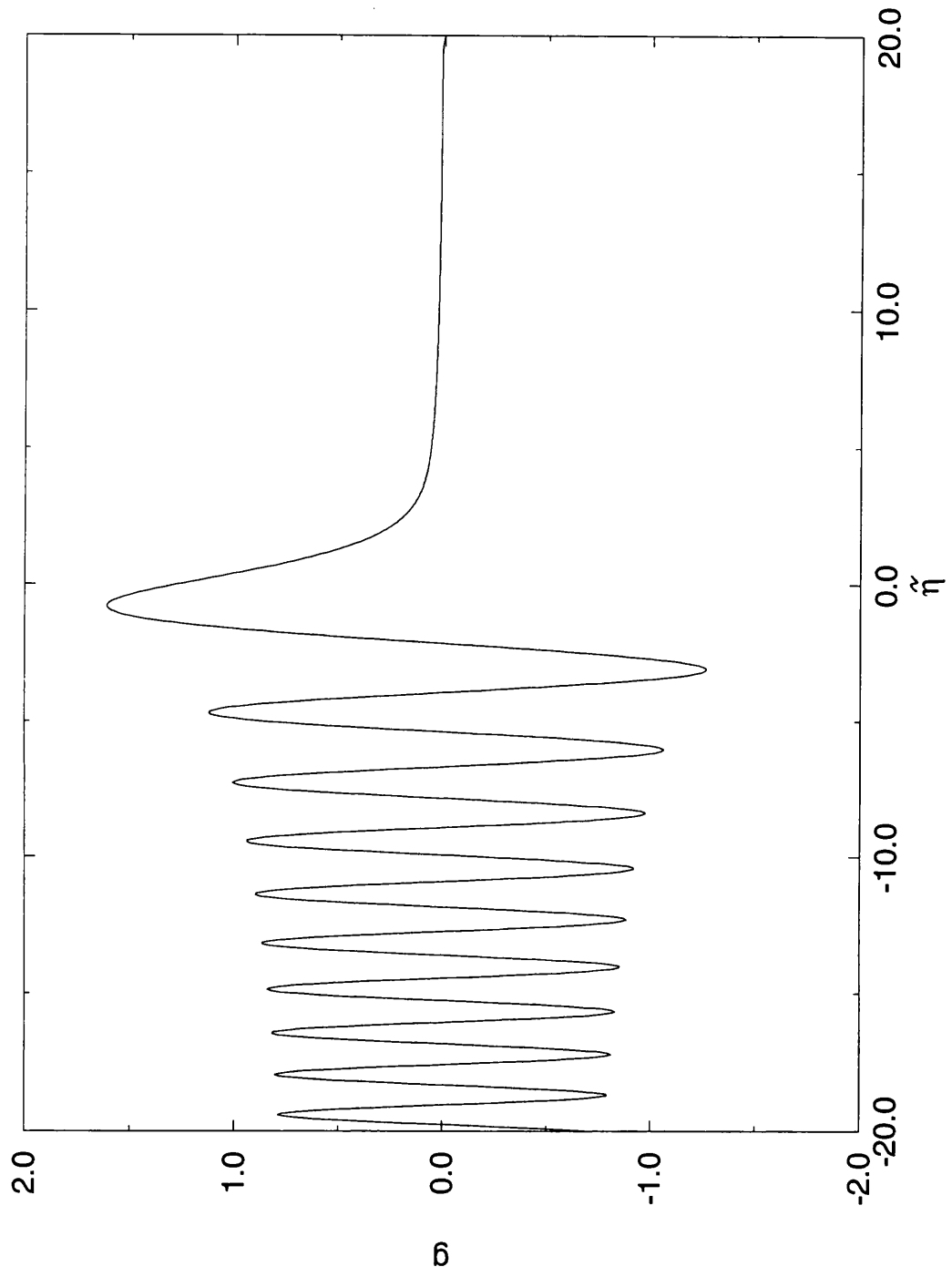

fig 2.11.3a

Solution computed for the wave contribution g (real part).

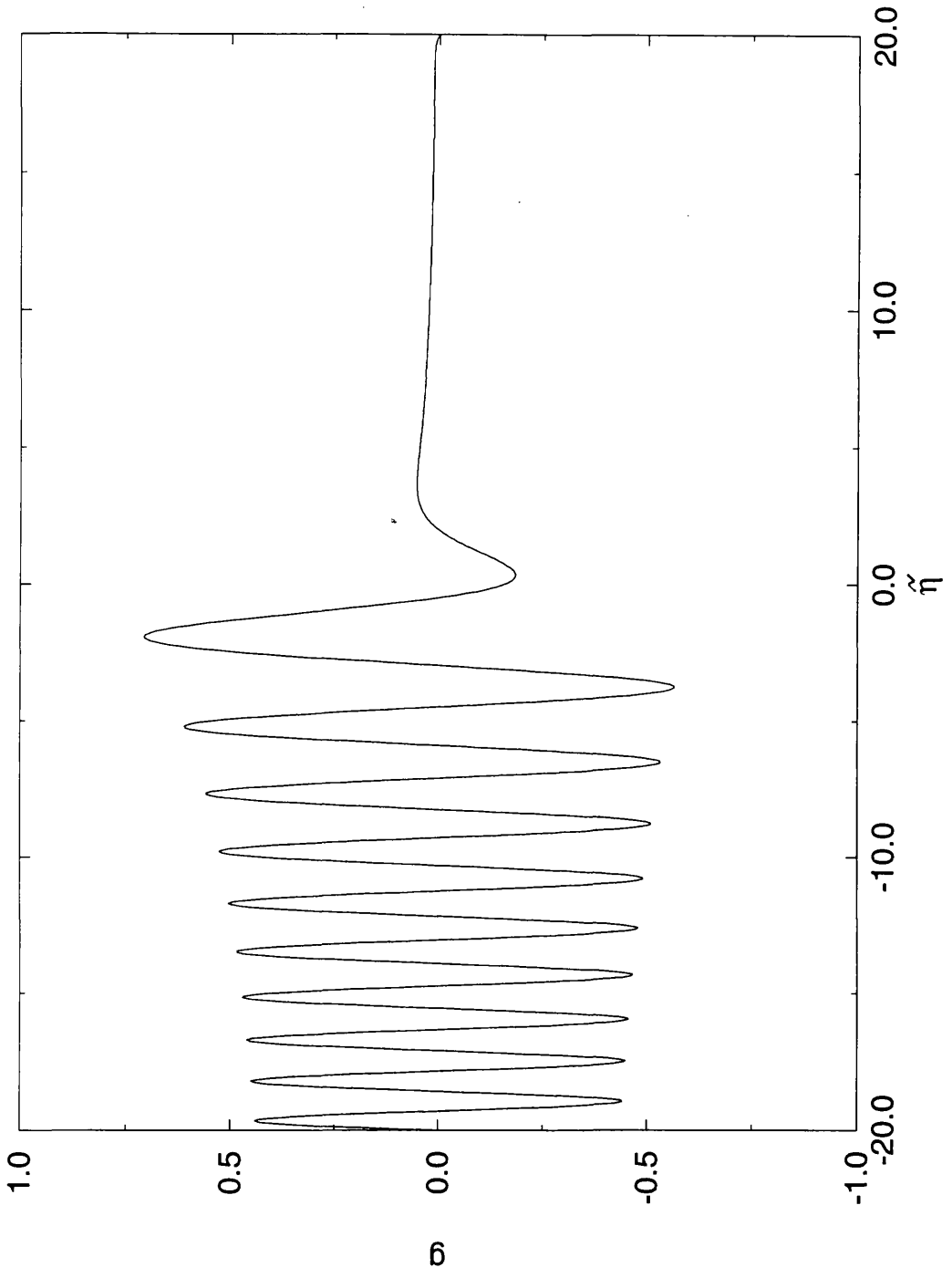

fig 2.11.3b

Solution computed for the wave contribution g (imaginary part).

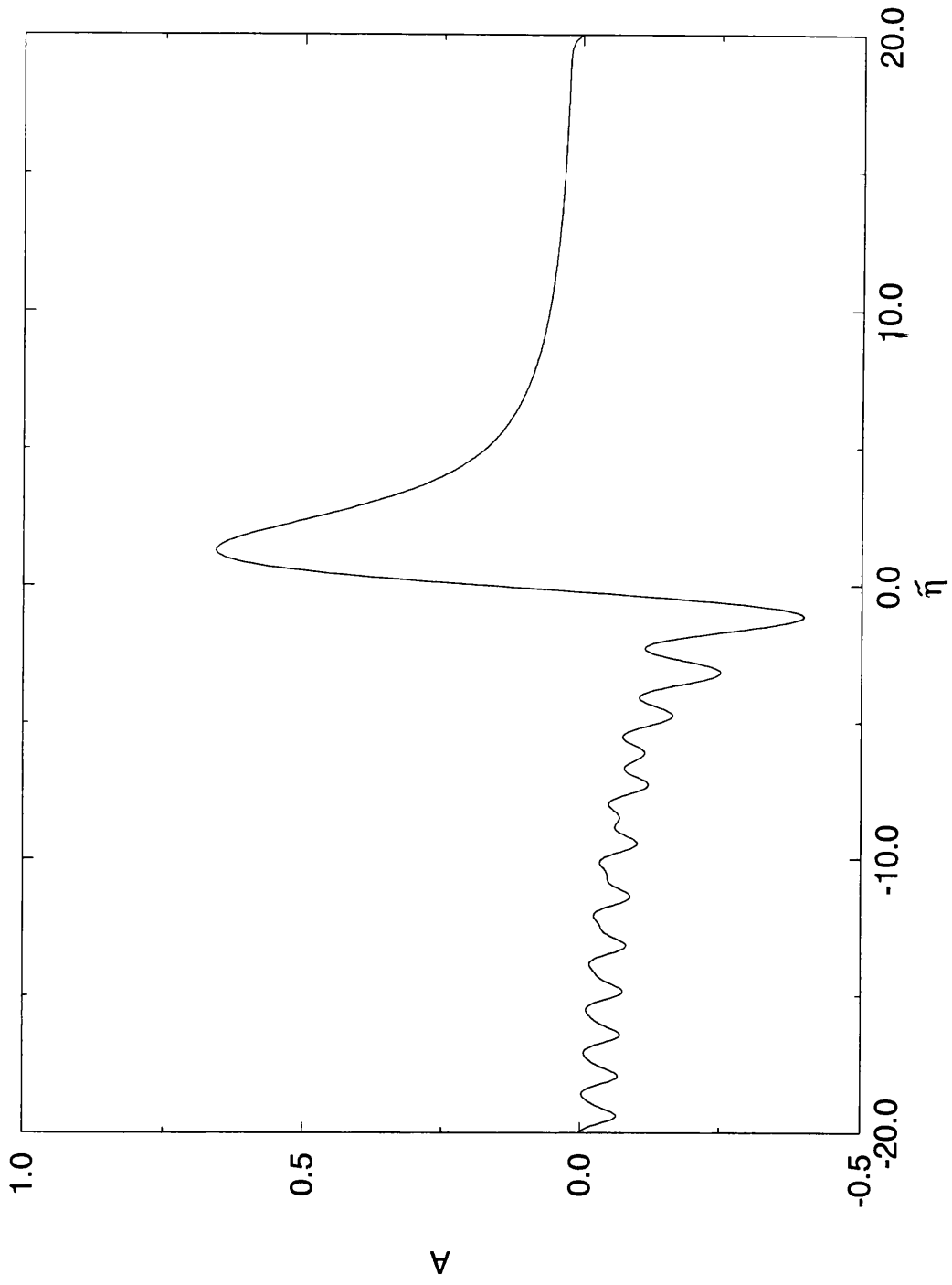

fig 2.11.3c

Solution computed for the mean amplitude A corresponding

to the wave contribution g in figs 2.11.3a, b.

CHAPTER 3

AMPLITUDE LEVEL II

§3.0 INTRODUCTION

The aim in this chapter is to understand the influence of raised amplitudes in the $O(T^{1/3})$ zone near the trailing edge of the spot, and to find whether the positions of maximum amplitude gradually move towards the middle of the spot's trailing edge.

We start below with the governing equations $(2.7.5a, b)$ of chapter 2 and consider what happens when the typical scale of $|\tilde{\eta}|$ expands like $\hat{\triangle}$ ($\hat{\triangle} \gg 1$) say, with $g \sim \hat{\triangle}^{5/4}\hat{G}_n \exp[i\hat{\triangle}^{3/2}\hat{F}_n]$ and $A \sim \hat{\triangle}^{3/2}a_m$ for consistency, where $\hat{G}_n$, $\hat{F}_n$, a_m are all generally $O(1)$ real functions of the new $O(1)$ coordinate $\check{\eta} = \hat{\triangle}^{-1}\tilde{\eta}$: see section 3.1. The leading-order equations obtained for $\hat{F}_n$, $\hat{G}_n$, a_m, are found to suggest at first sight three possible phase branches for $\hat{F}_n'$ for a given $a_m(\check{\eta})$, but after some working only one branch is felt to be mathematically consistent, as is explained in sections 3.2, 3.3.

A modified version of the above mentioned higher-amplitude system of equations is studied in section 3.4, since the modified version allows us to obtain more analytical insight about the actual system. The modified equations are studied computationally and analytically. On the analytical side we carry out a phase-plane analysis in section 3.4, which shows that three saddle-points are present; an alternative method using Taylor series expansions is also shown in section 3.5, which confirms these results. Numerically we use a classical fourth-order Runge-Kutta shooting method to solve the system, see section 3.6; again we observe that three saddle points are present. Other details are also presented.

Numerical solutions for the actual system are then shown ('shooting' forwards and backwards from $\check{\eta} = 0$). The effect of increased nonlinearity in the edge-layer is clearly seen from the solutions of this system, i.e. a definitive inward trend towards the middle of the spot for the amplitude a_m is obtained.

We note that the main governing equations at this amplitude level correspond to the higher amplitude limit of level II in the work of Smith et al (1994) for the boundary-layer spot (again see below).

§3.1 HIGHER AMPLITUDE EQUATIONS

We have from Chapter 2 (Part I) the governing equations

$$g_{\tilde{\eta}\tilde{\eta}\tilde{\eta}} - \tilde{\eta} g_{\tilde{\eta}} - g = -iAg, \tag{3.1.1a}$$

$$A_{\tilde{\eta}\tilde{\eta}\tilde{\eta}} - 3\left(\frac{A}{2} + \frac{\tilde{\eta} A_{\tilde{\eta}}}{3}\right) = (|g|^2)_{\tilde{\eta}}, \tag{3.1.1b}$$

to consider first. As mentioned in the introduction to this chapter, we examine what happens as the typical scale of $\tilde{\eta}$ (in the above notation) expands like

$$\tilde{\eta} = \hat{\triangle}\check{\eta},$$

say, where the constant factor $\hat{\triangle} \gg 1$. For g to satisfy (3.1.1a) at leading order at the current amplitude level we need the balance

$$\tilde{\eta} g' \sim iAg.$$

So taking $g \propto e^{\frac{2}{3}i|\tilde{\eta}|^{3/2}}$ at large $\tilde{\eta}$ as guided by the Airy function, we have

$$\tilde{\eta}|\tilde{\eta}|^{1/2} e^{\frac{2}{3}i|\tilde{\eta}|^{3/2}} \sim A e^{\frac{2}{3}i|\tilde{\eta}|^{3/2}},$$

i.e $A \sim \hat{\triangle}^{3/2}$. Hence we consider the pressure g and amplitude A to have the following expansions,

$$g = \hat{\triangle}^{c_1}(\hat{G}_1(\check{\eta})e_1 + \hat{G}_2(\check{\eta})e_2 + \ldots) + \ldots, \tag{3.1.2a}$$

$$A = \hat{\triangle}^{3/2} a_m(\check{\eta}) + \hat{\triangle}^{c_2}\tilde{A} e_2 e_1^{-1} + \ldots, \tag{3.1.2b}$$

where $e_n = exp[i\hat{\triangle}^{3/2}\hat{F}_n(\check{\eta})]$, $n = 1, 2, \ldots$. Here c_1 and c_2 are constants to be determined, and the e_n's give the fastest behaviour present. Substituting (3.1.2a, b) into (3.1.1b) gives for the right-hand-side,

$$(|g|^2)_{\tilde{\eta}} = \hat{\triangle}^{2c_1}(\hat{\triangle}^{-1}[(|\hat{G}_1|^2)_{\check{\eta}} + (|\hat{G}_2|^2)_{\check{\eta}} + \ldots] + \hat{\triangle}^{1/2}\hat{G}_2\hat{G}_1^* e_2 e_1^{-1} i\hat{F}_2' + \ldots), \tag{3.1.3a}$$

and for the left-hand-side we have

$$A_{\check{\eta}\check{\eta}\check{\eta}} - \left(\frac{3}{2}A + \check{\eta}A_{\check{\eta}}\right) = \hat{\triangle}^{3/2}\left(-\frac{3}{2}a_m - \check{\eta}a'_m\right)$$

$$+\hat{\triangle}^{c_2}\left(\tilde{A}e_2e_1^{-1}i^3\hat{F}_2'^3\hat{\triangle}^{3/2} - \check{\eta}\hat{\triangle}^{3/2}\tilde{A}e_2e_1^{-1}i\hat{F}_2' - \frac{3}{2}\tilde{A}e_2e_1^{-1}\right). \qquad (3.1.3b)$$

Balancing the leading-order terms from $(3.1.3a, b)$, we therefore have

$$\hat{\triangle}^{2c_1-1} = \hat{\triangle}^{3/2} \Rightarrow c_1 = 5/4,$$

and

$$\hat{\triangle}^{2c_1+1/2} = \hat{\triangle}^{c_2}\hat{\triangle}^{3/2} \Rightarrow c_2 = 3/2.$$

So we are left with the expansions

$$g = \hat{\triangle}^{5/4}(\hat{G}_1e_1 + \hat{G}_2e_2 + \ldots) + \ldots, \qquad (3.1.4a)$$

$$A = \hat{\triangle}^{3/2}a_m(\check{\eta}) + \hat{\triangle}^{3/2}\tilde{A}e_2e_1^{-1} + \ldots, \qquad (3.1.4b)$$

for the pressure and displacement respectively, cf. Smith et. al (1994). Further terms in the expansions can be obtained through a procedure similar to that above.

Substituting these higher-amplitude expansions $(3.1.4a, b)$ into the equations $(3.1.1a, b)$ yields the governing equations for the current amplitude level, i.e.

$$h_n^3 + \check{\eta}h_n = -a_m, \qquad (3.1.5a)$$

$$(3h_n^2 + \check{\eta})r_n' + (3h_nh_n' + 1)r_n = 0, \qquad (3.1.5b)$$

$$(r_1^2 + r_2^2 + r_3^2 + \ldots)_{\check{\eta}} = -\frac{3}{2}a_m - \check{\eta}a'_m, \qquad (3.1.5c)$$

for $n = 1, 2, 3, \ldots$, where $h_n = -\hat{F}_n'$ and $r_n = |\hat{G}_n|$, cf. Smith et. al. (1994).

§3.2 THREE NONLINEAR MODES

In this section we show that the system $(3.1.5a-c)$ has a 'cut-off' value (see below) at a finite value $\check{\eta}=\bar{\eta}_0$, there being only one nonlinear 'mode' r_n for $\check{\eta}>\bar{\eta}_0$ but three nonlinear 'modes' r_n for $\check{\eta}<\bar{\eta}_0$. Only one of these three modes turns out to be mathematically consistent however.

So for $\check{\eta}<0$ we put $\check{\eta}=-\xi$ say $(\xi>0)$ and set

$$\xi=\frac{3}{2^{2/3}}\bar{\xi}, \qquad h=2^{2/3}\bar{\xi}^{1/2}\bar{h}.$$

Substituting these into equation $(3.1.5a)$ yields

$$4\bar{h}^3-3\bar{h}=-\frac{a_m}{\bar{\xi}^{3/2}},$$

which we consider for now as an equation for $\bar{h}$, given a_m. This admits a solution of the form

$$\bar{h}=\cos\theta, \qquad \cos 3\theta=-\frac{a_m}{\bar{\xi}^{3/2}},$$

i.e.

$$\cos 3\theta=-\frac{1}{2}a_m\left(\frac{\xi}{3}\right)^{-3/2}$$

determines the three values of θ, or the three nonlinear 'modes', and is valid provided

$$\left|\frac{1}{2}a_m\left(\frac{\xi}{3}\right)^{-3/2}\right|\leq 1. \tag{3.2.1}$$

This implies a 'cut-off' value at

$$a_m=\pm 2\left(\frac{\xi}{3}\right)^{3/2}.$$

Similarly for $\check{\eta}>0$ we write

$$\check{\eta}=\frac{3}{2^{2/3}}\xi_1 \qquad \text{and} \qquad h=2^{2/3}\xi_1^{1/2}\bar{h}_1.$$

Therefore introducing $\bar{h}_1=\sinh\theta$, we obtain

$$\sinh 3\theta=-\frac{a_m}{\xi_1^{3/2}},$$

i.e.

$$\sinh 3\theta = -\frac{a_m}{2}\left(\frac{\check{\eta}}{3}\right)^{-3/2},$$

so that in general this suggests only one nonlinear mode for $\check{\eta} > 0$. The question of how many of these modes are present in the solution of the full system $(3.1.5a - c)$ now needs to be tackled.

§3.3 'CUT-OFF' ANALYSIS

We expect the amplitude a_m to have the form

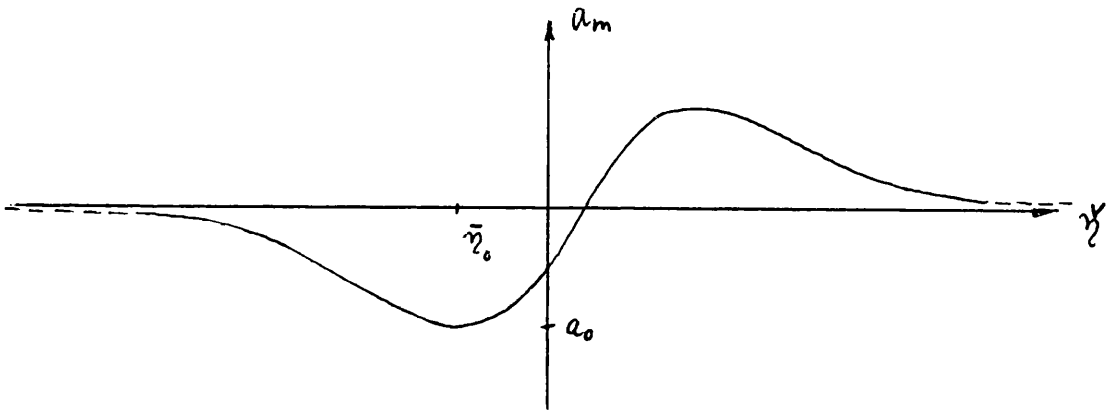

fig 3.3.1

See section 2.11. Now $(3.1.5a)$ gives

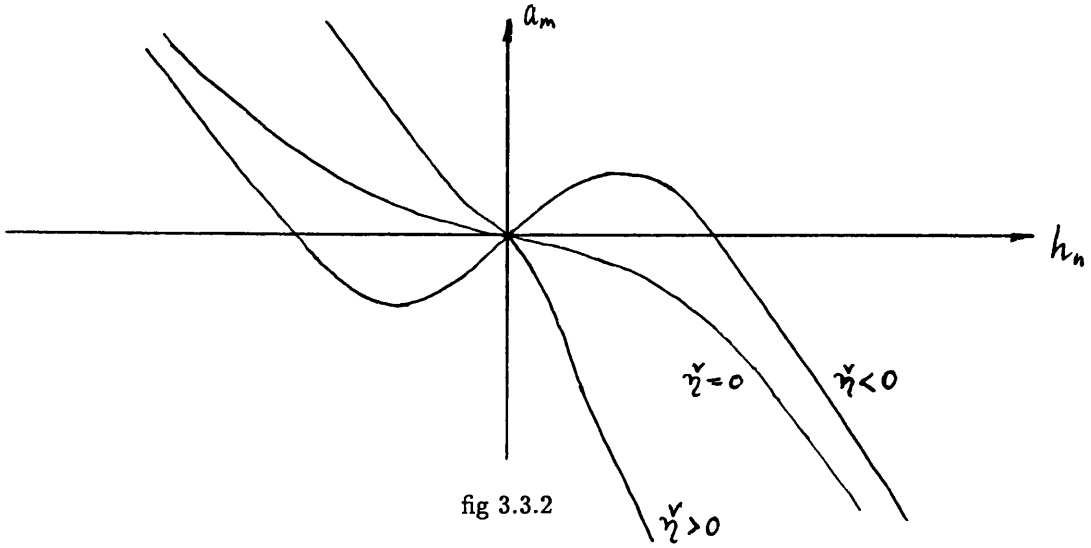

fig 3.3.2

Therefore we have a double root where,

$$h_n^3 + \check{\eta} h_n = -a_m \quad \text{and} \quad 3h_n^2 + \check{\eta} = 0,$$

i.e.

$$\bar{\eta}_0 = -3h_n^2 < 0, \tag{3.3.1a}$$

and

$$a_m = a_0 = \pm 2\left(\frac{-\bar{\eta}_0}{3}\right)^{3/2}, \tag{3.3.1b}$$

which agrees with (3.2.1). So assuming a_m has a finite value at the 'cut-off' point we consider a_m to have the form

$$a_m \sim a_0 + \gamma(\bar{\eta}_0 - \check{\eta})^{\delta} + \bar{\gamma}(\bar{\eta}_0 - \check{\eta})^{3\delta/2} + \ldots, \tag{3.3.2a}$$

as $\check{\eta} \to \bar{\eta}_0-$ for $0 < \delta \leq 1$, where $\gamma > 0$ if $\delta < 1$ (from fig 3.3.1). Then for h_1, h_3 say, we have the forms

$$h_{1,3} \sim \alpha \mp \beta(\bar{\eta}_0 - \check{\eta})^{\delta/2} + \bar{\beta}(\bar{\eta}_0 - \check{\eta})^{\delta} + \ldots \tag{3.3.2b}$$

from (3.1.5a), (3.3.1a, b), where $\alpha < 0$ and for r_1 and r_3 (corresponding to h_1, and h_3 respectively) we have

$$r_{1,3} \propto (\bar{\eta}_0 - \check{\eta})^{-\delta/4} + \lambda_1(\bar{\eta}_0 - \check{\eta})^{\delta/4} + \ldots \tag{3.3.2c}$$

Substituting the a_m, h_3, and r_3 combination into equation (3.1.5a) we obtain the following equations at various orders,

$$\alpha^3 + \bar{\eta}_0\alpha = -a_0, \tag{3.3.3}$$

from an $O(1)$ balance

$$3\alpha^2\beta + \bar{\eta}_0\beta = 0,$$

from an $O(\bar{\eta}_0 - \check{\eta})^{\delta/2}$ balance. This last balance implies

$$\alpha = -\left(-\frac{\bar{\eta}_0}{3}\right)^{1/2},$$

Substituting this expression for α into the $O(1)$ balance above we get

$$a_0 = -2\left(-\frac{\bar{\eta}_0}{3}\right)^{3/2},$$

which agrees with our expression for a_m at the 'cut-off' (3.3.1b). Now at $O(\bar{\eta}_0 - \check{\eta})^{\delta}$ we have

$$3\alpha^2\bar{\beta} + 3\alpha\beta^2 + \bar{\eta}_0\bar{\beta} = -\gamma,$$

i.e $3\alpha\beta^2 = -\gamma$ which implies $\gamma > 0$ (since $\alpha < 0$). If the forms for $h_{1,3}$ and $r_{1,3}$ are valid then

$$h_2 \sim -2\alpha + \hat{\beta}(\bar{\eta}_0 - \check{\eta})^N + \ldots,$$

since

$$h_1 + h_2 + h_3 = 0.$$

Substituting h_2 into (3.1.5a) yields

$$(2\alpha)^3 + \bar{\eta}_0(2\alpha) = a_0,$$

from as $O(1)$ balance, therefore if

$$\bar{\eta}_0 = -3\alpha^2,$$

then

$$a_0 = -2\left(-\frac{\bar{\eta}_0}{3}\right)^{3/2}$$

which again agrees with the earlier result, also

$$12\alpha^2\hat{\beta} + \bar{\eta}_0\hat{\beta} = -\gamma,$$

from an $O(\bar{\eta}_0 - \check{\eta})^\delta$ (if $N = \delta$) balance, which holds if

$$\hat{\beta} = -\frac{\gamma}{9\alpha^2} \qquad \text{and} \qquad \bar{\eta}_0 = -3\alpha^2,$$

Now equation (3.1.5b) implies

$$\frac{r_n'}{r_n} = -\frac{(3h_n h_n' + 1)}{(3h_n^2 + \check{\eta})}, \tag{3.3.4}$$

therefore substituting

$$h_2 \sim -2\alpha + \hat{\beta}(\bar{\eta}_0 - \check{\eta})^\delta, \qquad h_2' = -\delta\hat{\beta}(\bar{\eta}_0 - \check{\eta})^{\delta-1},$$

into (3.3.4) and using $\bar{\eta}_0 = -3\alpha^2$ we obtain

$$\frac{r_2'}{r_2} \sim -\frac{2}{3}\frac{\hat{\beta}\delta(\bar{\eta}_0 - \check{\eta})^{\delta-1}}{\alpha},$$

after some working, i.e

$$r_2 \sim O(1) + (\bar{\eta}_0 - \check{\eta})^\delta + \ldots.$$

Having established through the working above that the expressions for a_m, (h_1, h_2, h_3), (r_1, r_2, r_3) are consistent, we examine equation (3.1.5c) near the 'cut-off' value $\bar{\eta}_0$. We first take the r_1 (or r_3) asymptote which becomes singular at $\check{\eta} = \bar{\eta}_0$, i.e

$$(\bar{\eta}_0 - \check{\eta})^{-\delta/2-1} \sim -\bar{\eta}_0 a'_m,$$

from (3.1.5c), so

$$a_m \sim (\bar{\eta}_0 - \check{\eta})^{-\delta/2}$$

which contradicts (3.3.2a). So we are left with a (a_m, h_2, r_2) combination, i.e one nonlinear mode for $\check{\eta} < \bar{\eta}_0$ and one nonlinear mode for $\check{\eta} > \bar{\eta}_0$ (below we drop the subscript '2' for convenience).

§3.4 PHASE-PLANE ANALYSIS

Initially an attempt was made to solve the reduced system above numerically, using iterative techniques and a Runge-Kutta shooting method, but no conclusive results were obtained. The Runge-Kutta algorithm did however suggest that singularities may be present at certain critical points. To gain some analytical insight into the structure of these critical points we therefore study now a modified system, namely

$$h^3 + \check{\eta} h = -a_m, \tag{3.4.1a}$$

$$(3h^2 + \check{\eta})r' + (3hh' + 1)r = 0, \tag{3.4.1b}$$

$$(r^2)_{\check{\eta}} = -\frac{3}{2}(a_m + \check{\eta} a'_m). \tag{3.4.1c}$$

The change that we have made to the original reduced system is to multiply the term $-\check{\eta} a'_m$ with the coefficient $3/2$, which enables us to integrate (3.4.1c). Making the transformation

$$\frac{d}{d\check{\eta}} = \frac{d}{dh}\frac{dh}{d\check{\eta}},$$

yields

$$h^3 + \check{\eta} h = -a_m, \tag{3.4.2a}$$

$$(3h^2+\check{\eta})\frac{dr}{dh}+(3h+\frac{d\check{\eta}}{dh})r=0, \qquad (3.4.2b)$$

$$2r\frac{dr}{dh}=-\frac{3}{2}\left(a_m\frac{d\check{\eta}}{dh}+\check{\eta}\frac{da_m}{dh}\right), \qquad (3.4.2c)$$

where r, a_m, $\check{\eta}$ are now functions of h. Integrating (3.4.2c) we obtain

$$r^2=-\frac{3}{2}a_m\check{\eta}+r_c, \qquad (3.4.2d)$$

for some constant r_c say ($r=r_c^{1/2}$ at $\check{\eta}=0$). After some manipulation of equations (3.4.2a,b,d) the following form is obtained,

$$\frac{dh}{dt}=2r_c+\frac{3}{2}h\left[\left(2\check{\eta}+\frac{9}{4}h^2\right)^2-\frac{33}{16}h^4\right], \qquad (3.4.3a)$$

$$\frac{d\check{\eta}}{dt}=-6hr_c-\frac{3}{2}\check{\eta}\left[(\check{\eta}+6h^2)^2-21h^4\right]. \qquad (3.4.3b)$$

We can now carry out a phase-plane analysis, based on finding where (3.4.3a,b) are simultaneously identically zero to determine the critical points. So putting $\check{\eta}=h^2v$ into (3.4.3a,b) yields

$$\frac{dh}{dt}=2r_c+\frac{3}{2}h^5\left[\left(2v+\frac{9}{4}\right)^2-\frac{33}{16}\right]=0, \qquad (3.4.4a)$$

$$\frac{d\check{\eta}}{dt}=-6hr_c-\frac{3}{2}h^6v[(v+6)^2-21]=0, \qquad (3.4.4b)$$

and hence we need to solve the cubic equation

$$3\left[\left(2v+\frac{9}{4}\right)^2-\frac{33}{16}\right]=v\left[(v+6)^2-21\right]$$

for v. The solutions are

$$v_1=-3, \qquad v_2=\frac{3+(21)^{1/2}}{2}, \qquad v_3=\frac{3-(21)^{1/2}}{2}.$$

Therefore choosing $r_c=0.5$ (without loss of generality) we can locate the three critical points, which are found to be

$$v_1=-3, \qquad h_1=-0.560977572, \qquad \check{\eta}_1=-0.944087511,$$

$$v_2 = \frac{3+(21)^{1/2}}{2}, \qquad h_2 = -0.371182824, \qquad \check{\eta}_2 = 0.522351087,$$

$$v_3 = \frac{3-(21)^{1/2}}{2}, \qquad h_3 = 0.83760129, \qquad \check{\eta}_3 = -0.555148501,$$

using (3.4.4a).

To determine the nature of these critical points we perform a local analysis. So if in general we have a critical point at $(\check{\eta}_i, h_i)$ then we set

$$h = h_i + Y, \quad \check{\eta} = \check{\eta}_i + X,$$

with X, Y small. Substituting these into (3.4.4a, b) gives

$$\frac{dY}{dt} = \frac{3}{2}h_i[8\check{\eta}_i + 9h_i^2]X + \frac{3}{2}[27h_i^2\check{\eta}_i + 15h_i^4 + 4\check{\eta}_i^2]Y, \qquad (3.4.5a)$$

$$\frac{dX}{dt} = -\frac{3}{2}[3\check{\eta}_i^2 + 24\check{\eta}_i h_i^2 + 15h_i^4]X - \frac{3}{2}[2 + 24\check{\eta}_i^2 h_i + 60\check{\eta}_i h_i^3]Y, \qquad (3.4.5b)$$

after some working. Inserting the $\check{\eta}$, h values for the critical points into (3.4.5a, b), we find that all three points are saddle points, again after some standard phase-plane analysis. We now briefly examine (3.4.3a,b):

$$\text{when} \quad h = 0, \quad \frac{dh}{d\check{\eta}} \approx -\frac{2}{3\check{\eta}^3},$$

$$\text{so} \quad \frac{dh}{d\check{\eta}} \to \mp 0 \quad \text{as} \quad \check{\eta} \to \pm\infty;$$

$$\text{when} \quad \check{\eta} = 0, \quad \frac{dh}{d\check{\eta}} \approx -\frac{(1+\frac{9}{2}h^5)}{3h},$$

$$\text{so} \quad \frac{dh}{d\check{\eta}} \to -\infty \quad \text{as} \quad h \to \pm\infty,$$

but $\frac{dh}{d\check{\eta}}$ is positive when h is small and negative for $(1+\frac{9}{2}h^5) > 0$, i.e in the region $-\left(\frac{2}{9}\right)^{1/5} < h < 0$.

See figure 3.4.2a for a plot of the phase-plane. We see from the plot of the phase-plane that a possible solution or phase trajectory has $h < 0$ for all $\check{\eta}$, i.e.

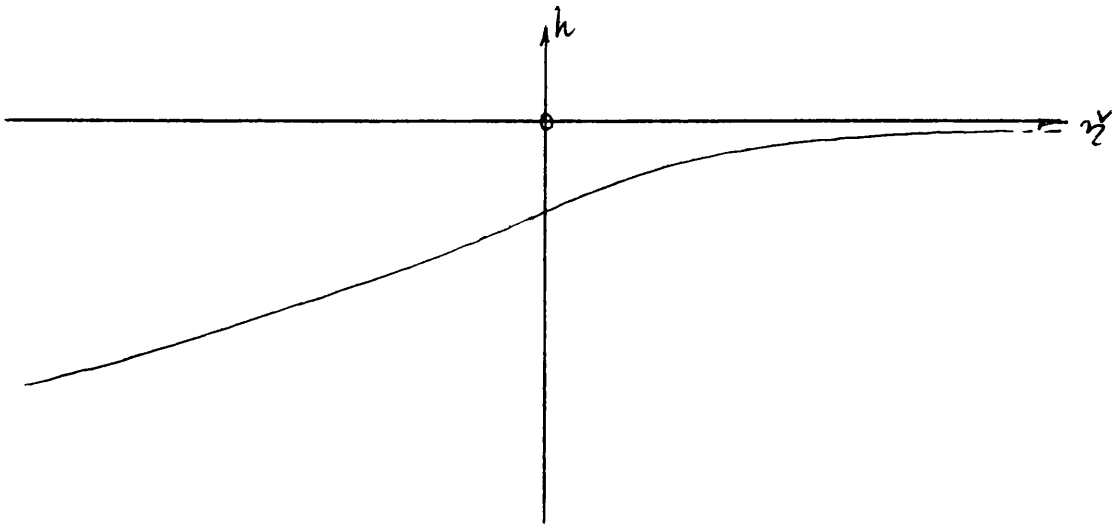

fig 3.4.1

and all the analytical features from the above phase-plane analysis are present. Having studied the modified system we turn our attention back to the actual equations, for which we might expect to obtain a solution similar to that above for h. However before moving on we see from the phase-plane plot that the h_2 solution which we obtained from the analytical analysis, is no longer a suitable possibility because of the location of the critical points, but an alternative solution, phase trajectory does exist, which is smooth throughout as sketched above.

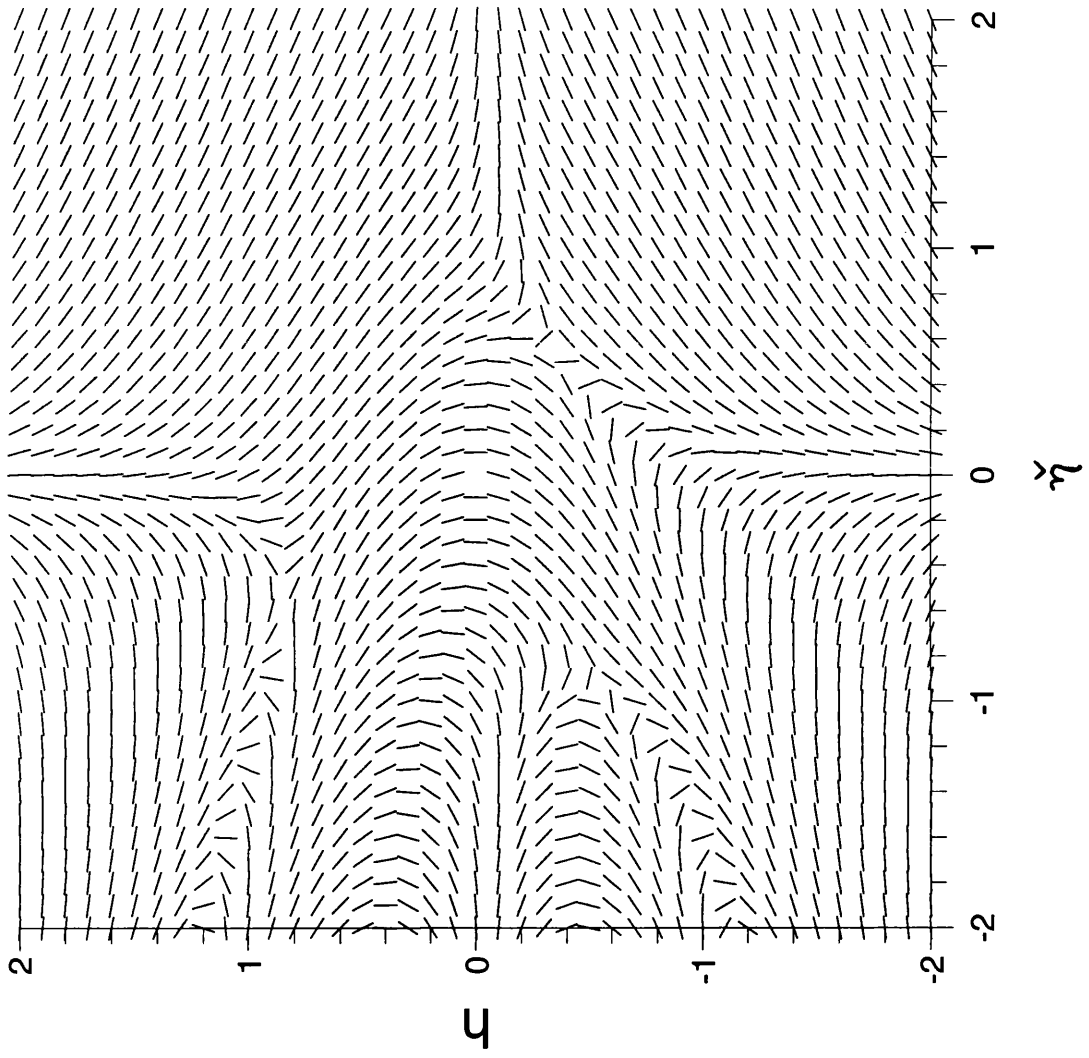

fig 3.4.2a

Phase plane plot for the system $(3.4.1a-c)$

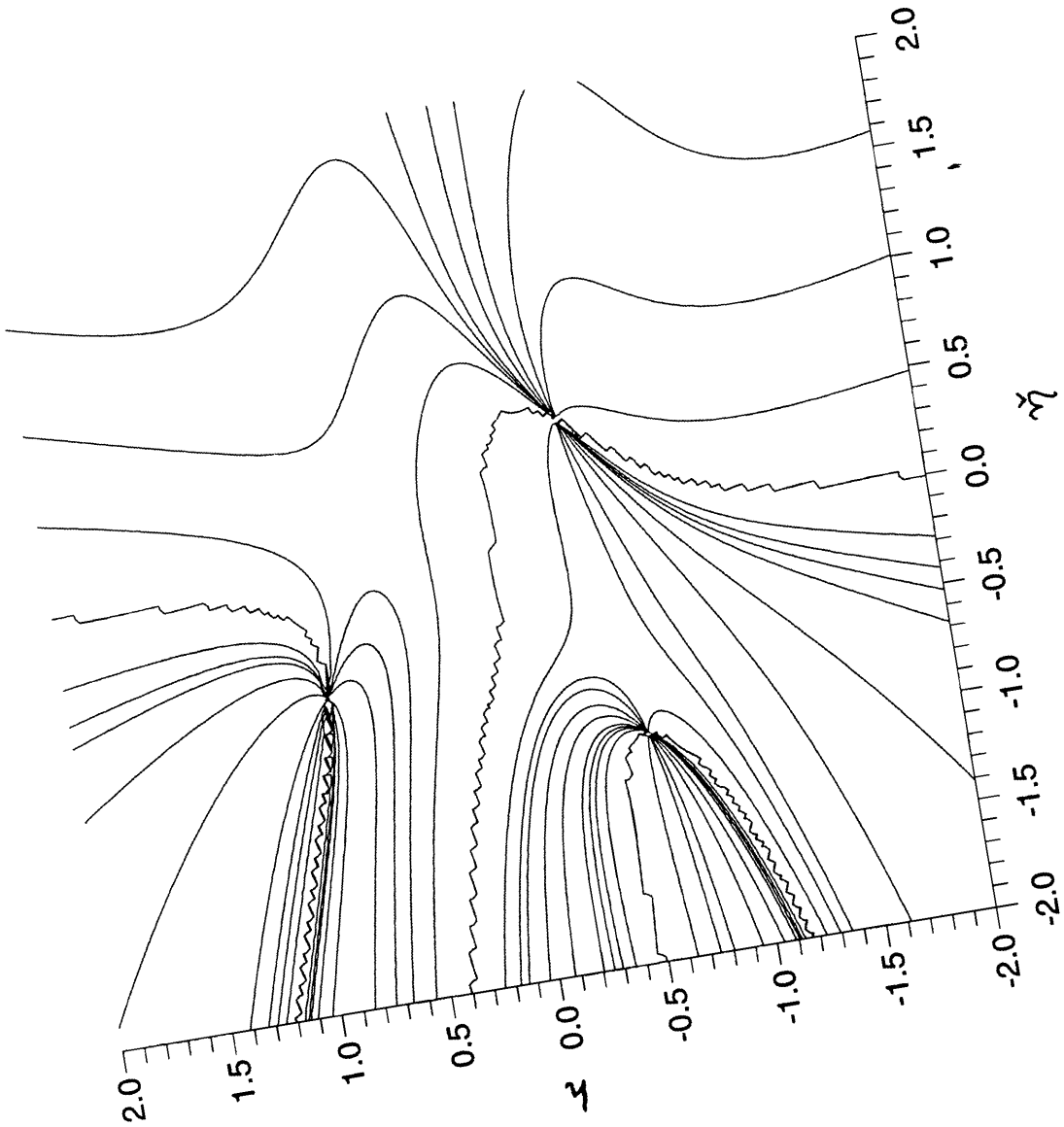

fig 3.4.2b

Contour plot for equations $(3.4.1a-c)$

§3.5 TAYLOR SERIES METHOD

Before moving on to solving the actual system numerically we examine the modified equations locally near the singular points using Taylor-series expansions for the variables h, r, a_m, as an alternative to the phase-plane analysis. Thus, near the singularity η_i, say we set $\check{\eta} = \eta_i + s$ $(s > 0)$ and substitute the following Taylor-series expansions in s into (3.4.1a, b), (3.4.2d),

$$h = h_i + \bar{h}_1 s + \ldots,$$

$$a = a_i + \bar{a}_1 s + \ldots,$$

$$r = r_i + \bar{r}_1 s + \ldots.$$

The leading-order equations obtained from (3.4.1a) are

$$h_i^3 + \eta_i h_i = -a_i,$$

$$(3h_i^2 + \eta_i)\bar{h}_1 + h_i = -\bar{a}_1,$$

while equation (3.4.1b) gives

$$(3h_i^2 + \eta_i)\bar{r}_1 + (3h_i\bar{h}_1 + 1)r_i = 0,$$

and equation (3.4.2d) gives

$$r_i^2 = -\frac{3}{2}a_i\eta_i + r_c,$$

$$2r_i\bar{r}_1 = -\frac{3}{2}(\bar{a}_1\eta_i + a_i).$$

After manipulation of these five leading-order equations we obtain an expression for $\bar{h}_1$,

$$\bar{h}_1 = -\frac{2r_c + \frac{3}{2}h_i\left[(2\eta_i + \frac{9}{4}h_i^2)^2 - \frac{33}{16}h_i^4\right]}{6h_i r_c + \frac{3}{2}\eta_i\left[(\eta_i + 6h_i^2)^2 - 21h_i^4\right]},$$

which matches with the expression from $(3.4.3a,b)$ for $dh/d\check{\eta}$. So, near the critical points, the above Taylor series method yields the same structure as the phase-plane analysis. This analysis provides a check on the previous working for the modified system.

§3.6 NUMERICAL RESULTS

Below we show numerical results derived for the actual system (A/S),

$$h^3 + \check{\eta}h = -a_m, \tag{3.6.1a}$$

$$(3h^2 + \check{\eta})r' + (3hh' + 1)r = 0, \tag{3.6.1b}$$

$$(r^2)_{\check{\eta}} = -\frac{3}{2}a_m - \check{\eta}a'_m, \tag{3.6.1c}$$

and for the modified system (M/S) for comparison. A classical fourth-order Runge-Kutta shooting method is used, where we shoot forwards and backwards from $\check{\eta} = 0$, for different h, r and a_m values. In particular we choose a value for r at $\check{\eta} = 0$ and then try different values for h at $\check{\eta} = 0$ until we obtain a valid solution; we note that choosing h fixes a_m at $\check{\eta} = 0$ from $(3.6.1a)$.

Different step lengths (e.g steps of size 0.001, 0.00125, 0.004 were tried, however we find that apart from obtaining a slightly more accurate solution when using refined grids the solution form remains the same) and ranges for $\check{\eta}$ are used, although since all the critical points are located near the origin, the range $\check{\eta}_{-\infty} = -20$ to $\check{\eta}_{+\infty} = 20$ is sufficient. We conclude from the results below that solutions exist which stretch from $-\infty$ to ∞ in $\check{\eta}$, which was part of our aim and that the solution at this amplitude level confirms that the positions of maximum amplitude move towards the centre of the spot, and hence the spread angle is reduced. We note that the Runge-Kutta shoots back-up the phase-plane plot, and that the critical points present are clearly evident. However numerically it is difficult to obtain the unique solution which exists, for each set of initial values $r(0)$, $h(0)$, $a_m(0)$.

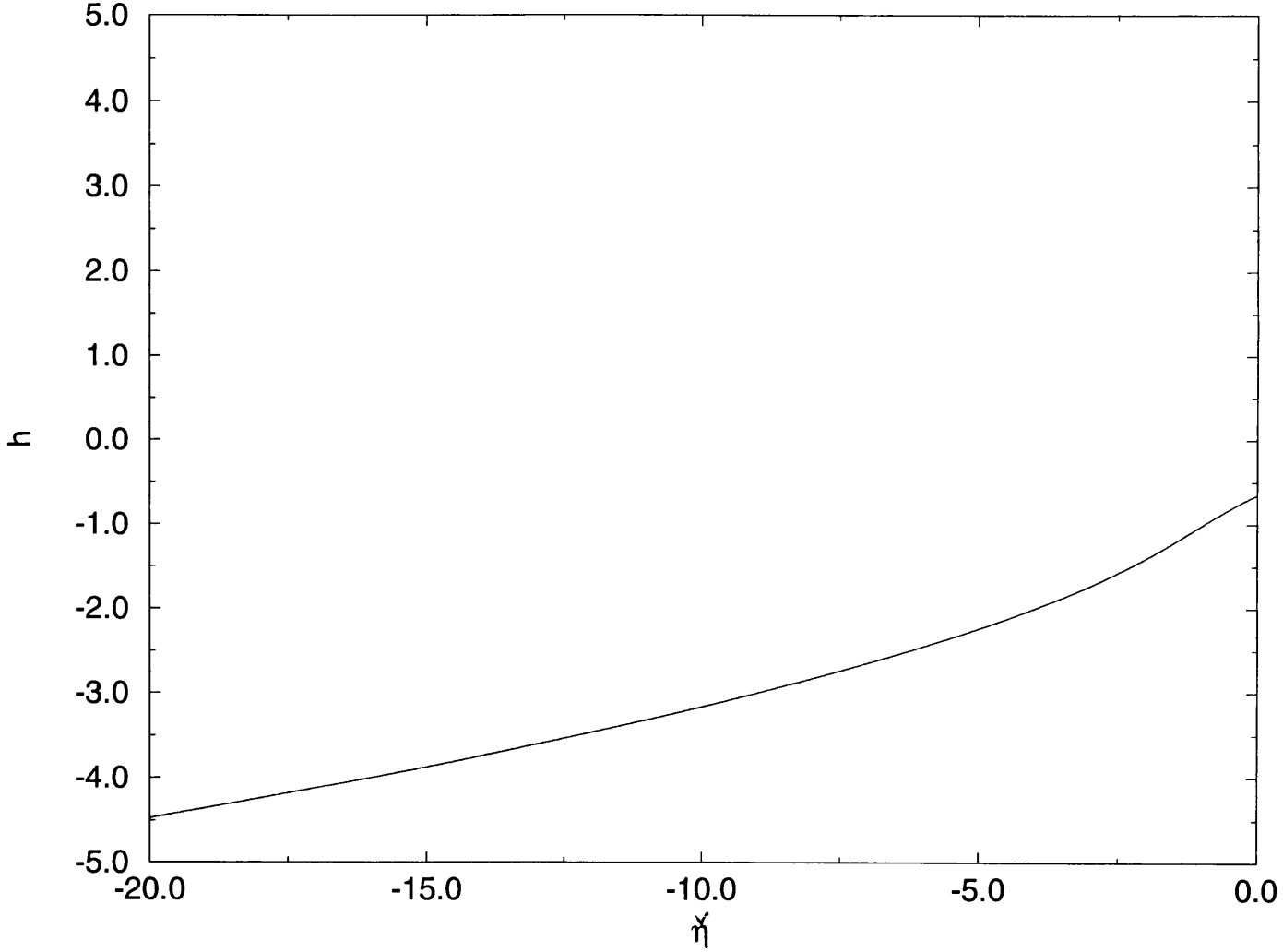

fig 3.6.1a

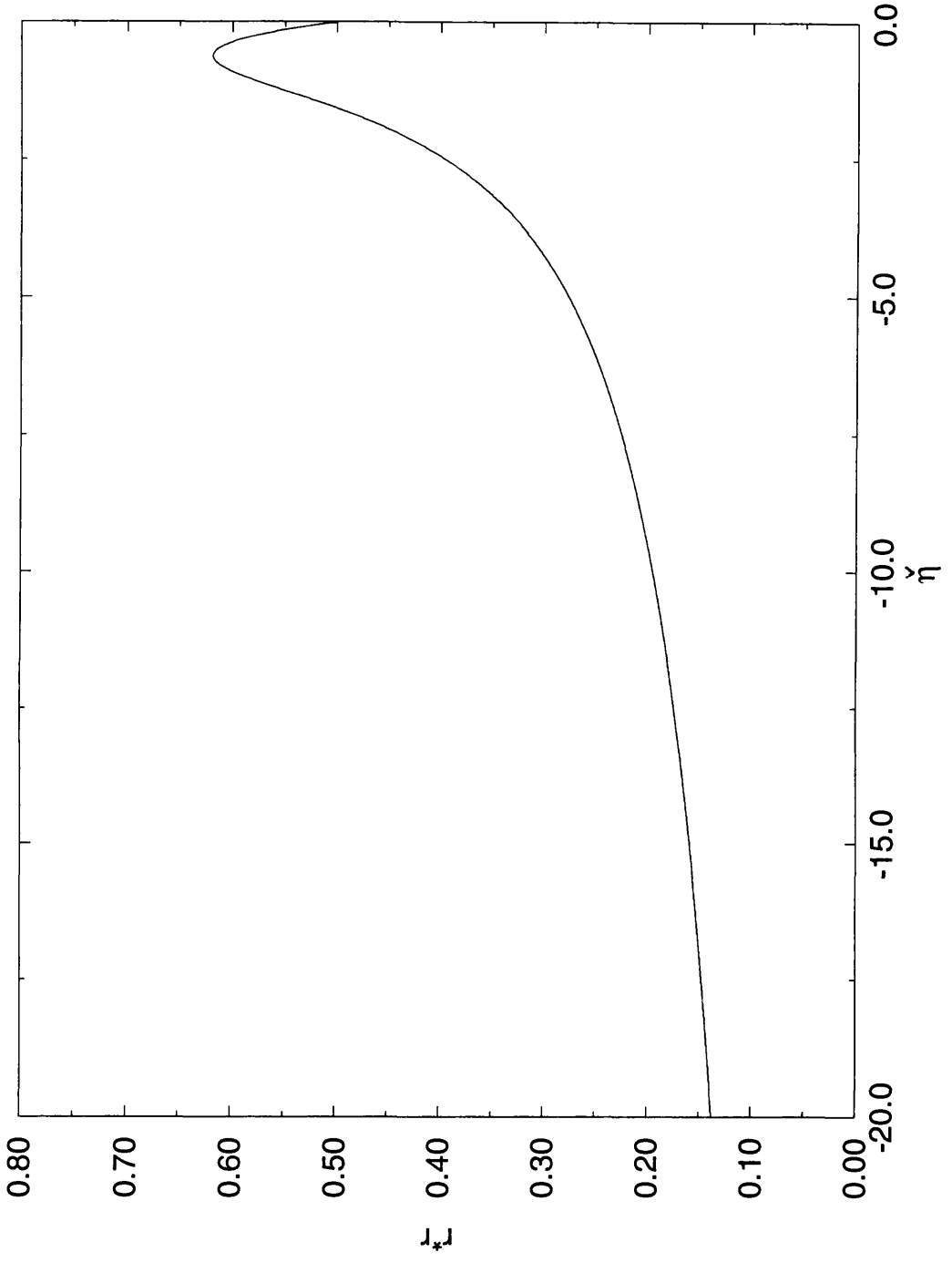

fig 3.6.1b

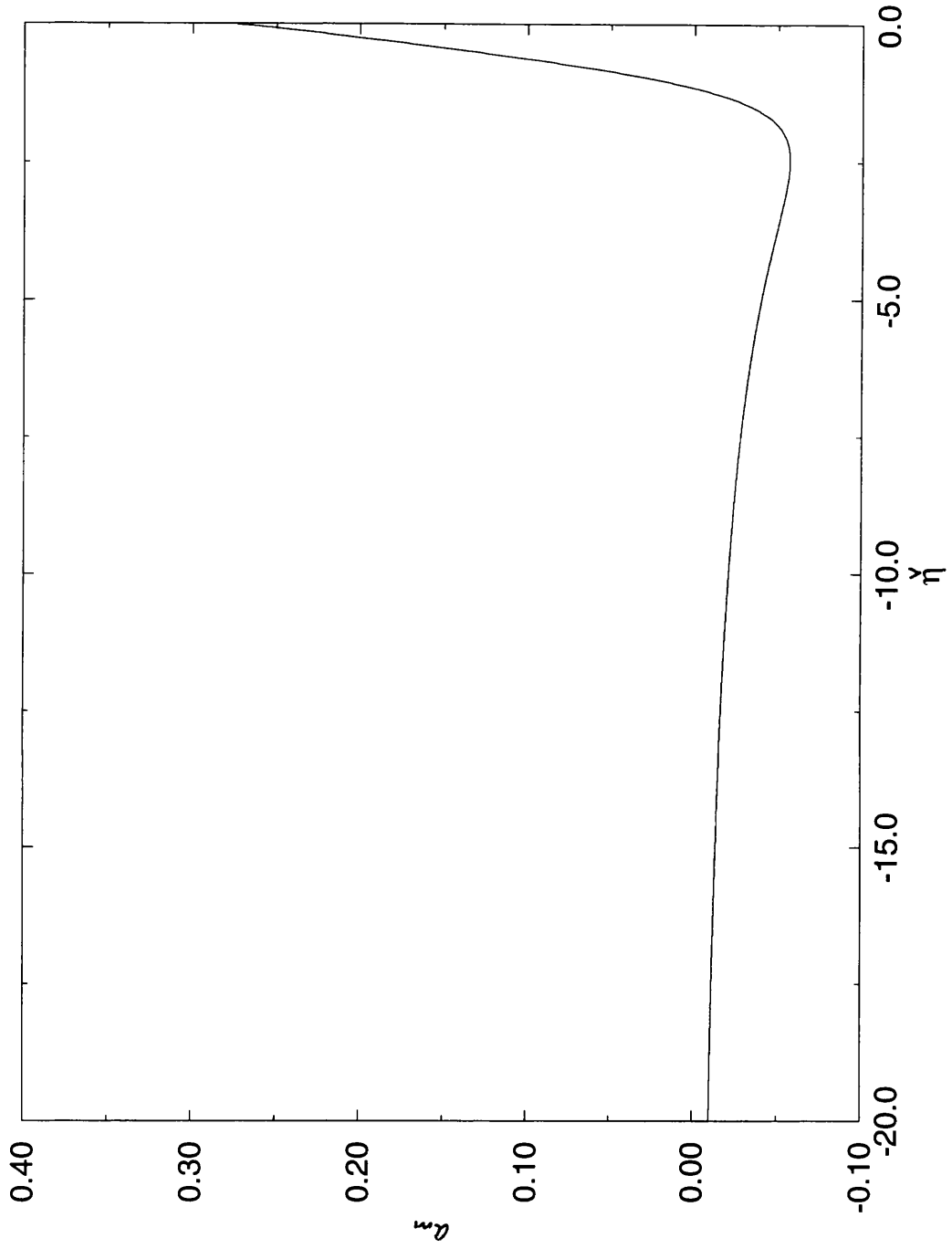

fig 3.6.1c

In figures $(3.6.1a-c)$ numerical solutions for the actual system are shown. Shooting backwards from $h(0) = -0.649, \quad r(0) = 0.707106, \quad a_m(0) = 0.273359.$

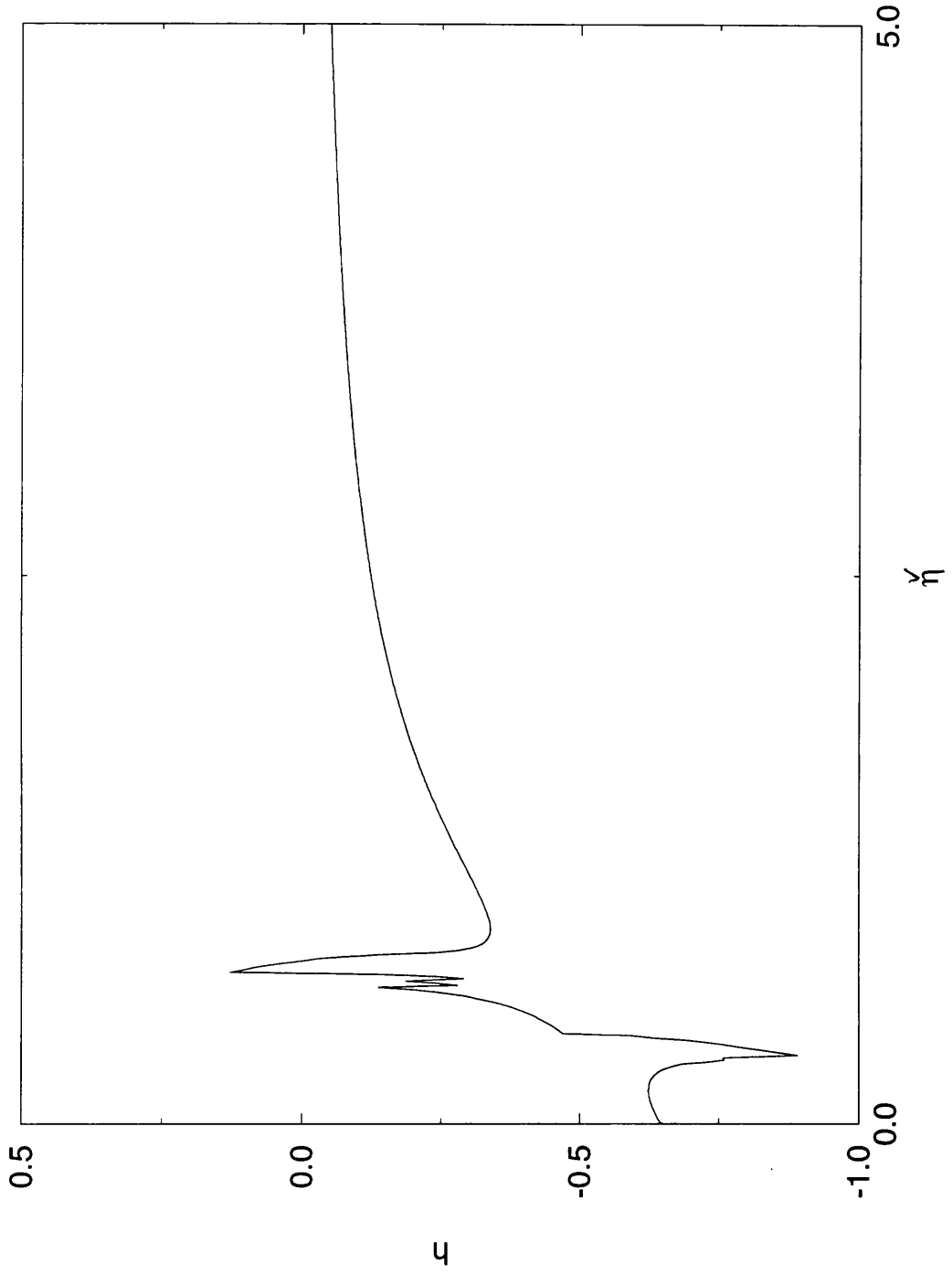

fig 3.6.2a

fig 3.6.2b

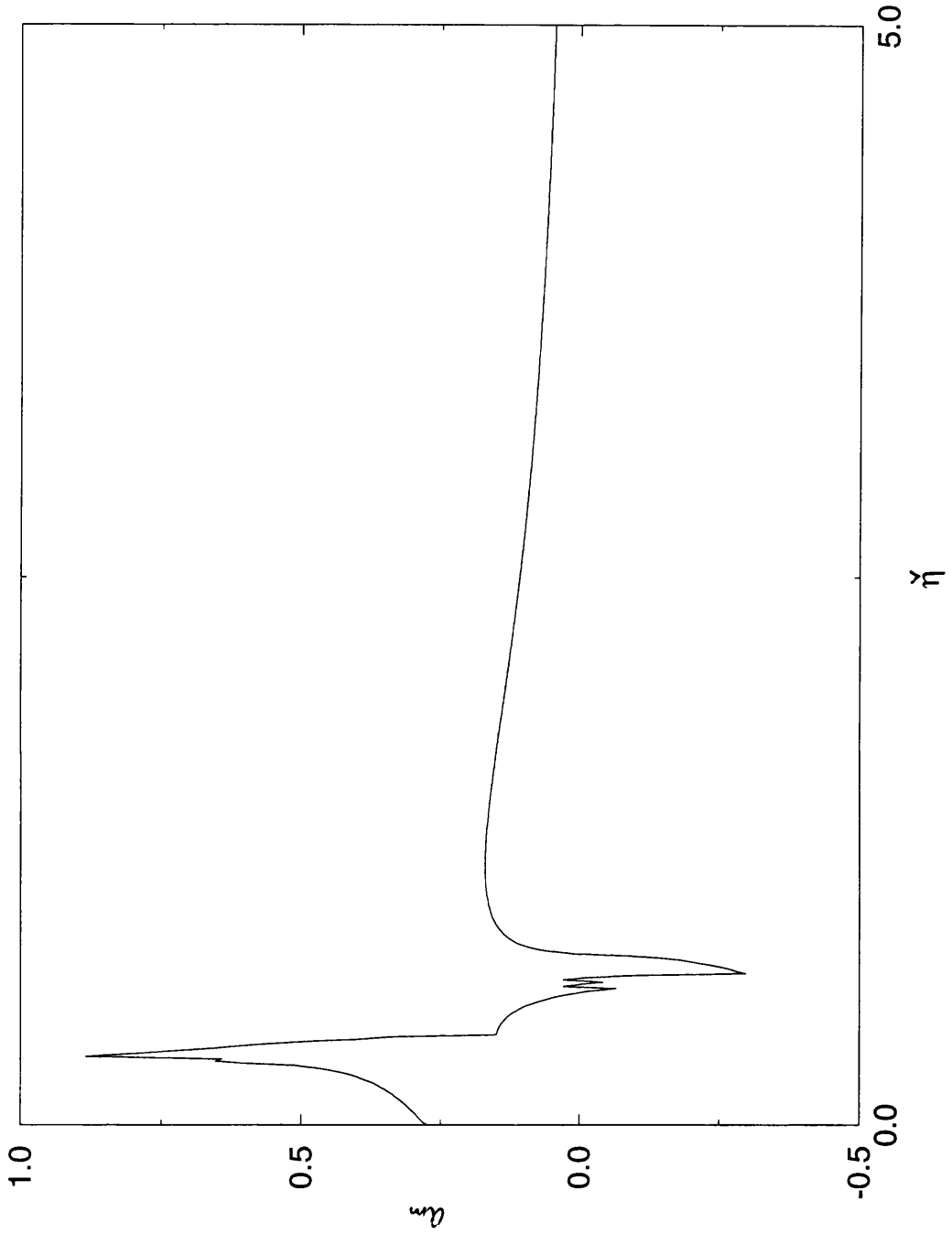

fig 3.6.2c

In figures $(3.6.2a-c)$ numerical solutions for the actual system are shown. Shooting forwards from $h(0) = -0.649, \quad r(0) = 0.707106, \quad a_m(0) = 0.273359.$

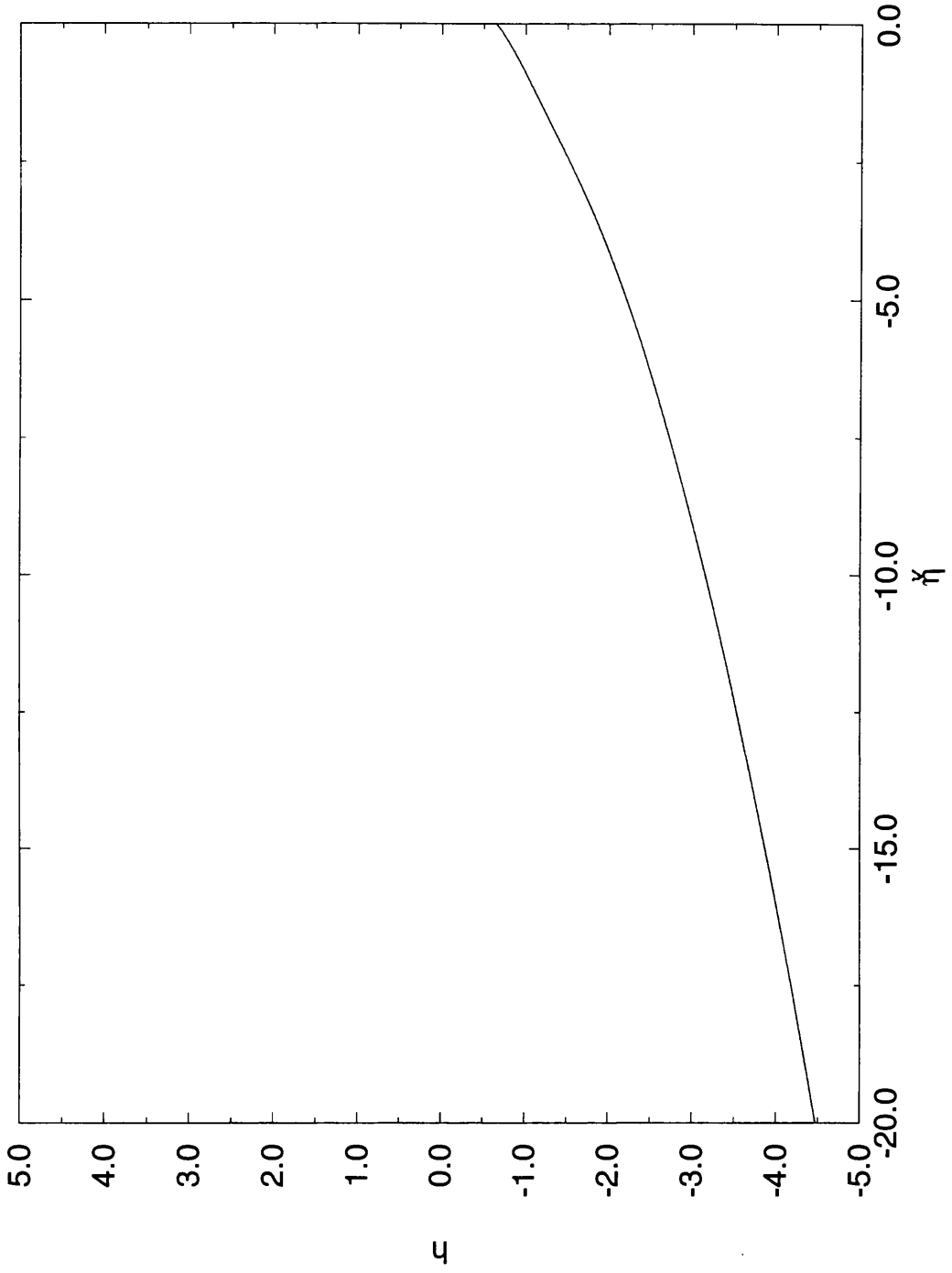

fig 3.6.3a

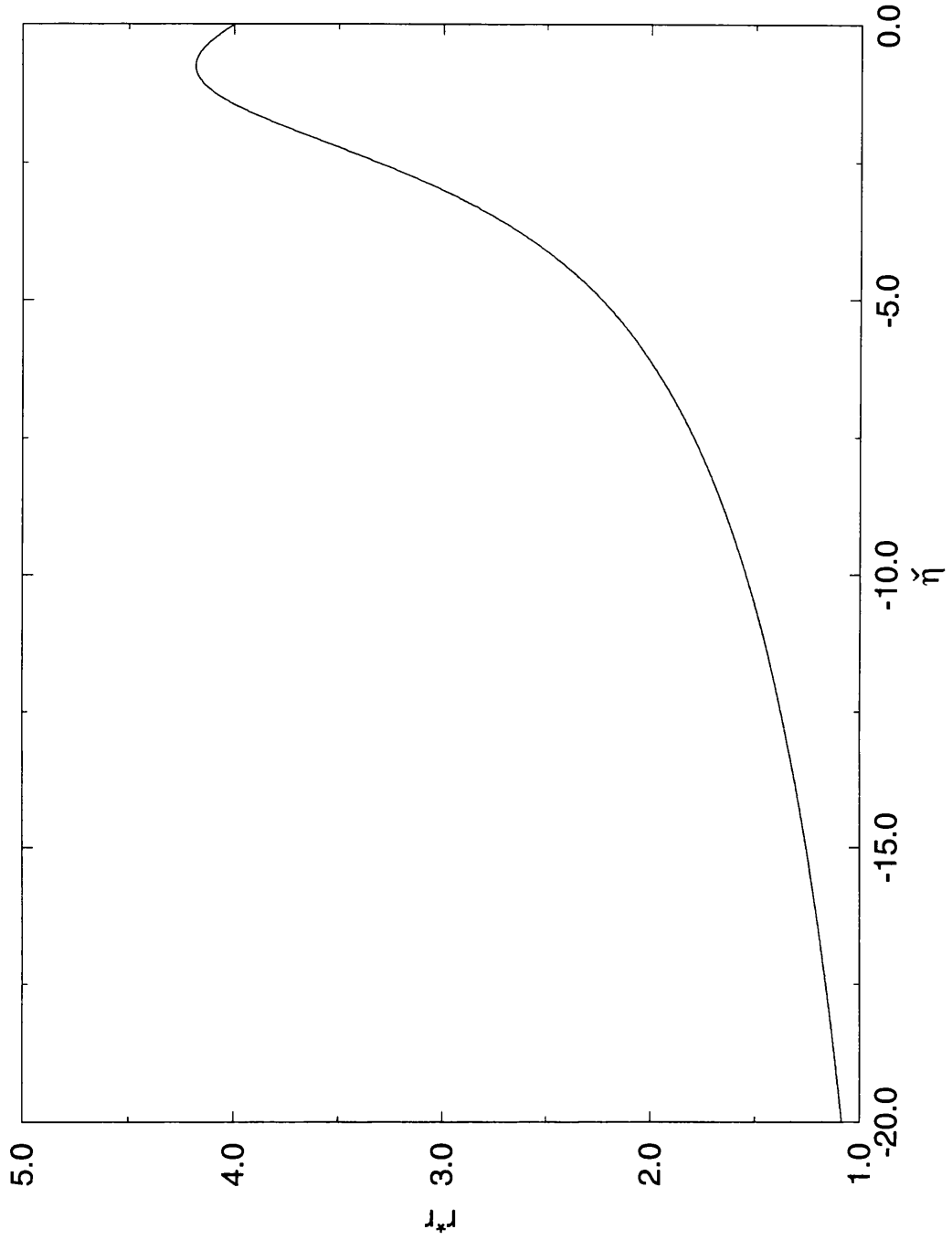

fig 3.6.3b

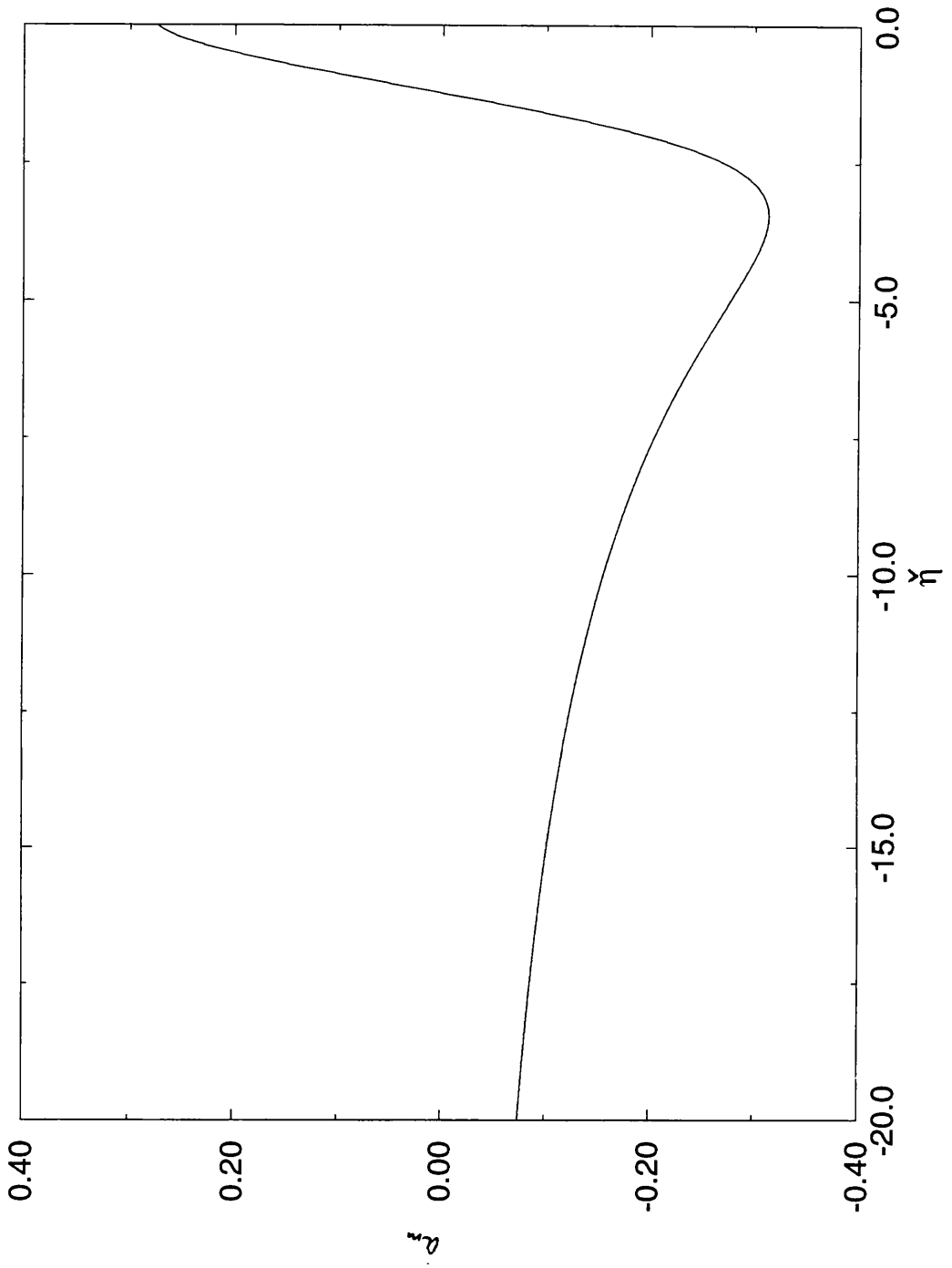

fig 3.6.3c

In figures $(3.6.3a-c)$ we shoot backwards (for the A/S) with

$$h(0) = -0.649, \quad r(0) = 2.0, \quad a_m(0) = 0.273359.$$

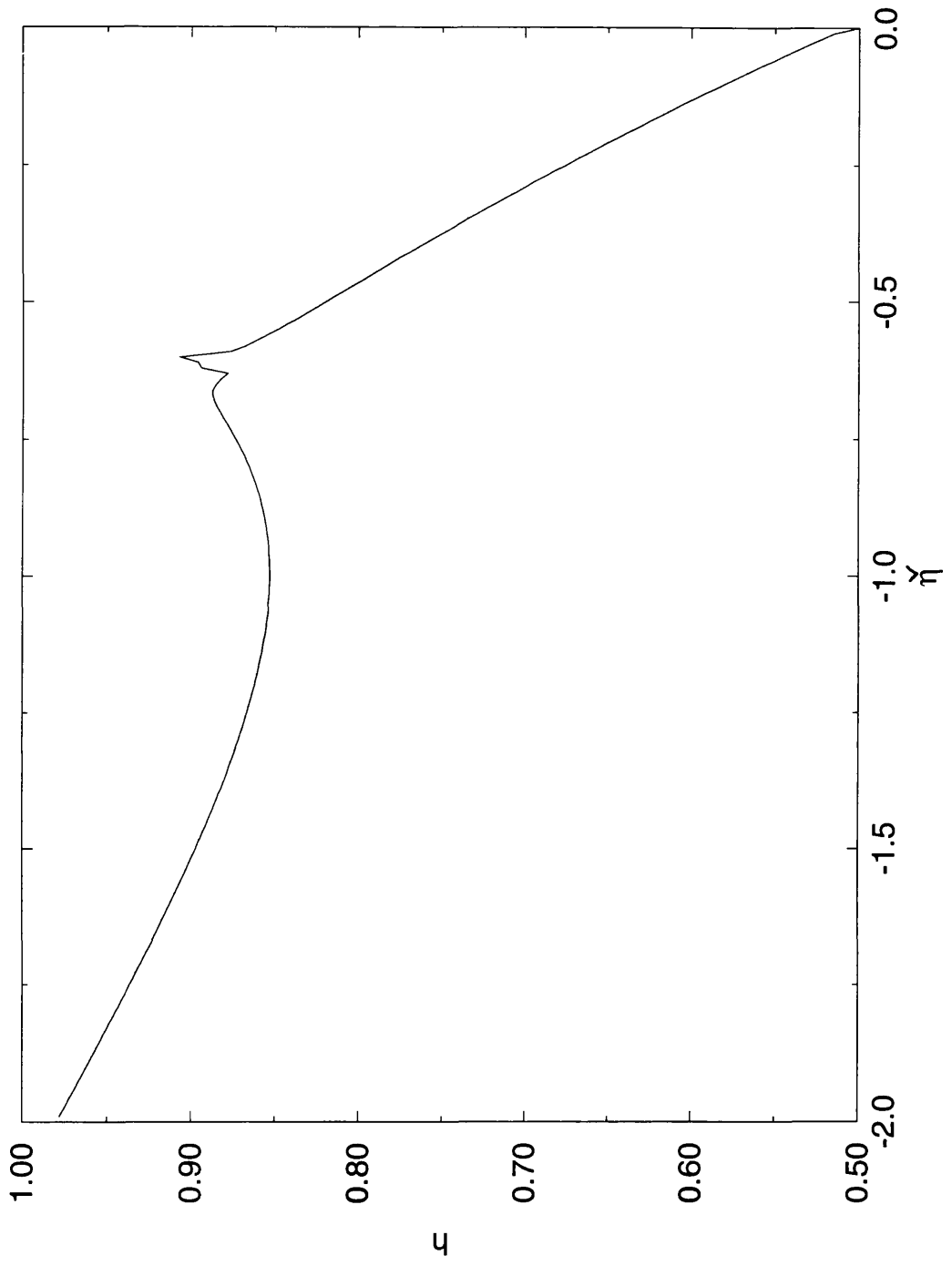

fig 3.6.4

For completeness we shoot backwards (for the A/S) with

$h(0) = 0.5, \quad r(0) = 0.707106, \quad a_m(0) = -0.125,$

and note the presence of the critical point

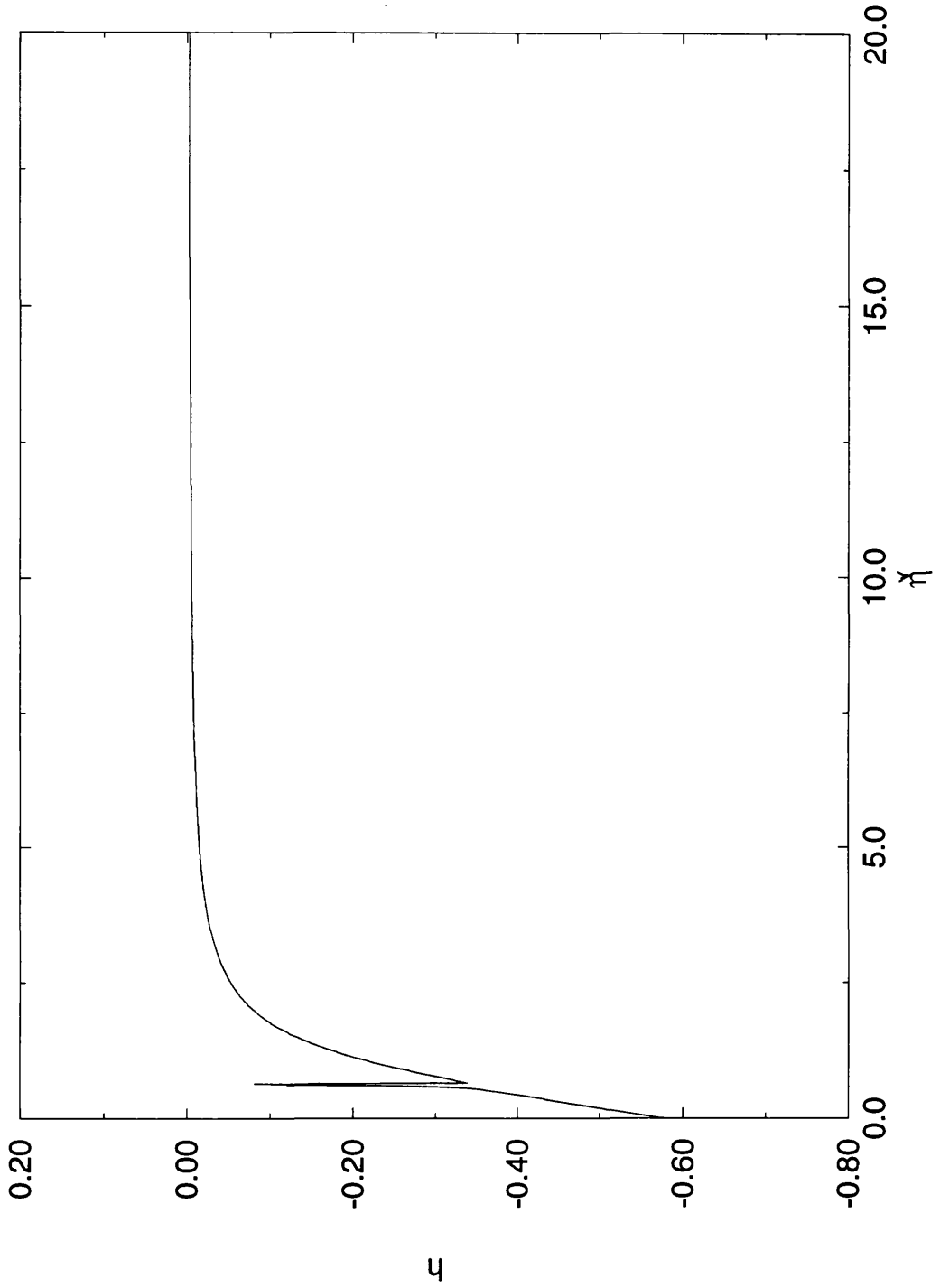

fig 3.6.5a

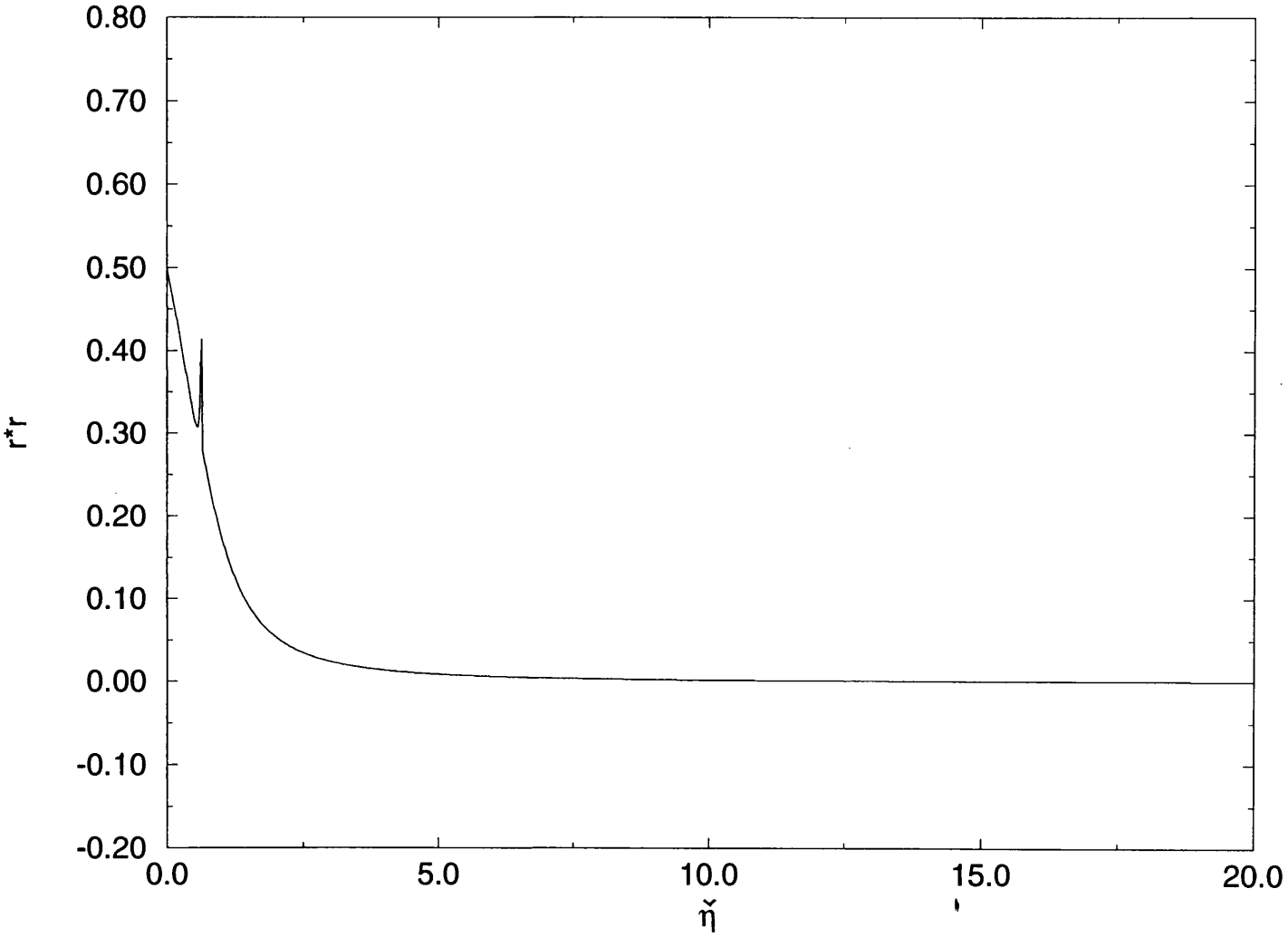

fig 3.6.5b

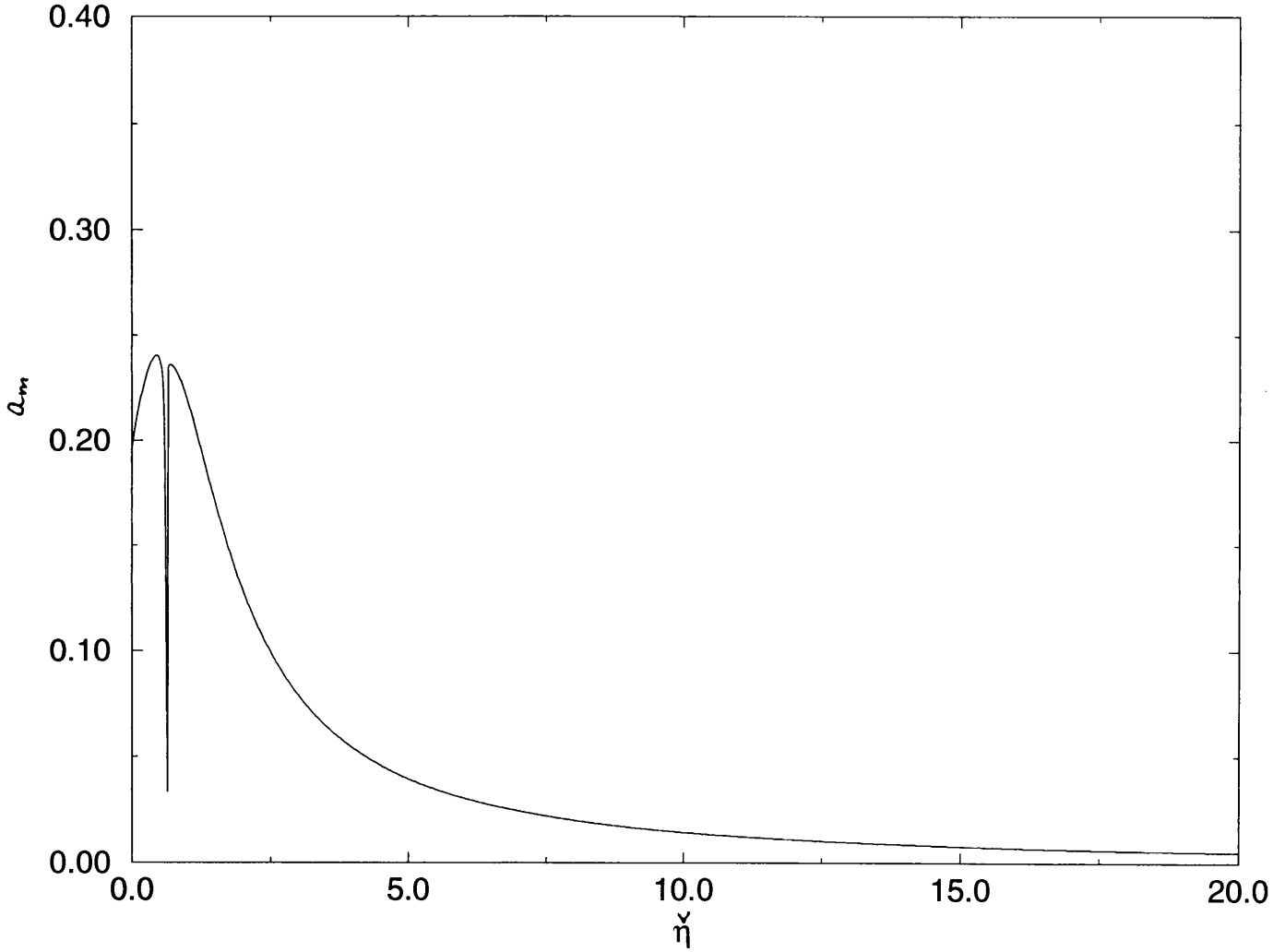

fig 3.6.5c

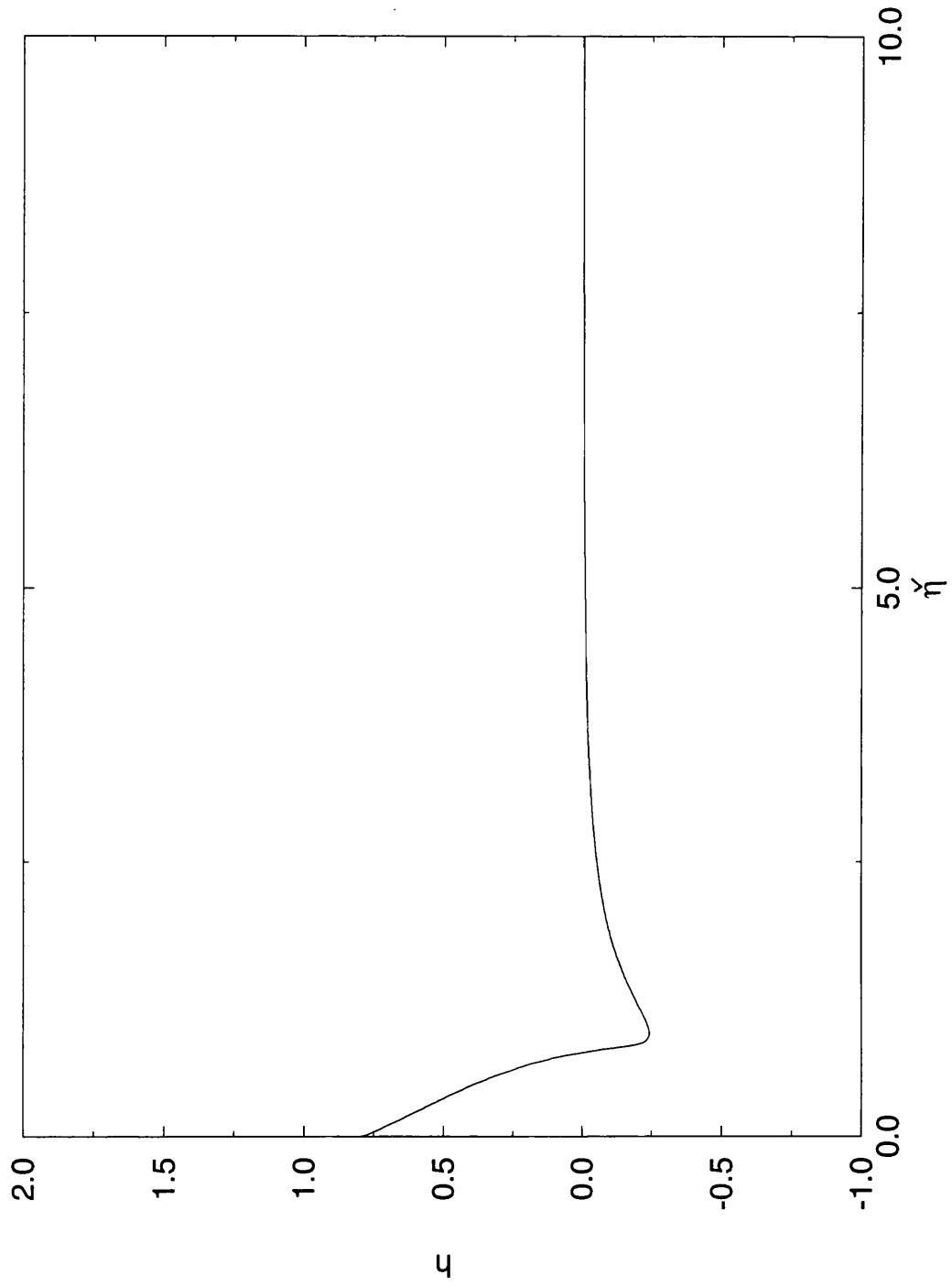

fig 3.6.6a

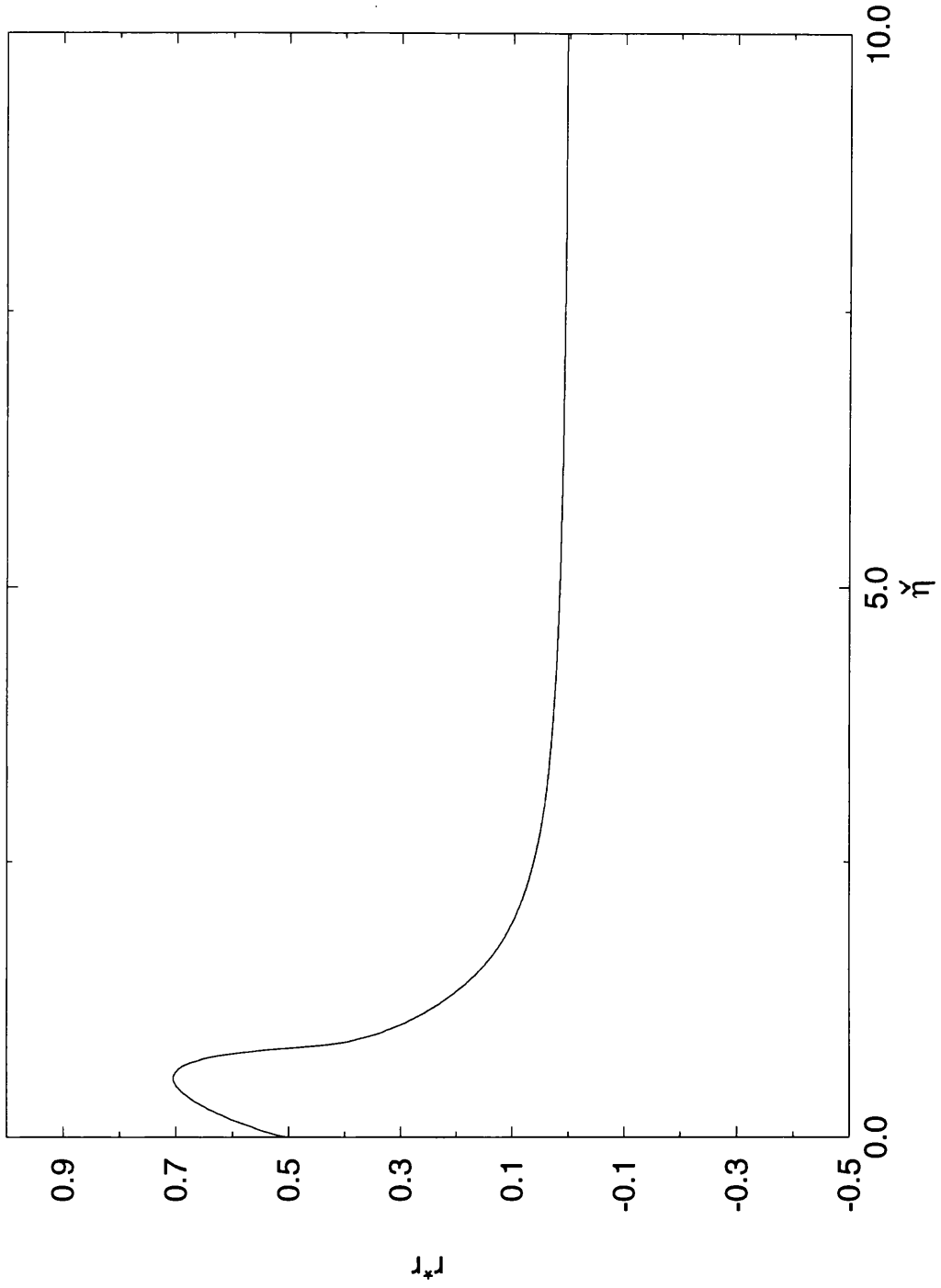

fig 3.6.6b

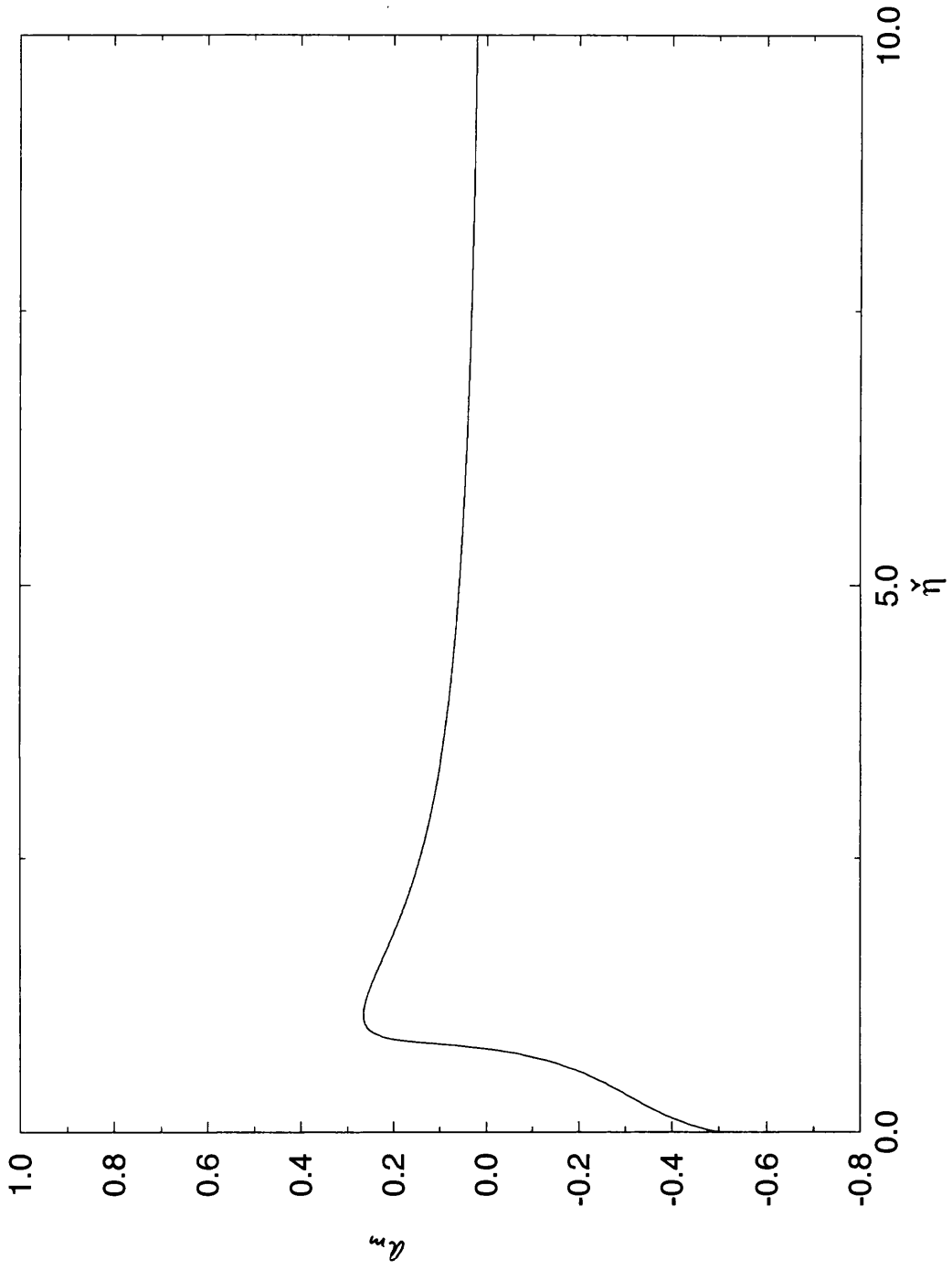

fig 3.6.6c

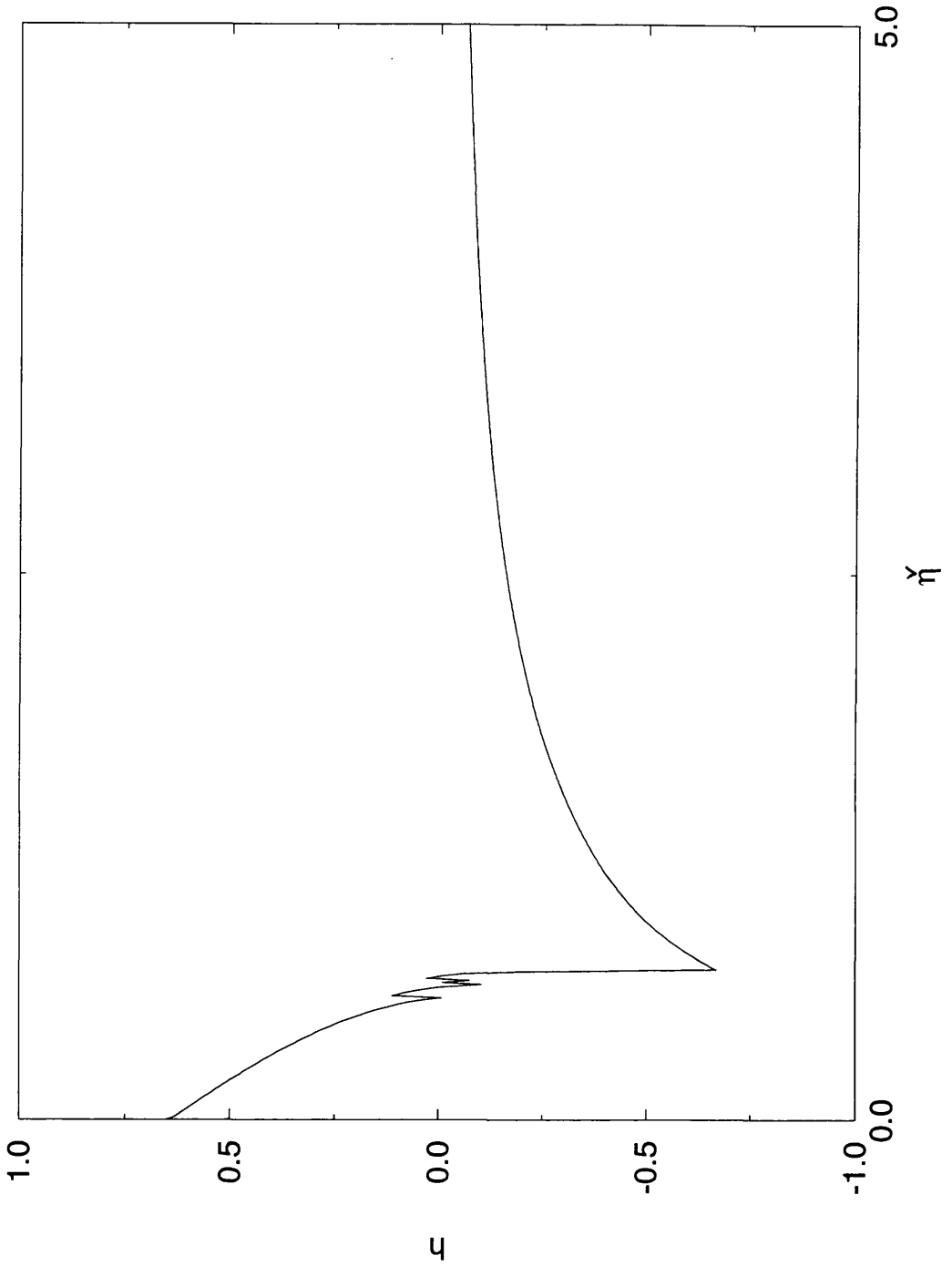

fig 3.6.7

We shoot forwards in figures $(3.6.5a-c)$, $(3.6.6a-c)$, (3.6.7) (for the A/S) so as to emphasize the existence and location of the critical point.

fig $(3.6.5a-c)$, $h(0)=-0.58$, $r(0)=0.707106$, $a_m(0)=0.195112$.

fig $(3.6.6a-c)$, $h(0)=0.8$, $r(0)=0.707106$, $a_m(0)=-0.512$.

fig (3.6.7), $h(0)=0.65$, $r(0)=0.707106$, $a_m(0)=-0.274625$.

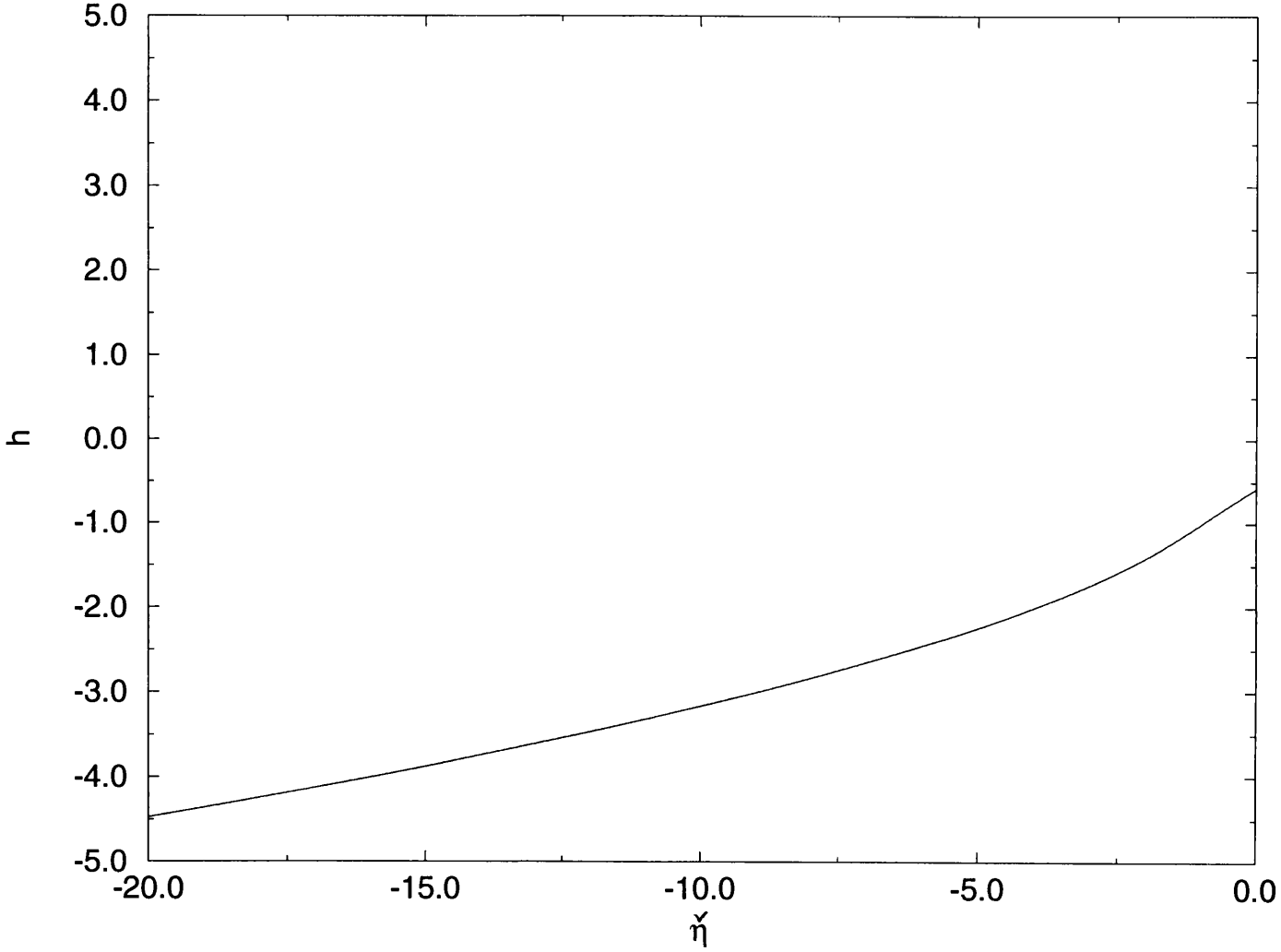

fig 3.6.8a

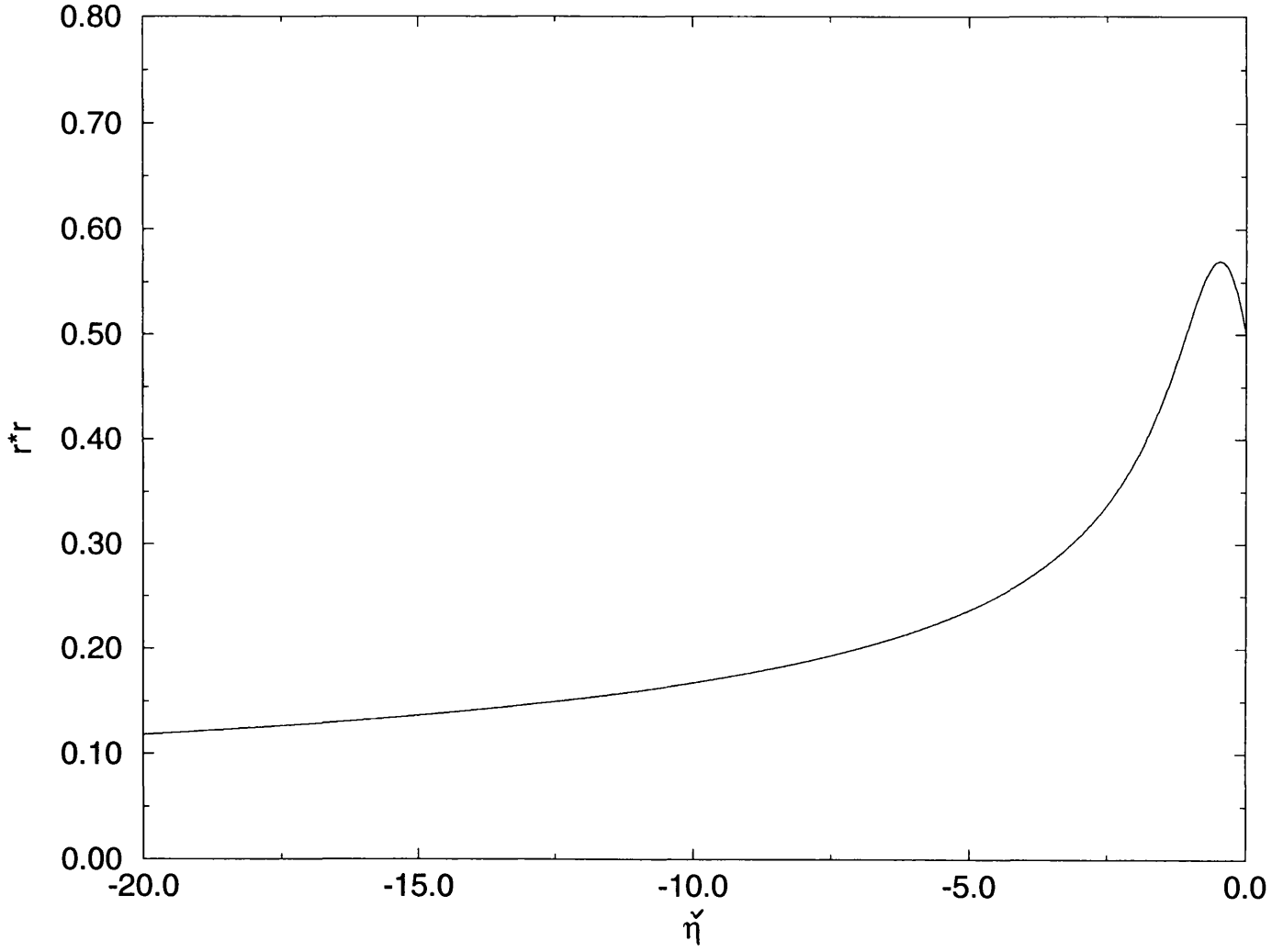

fig 3.6.8b

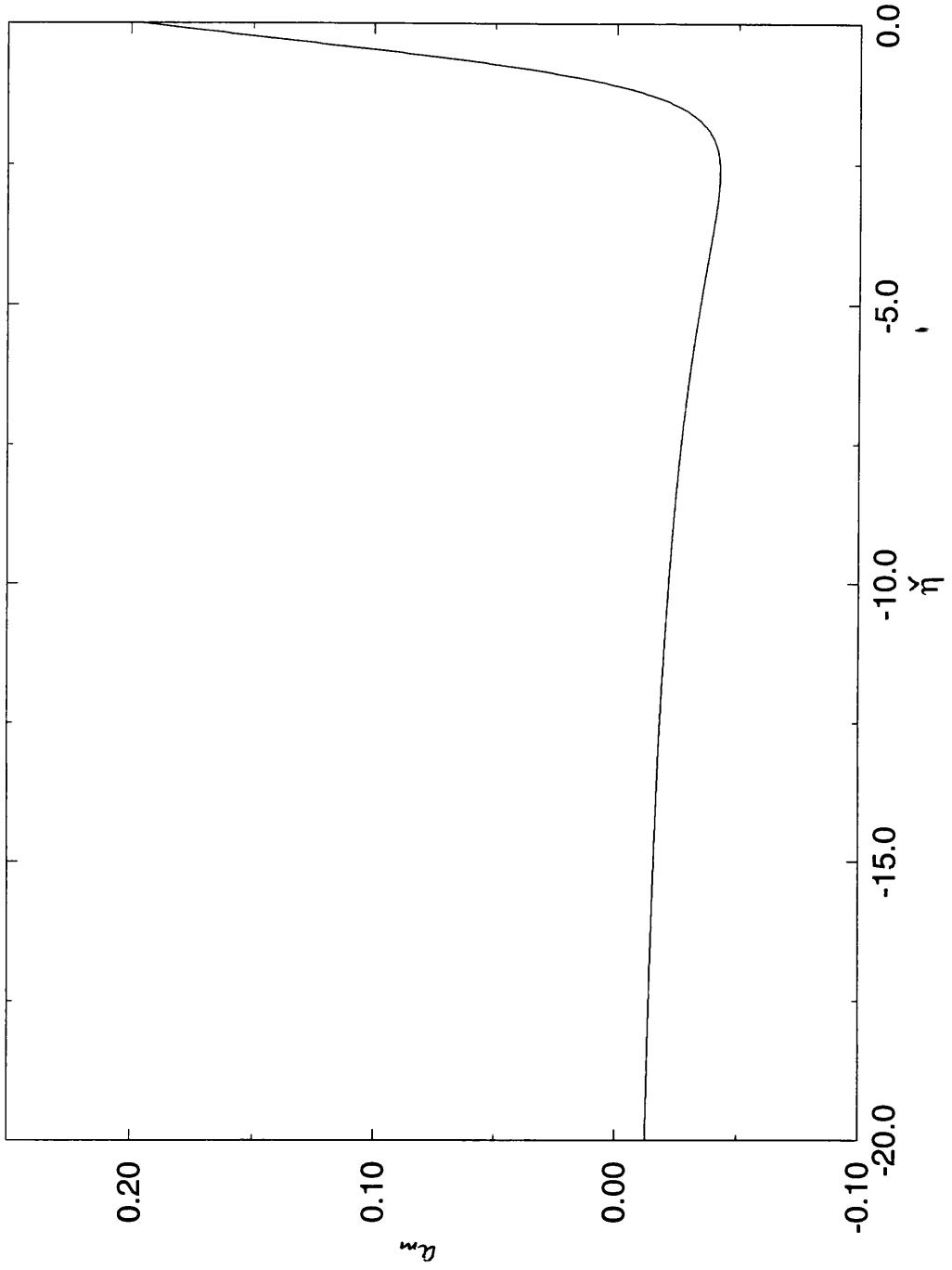

fig 3.6.8c

Numerical solutions for the modified system. Shooting backwards with, $h(0) = -0.58$, $r(0) = 0.707106$, $a_m(0) = 0.195112$.

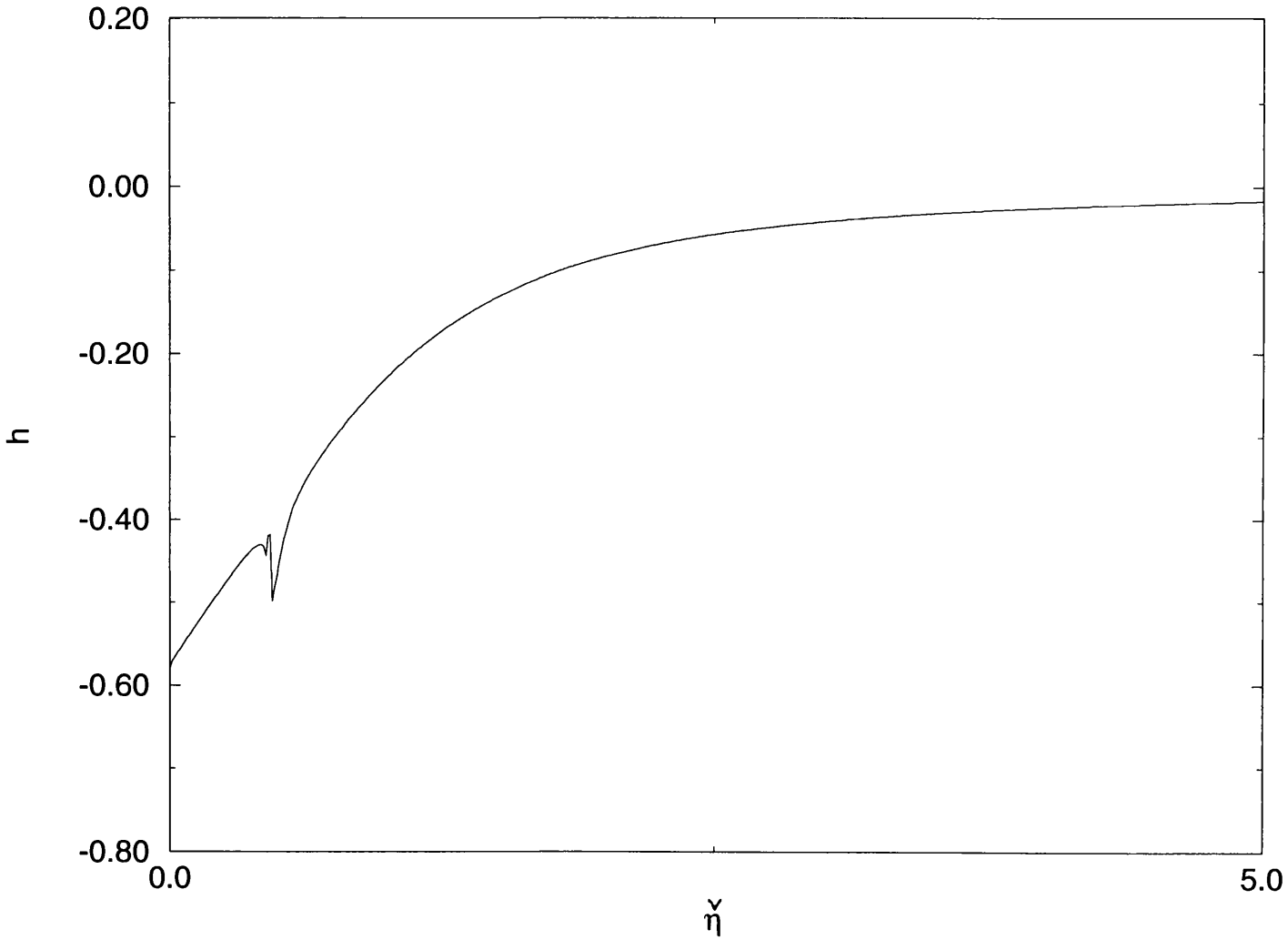

fig 3.6.9a

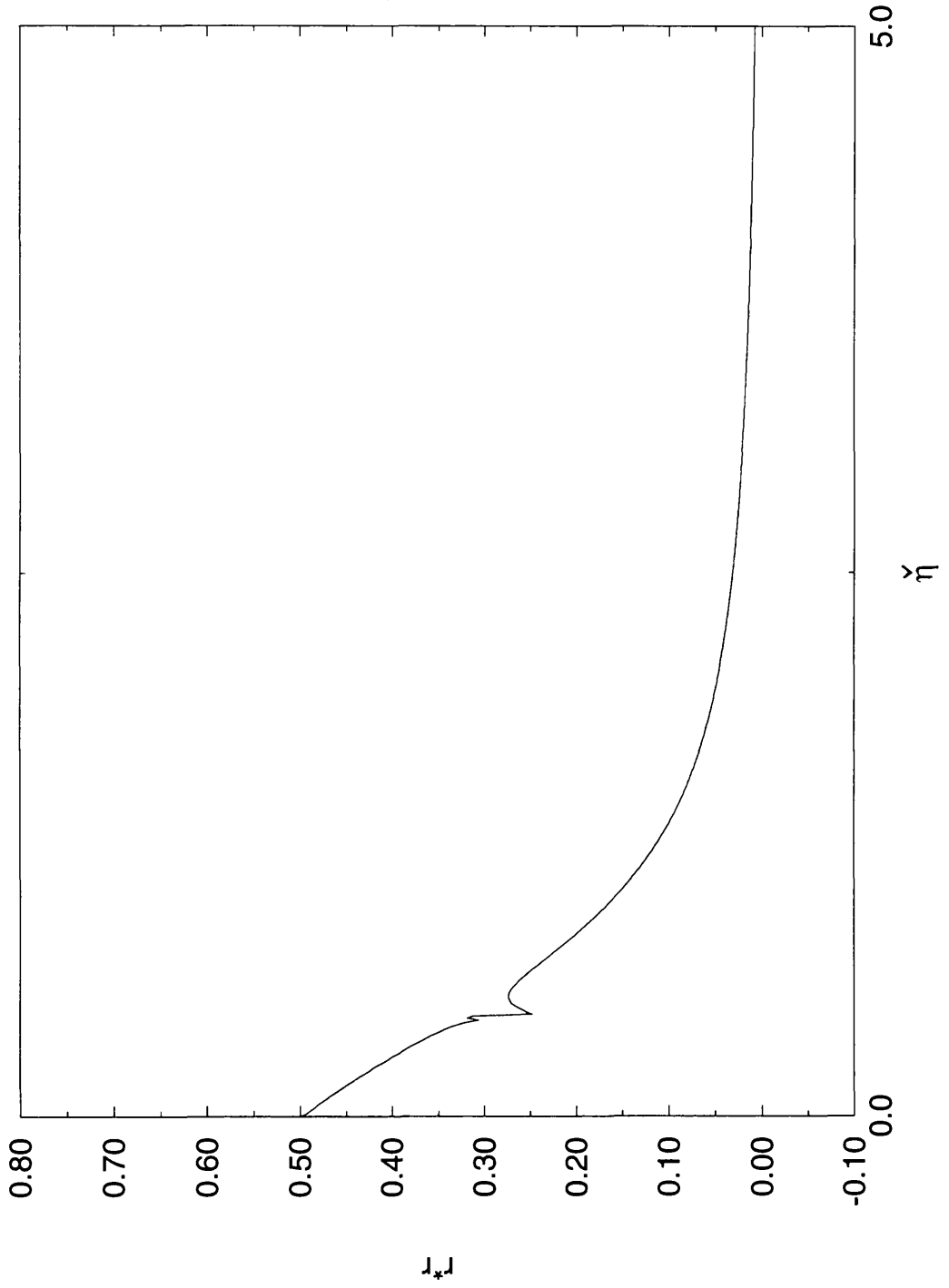

fig 3.6.9b

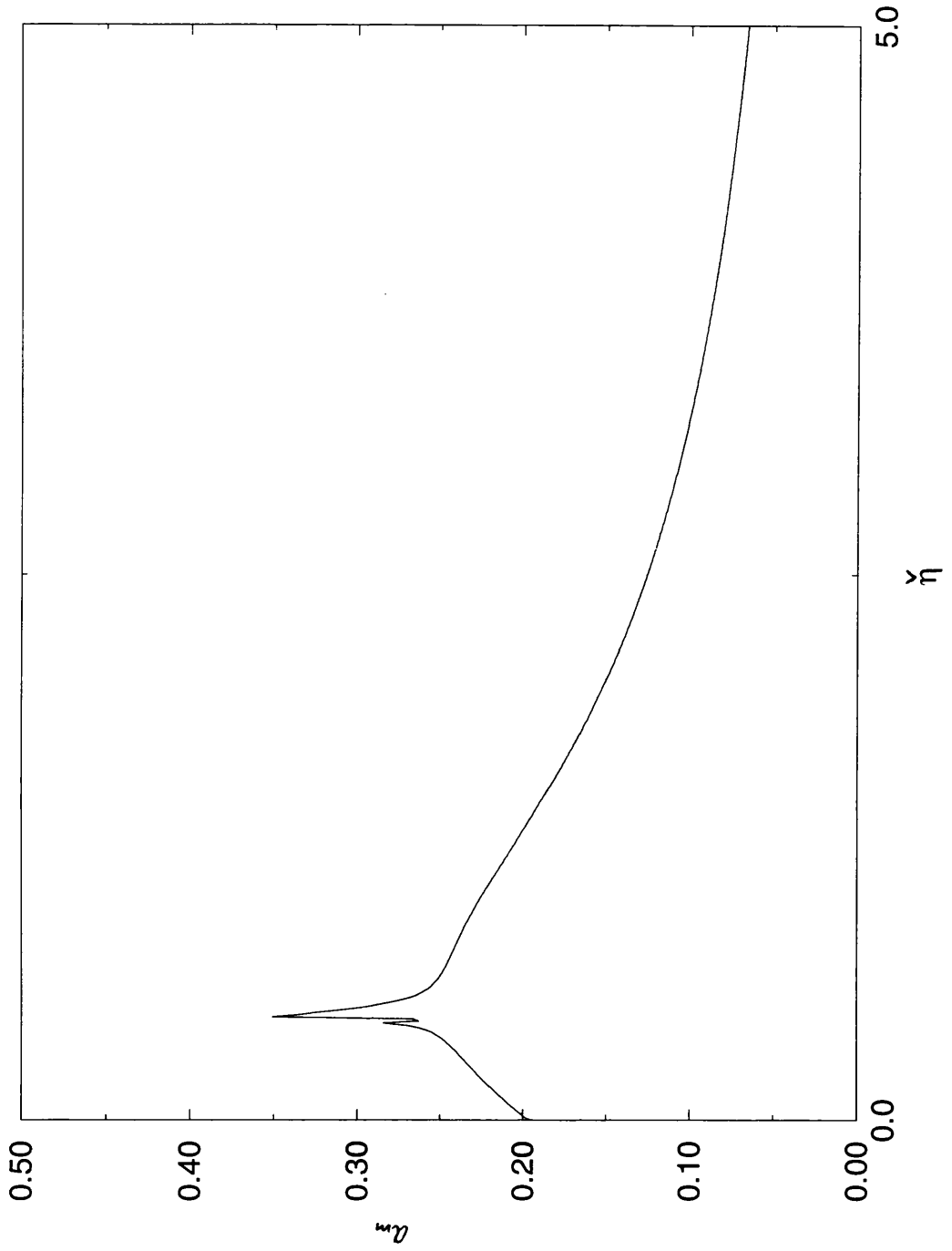

fig 3.6.9c

Numerical solutions for the modified system of equations.

Shooting forwards with, $h(0) = -0.58$, $r(0) = 0.707106$, $a_m(0) = 0.195112$.

§3.7 SUMMARY

In this chapter the governing equations relevant to the current higher-amplitude level-II have been derived, in sections 3.1, 3.2, 3.3. A 'cut-off' value at a finite value $\check{\eta} = \bar{\eta}_0$ has been identified. We note here for comparison purposes that the solution for the governing system $(3.6.1a - c)$ is different from the solution for the boundary-layer higher-amplitude equations of Smith et al (1994). The reason for this is that the pressure-displacement laws yield different governing relations. For the present wall-jet case we have

$$(r^2)_{\check{\eta}} = -\frac{3}{2}a_m - \check{\eta}a'_m, \tag{3.7.1}$$

whereas in the boundary-layer case

$$-r^2 = \frac{1}{\pi}\int_{-\infty}^{\infty} \frac{a'_m(q)}{\check{\eta} - q}dq$$

in our notation (Smith et al 1994). Nevertheless as the amplitudes increase in the boundary-layer spot case an analogue of $(3.6.1c)$ eventually holds, i.e.

$$-\frac{1}{2}\hat{A}_m - \check{\eta}\hat{A}'_m = (|\hat{p}_0|^2)'$$

in the notation of the last-named paper. Finally we observe here that as the typical value of the pressure r at $\check{\eta} = 0$ increases, the maximum amplitude moves towards the middle of the spot's trailing edge.

The next move is to consider the new stage that must arise as the amplitude is raised still further. At this new amplitude level the entire trailing-edge region becomes affected by nonlinearity. In effect we have $\hat{Z} - \bar{q}\hat{X}$ increasing to $O(\hat{X})$, which corresponds to $\hat{\Delta}$ increasing to $O(\hat{X})$. So $|A_{10}|$, $|u_{10}|$ increase to $O(\hat{X}^{3/2})$ as they are comparable and hence the mean-flow correction becomes comparable with the basic mean-flow $\hat{X}s$, formally. As a result a strongly nonlinear effect is implied at that level, with the fluctuating part $\propto \hat{X}^{-1/4}A_0$ also increasing to the order $\hat{X}$ since $|A_0| \propto |g_0| \sim \hat{X}^{5/4}$. In chapter 5 we investigate this in further detail.

CHAPTER 4

THE EDGE LAYER FURTHER DOWNSTREAM

§4.0 INTRODUCTION

In this chapter, to help complete the overall picture of the spot, we investigate the edge-layer further downstream in the $x = O(t)$ region which forms the bulk of the spot, this $O(t)$ scaling being suggested by the analysis of section 2.2. We begin by considering the thin-layer versions of the three-dimensional unsteady nonlinear Euler equations, which are valid for all scaled time, along with the rescaled versions of (2.4.2), (2.4.3a, b) in section 4.1 below. The general approach here is similar to that in chapter 2, i.e. we obtain the relevant controlling relations from the momentum, continuity and pressure-amplitude balances and then we manipulate these controlling equations to obtain the main governing amplitude equations at $x = O(t)$. We note that the amplitude equations at this order are partial differential equations (whereas at $x = O(t^{1/3})$ we have ordinary differential equations), see section 4.3.

In section 4.4 we modify the linear theory of chapter 2, by increasing the distances x, z to $O(t)$. At this distance the major contributions to the integral (2.2.3) come from $O(1)$ values of α, β. So the new feature emerging here is that the detailed distribution $\tilde{Q}(\alpha, \beta)$ now modifies the solution amplitude at leading order, and in particular it has a damping effect on the amplitude. There are again two wave families present containing an infinite number of waves analogous with those in (2.2.6). Moreover, the wake remains confined to $|\theta| < \theta_c$, with a modified form of (2.2.7) applying in the edge region, the caustic zone of the spot disturbance.

In sections 4.3 and 4.4 we match the nonlinear and linear theories. As a consequence of using the thin-layer Euler equations in examining the nonlinear theory, we find that in the lower amplitude limit (i.e. matching back to the linear theory) we regain Airy's equation, damped down by an exponentially decaying factor from $\tilde{Q}(\alpha, \beta)$; also the governing relations in the $O(t)$ zone are analogous with those for the trailing-edge region.

§4.1 THE ORDER t REGION: NONLINEAR THEORY

The governing equations to be addressed here are the thin-layer versions of $(2.1.1a-d)$, namely

$$u_x + v_y + w_z = 0, \tag{4.1.1a}$$

$$u_t + uu_x + vu_y + wu_z = -p_x, \tag{4.1.1b}$$

$$w_t + uw_x + vw_y + ww_z = -p_z, \tag{4.1.1c}$$

which are valid for all scaled time in the present context. Our new scalings for the spatial variables are

$$(x, y, z) = (t\tilde{X}, \tilde{Y}, t\tilde{Z})$$

where $\tilde{X}$, $\tilde{Y}$, $\tilde{Z}$ are all $O(1)$ generally. The normal scaling in the current $O(t)$ region follows from $(2.3.1b)$ and $(2.4.3a)$, while the x, z scalings define the current region of interest. Substituting these scalings into (2.4.2) and $(2.4.3b)$ we obtain after some manipulation

$$E \equiv exp(i[t\tilde{h}(\tilde{X}) + t^{1/3}\hat{\eta}\tilde{g}(\tilde{X})]), \tag{4.1.2a}$$

$$z - \bar{q}x = t^{1/3}\hat{\eta}, \tag{4.1.2b}$$

respectively, where $\tilde{h}$, $\tilde{g}$ are generally of $O(1)$ at most $\tilde{X}$ values of $O(1)$ but

$$\tilde{h}(\tilde{X}) \sim \tilde{X}^{3/2}, \quad \tilde{g}(\tilde{X}) \sim \tilde{X}^{1/2} \text{ as } \tilde{X} \to 0$$

to match with the previous work. Also rescaling the expansions $(2.4.1a-e)$ of the flow solution we have now

$$u = \tilde{Y} + t^{-5/6}(E\tilde{u}_0 + E^{-1}\tilde{u}_0^*) + \ldots + t^{-2/3}(E^2\tilde{u}_{12}t^{-1} + E\tilde{u}_{11}t^{-1/2} + \tilde{u}_{10}t^{-1/3} + c.c) +$$

$$\ldots + t^{-2/3}t^{-1/3}(E^3\tilde{u}_{23}t^{-3/2} + E^2\tilde{u}_{22}t^{-1} + E\tilde{u}_{21}t^{-1/2} + \tilde{u}_{20}t^{-1/3} + c.c) + \ldots$$

$$+ t^{-2/3}t^{-2/3}(E^4\tilde{u}_{34}t^{-2} + E^3\tilde{u}_{33}t^{-3/2} + E^2\tilde{u}_{32}t^{-1} +$$

$$E\tilde{u}_{31}t^{-1/2} + \tilde{u}_{30}t^{-1/3} + c.c) + \ldots, \tag{4.1.3a}$$

$$v = t^{-5/6}(E\tilde{v}_0 + E^{-1}\tilde{v}_0^*) + \ldots + t^{-5/3}(E^2\tilde{v}_{12} + E\tilde{v}_{11}t^{1/2} + \tilde{v}_{10}t^{2/3} + c.c) +$$

$$\ldots + t^{-5/3}t^{2/3}(E^3\tilde{v}_{23}t^{-3/2} + E^2\tilde{v}_{22}t^{-1} + E\tilde{v}_{21}t^{-1/2} + \tilde{v}_{20}t^{-1/3} + c.c) + \ldots$$

$$+t^{-5/3}t^{1/3}(E^4\tilde{v}_{34}t^{-2} + E^3\tilde{v}_{33}t^{-3/2} +$$

$$E^2\tilde{v}_{32}t^{-1} + E\tilde{v}_{31}t^{-1/2} + \tilde{v}_{30}t^{-1/3} + c.c) + \ldots, \qquad (4.1.3b)$$

$$w = t^{-5/6}(E\tilde{w}_0 + E^{-1}\tilde{w}_0^*) + \ldots + t^{-2/3}(E^2\tilde{w}_{12}t^{-1} + E\tilde{w}_{11}t^{-1/2} + \tilde{w}_{10}t^{-1/3} + c.c) +$$

$$\ldots + t^{-2/3}t^{-1/3}(E^3\tilde{w}_{23}t^{-3/2} + E^2\tilde{w}_{22}t^{-1} + E\tilde{w}_{21}t^{-1/2} + \tilde{w}_{20}t^{-1/3} + c.c) + \ldots$$

$$t^{-2/3}t^{-2/3}(E^4\tilde{w}_{34}t^{-2} + E^3\tilde{w}_{33}t^{-3/2} +$$

$$E^2\tilde{w}_{32}t^{-1} + E\tilde{w}_{31}t^{-1/2} + \tilde{w}_{30}t^{-1/3} + c.c) + \ldots, \qquad (4.1.3c)$$

for the velocity components, and

$$p = t^{-4/3}t^{1/2}(E\tilde{p}_0 + E^{-1}\tilde{p}_0^*) + \ldots + t^{-4/3}(E^2\tilde{p}_{12}t^{-1/3} + E\tilde{p}_{11}t^{1/6} + \tilde{p}_{10}t^{-1/3} + \ldots)$$

$$+t^{-4/3}t^{1/3}(E^3\tilde{p}_{23}t^{-3/2} + E^2\tilde{p}_{22}t^{-1} + E\tilde{p}_{21}t^{-1/2} + \tilde{p}_{20}t^{-1} + c.c) + \ldots$$

$$t^{-4/3}(E^4\tilde{p}_{34}t^{-2} + E^3\tilde{p}_{33}t^{-3/2} +$$

$$E^2\tilde{p}_{32}t^{-1} + E\tilde{p}_{31}t^{-1/2} + \tilde{p}_{30}t^{-1} + c.c) + \ldots, \qquad (4.1.3d)$$

$$A = t^{-2/3}t^{-1/6}(E\tilde{A}_0 + E^{-1}\tilde{A}_0^*) + \ldots + t^{-2/3}(E^2\tilde{A}_{12}t^{-1} + E\tilde{A}_{11}t^{-1/2} +$$

$$\tilde{A}_{10}t^{-1/3} + c.c) + \ldots + t^{-2/3}t^{-1/3}(E^3\tilde{A}_{23}t^{-3/2} + E^2\tilde{A}_{22}t^{-1} + E\tilde{A}_{21}t^{-1/2} +$$

$$\tilde{A}_{20}t^{-1/3} + c.c) + \ldots t^{-2/3}t^{-2/3}(E^4\tilde{A}_{34}t^{-2} + E^3\tilde{A}_{33}t^{-3/2} + E^2\tilde{A}_{32}t^{-1} +$$

$$E\tilde{A}_{31}t^{-1/2} + \tilde{A}_{30}t^{-1/3} + c.c) + \ldots, \qquad (4.1.3e)$$

for the pressure and displacement respectively, where $\tilde{u}_n$, $\tilde{v}_n$, $\tilde{w}_n$ are functions of $\tilde{X}$, $\hat{\eta}$, $\tilde{Y}$ and $\tilde{p}_n$, $\tilde{A}_n$ are functions of $\hat{\eta}$ and $\tilde{X}$ only. Equations $(4.1.1a - c)$ apply subject to the constraints.

$$u \sim y + A, \quad w \to 0 \quad \text{as} \quad y \to \infty, \qquad (4.1.4a)$$

$$v = 0 \quad \text{at} \quad y = 0, \tag{4.1.4b}$$

and the pressure-displacement relation is, from (2.1.6b),

$$p = -A_{xx}. \tag{4.1.5}$$

In the analysis which follows below we use the transformations

$$\partial_x \to t^{-1}\partial_{\tilde{X}} - \bar{q}t^{-1/3}\partial_{\hat{\eta}},$$

$$\partial_y \to \partial_{\tilde{Y}},$$

$$\partial_z \to t^{-1/3}\partial_{\hat{\eta}},$$

$$\partial_t \to \partial_t - t^{-1}\tilde{X}\partial_{\tilde{X}} - (1/3)t^{-1}\hat{\eta}\partial_{\hat{\eta}},$$

and

$$E_{\tilde{X}} \to i(t\tilde{h}_{\tilde{X}} + \hat{\eta}t^{1/3}\tilde{g}_{\tilde{X}})E,$$

$$E_{\hat{\eta}} \to it^{1/3}\tilde{g}E,$$

$$E_t \to i(\tilde{h} + (1/3)t^{-2/3}\hat{\eta}\tilde{g})E,$$

from above.

Substituting (4.1.3$a-d$) into the governing thin-layer system (4.1.1$a-c$) yields the successive controlling equations as follows. At first order (E terms only) we have

$$i\tilde{u}_0(\tilde{h}_{\tilde{X}} - \bar{q}\tilde{g}) + \tilde{v}_{0\tilde{Y}} + i\tilde{w}_0\tilde{g} = 0, \tag{4.1.6a}$$

$$i\tilde{u}_0(\tilde{h} - \tilde{X}\tilde{h}_{\tilde{X}} + \tilde{Y}\tilde{h}_{\tilde{X}} - \bar{q}\tilde{Y}\tilde{g}) + \tilde{v}_0 = -i\tilde{p}_0(\tilde{h}_{\tilde{X}} - \bar{q}\tilde{g}), \tag{4.1.6b}$$

$$i\tilde{w}_0(\tilde{h} - \tilde{X}\tilde{h}_{\tilde{X}} + \tilde{Y}\tilde{h}_{\tilde{X}} - \bar{q}\tilde{Y}\tilde{g}) = -i\tilde{g}\tilde{p}_0, \qquad (4.1.6c)$$

from the continuity, streamwise and spanwise balances respectively. These controlling equations apply subject to the constraints

$$\tilde{v}_0 = 0 \ \text{ at } \ \tilde{Y} = 0, \ \ \tilde{u}_0 \to \tilde{A}_0 \ \text{ as } \ \tilde{Y} \to \infty.$$

The solutions for $\tilde{u}_0$, $\tilde{v}_0$, $\tilde{w}_0$ hence obtained are

$$\tilde{u}_0 = \frac{\tilde{g}^2\tilde{p}_0}{\tilde{\alpha}\tilde{\beta}} + \tilde{A}_0, \qquad (4.1.7a)$$

$$\tilde{v}_0 = -i\tilde{\alpha}\tilde{A}_0\tilde{Y}, \qquad (4.1.7b)$$

$$\tilde{w}_0 = \frac{-\tilde{g}\tilde{p}_0}{\tilde{\beta}}, \qquad (4.1.7c)$$

with the resulting 'internal' pressure displacement relation being

$$\tilde{A}_0 = \Gamma\tilde{p}_0, \qquad (4.1.8)$$

where

$$\Gamma = -\frac{(\tilde{\alpha} + \tilde{g}^2/\tilde{\alpha})}{(\tilde{h} - \tilde{X}\tilde{h}_{\tilde{X}})}, \ \ \tilde{\alpha} = \tilde{h}_{\tilde{X}} - \bar{q}\tilde{g},$$

$$\tilde{\beta} = \tilde{\Phi} + \tilde{Y}\tilde{\alpha}, \ \ \tilde{\Phi} = \tilde{h} - \tilde{X}\tilde{h}_{\tilde{X}}.$$

At second order (E terms only) the continuity, streamwise and spanwise momentum balances yield

$$i\tilde{u}_{11}(\tilde{h}_{\tilde{X}} - \bar{q}\tilde{g}) + \tilde{v}_{11\tilde{Y}} + i\tilde{w}_{11}\tilde{g} - \bar{q}\tilde{u}_{0\hat{\eta}} + \tilde{w}_{0\hat{\eta}} = 0, \qquad (4.1.9a)$$

$$i\tilde{u}_{11}(\tilde{h} - \tilde{X}\tilde{h}_{\tilde{X}} + \tilde{Y}\tilde{h}_{\tilde{X}} - \bar{q}\tilde{Y}\tilde{g}) + \tilde{v}_{11} - \bar{q}\tilde{Y}\tilde{u}_{0\hat{\eta}} = -i\tilde{p}_{11}(\tilde{h}_{\tilde{X}} - \bar{q}\tilde{g}) + \bar{q}\tilde{p}_{0\hat{\eta}}, \qquad (4.1.9b)$$

$$i\tilde{w}_{11}(\tilde{h} - \tilde{X}\tilde{h}_{\tilde{X}} + \tilde{Y}\tilde{h}_{\tilde{X}} - \bar{q}\tilde{Y}\tilde{g}) - \bar{q}\tilde{Y}\tilde{w}_{0\hat{\eta}} = -i\tilde{g}\tilde{p}_{11} - \tilde{p}_{0\hat{\eta}}, \qquad (4.1.9c)$$

respectively. The solutions for $\tilde{u}_{11}$, $\tilde{v}_{11}$, $\tilde{w}_{11}$ subject to the constraints

$$\tilde{v}_{11} = 0 \ \text{ at } \ \tilde{Y} = 0, \ \ \tilde{u}_{11} \to \tilde{A}_{11} \ \text{ as } \ \tilde{Y} \to \infty,$$

are therefore

$$\tilde{u}_{11} = \tilde{A}_{11} + \frac{i}{\tilde{\alpha}}\left(\frac{\tilde{\sigma}}{\tilde{\beta}} + \frac{\tilde{\tau}}{\tilde{\beta}^2}\right), \tag{4.1.10a}$$

where

$$\tilde{\sigma} = -[i\tilde{g}\tilde{p}_{11} + 2\tilde{p}_{0\hat{\eta}} + 2\bar{q}\tilde{g}\tilde{p}_{0\hat{\eta}}/\tilde{\alpha}]\tilde{g},$$

$$\tilde{\tau} = \bar{q}\tilde{g}^2\tilde{\Phi}\tilde{p}_{0\hat{\eta}}/\tilde{\alpha},$$

$$\tilde{v}_{11} = \bar{q}\tilde{Y}\left[\frac{\tilde{g}^2\tilde{p}_{0\hat{\eta}}}{\tilde{\alpha}\tilde{\beta}} + \tilde{A}_{0\hat{\eta}}\right] - i\tilde{\alpha}\tilde{p}_{11} + \bar{q}\tilde{p}_{0\hat{\eta}} - i\tilde{\beta}\tilde{u}_{11}, \tag{4.1.10b}$$

$$\tilde{w}_{11} = -i\tilde{\beta}^{-1}[\bar{q}\tilde{Y}\tilde{w}_{0\hat{\eta}} - i\tilde{g}\tilde{p}_{11} - \tilde{p}_{0\hat{\eta}}]. \tag{4.1.10c}$$

The internal pressure-displacement relation between $\tilde{p}_{11}$, $\tilde{A}_{11}$ here takes the form

$$i\tilde{p}_{11}\Gamma\tilde{\Phi} = i\tilde{\Phi}\tilde{A}_{11} - \tilde{p}_{0\hat{\eta}}[\bar{q} - 2\tilde{g}/\tilde{\alpha} - \bar{q}\tilde{g}^2/\tilde{\alpha}^2]. \tag{4.1.11}$$

Similarly at third order (E terms only) the controlling equations are

$$i\tilde{u}_{21}(\tilde{h}_{\tilde{X}} - \bar{q}\tilde{g}) + \tilde{v}_{21\tilde{Y}} + i\tilde{w}_{21}\tilde{g} - \bar{q}\tilde{u}_{11\hat{\eta}} + \tilde{w}_{11\hat{\eta}} + i\tilde{u}_0\hat{\eta}\tilde{g}_{\tilde{X}} = 0, \tag{4.1.12a}$$

$$i\tilde{u}_{21}(\tilde{h} - \tilde{X}\tilde{h}_{\tilde{X}} + \tilde{Y}\tilde{h}_{\tilde{X}} - \tilde{Y}\bar{q}\tilde{g}) + \tilde{v}_{21} - \tilde{Y}\bar{q}\tilde{u}_{11\hat{\eta}} + i\tilde{u}_0(\tilde{Y}\hat{\eta}\tilde{g}_{\tilde{X}} - \tilde{X}\hat{\eta}\tilde{g}_{\tilde{X}})$$

$$= -i\tilde{p}_{21}(\tilde{h}_{\tilde{X}} - \bar{q}\tilde{g}) + \bar{q}\tilde{p}_{11\hat{\eta}} - i\hat{\eta}\tilde{g}_{\tilde{X}}\tilde{p}_0, \tag{4.1.12b}$$

$$i\tilde{w}_{21}(\tilde{h} - \tilde{X}\tilde{h}_{\tilde{X}} + \tilde{Y}\tilde{h}_{\tilde{X}} - \tilde{Y}\bar{q}\tilde{g}) - \tilde{Y}\bar{q}\tilde{w}_{11\hat{\eta}} + i\tilde{w}_0(\tilde{Y}\hat{\eta}\tilde{g}_{\tilde{X}} - \tilde{X}\hat{\eta}\tilde{g}_{\tilde{X}})$$

$$= -i\tilde{g}\tilde{p}_{21} - \tilde{p}_{11\hat{\eta}}, \tag{4.1.12c}$$

from the continuity, streamwise and spanwise momentum balances respectively. These are subject to

$$\tilde{v}_{21} = 0 \ \text{ at } \ \tilde{Y} = 0, \ \ \tilde{u}_{21} \to \tilde{A}_{21} \ \text{ as } \ \tilde{Y} \to \infty.$$

Hence we have for $(\tilde{u}_{21}, \tilde{v}_{21}, \tilde{w}_{21})$

$$\tilde{u}_{21} = \tilde{A}_{21} - i\int_{\infty}^{\tilde{Y}} \frac{1}{\tilde{\beta}}[\tilde{Y}\bar{q}\tilde{u}_{11\hat{\eta}\tilde{Y}} - i\hat{\eta}\tilde{g}_{\tilde{X}}(\tilde{Y}-\tilde{X})\tilde{u}_{0\tilde{Y}} + \tilde{w}_{11\hat{\eta}} + \tilde{g}\tilde{\beta}^{-1}\tilde{Y}\bar{q}\tilde{w}_{11\hat{\eta}}$$

$$-\tilde{g}\tilde{\beta}^{-1}i\tilde{w}_0\hat{\eta}\tilde{g}_{\tilde{X}}(\tilde{Y}-\tilde{X}) - \tilde{g}\tilde{\beta}^{-1}i\tilde{g}\tilde{p}_{21} - \tilde{g}\tilde{\beta}^{-1}\tilde{p}_{11\hat{\eta}}] \ d\tilde{Y}, \qquad (4.1.13a)$$

$$\tilde{v}_{21} = -i\tilde{p}_{21}\tilde{\alpha} + \bar{q}\tilde{p}_{11\hat{\eta}} - i\hat{\eta}\tilde{g}_{\tilde{X}}\tilde{p}_0 - i\tilde{u}_{21}\tilde{\beta} + \tilde{Y}\bar{q}\tilde{u}_{11\hat{\eta}} - i\tilde{u}_0\hat{\eta}\tilde{g}_{\tilde{X}}(\tilde{Y}-\tilde{X}), \ (4.1.13b)$$

$$\tilde{w}_{21} = -i\tilde{\beta}^{-1}(\tilde{Y}\bar{q}\tilde{w}_{11\hat{\eta}} - i\tilde{w}_0\hat{\eta}\tilde{g}_{\tilde{X}}(\tilde{Y}-\tilde{X}) - i\tilde{g}\tilde{p}_{21} - \tilde{p}_{11\hat{\eta}}). \qquad (4.1.13c)$$

The resulting internal pressure-displacement relation between $\tilde{p}_{21}$, $\tilde{A}_{21}$ is

$$-i\tilde{p}_{21}\left(\tilde{\alpha} + \frac{\tilde{g}^2}{\tilde{\alpha}}\right) - i\tilde{\Phi}\tilde{A}_{21} + \tilde{p}_{11\hat{\eta}}\left(\bar{q} - \frac{\bar{q}\tilde{g}^2}{\tilde{\alpha}^2} - \frac{2\tilde{g}}{\tilde{\alpha}}\right)$$

$$+i\tilde{p}_{0\hat{\eta}\hat{\eta}}\left(\frac{2\bar{q}\tilde{g}}{\tilde{\alpha}^2} + \frac{\bar{q}^2\tilde{g}^2}{\tilde{\alpha}^3} + \frac{1}{\tilde{\alpha}}\right) + \tilde{A}_0 i\hat{\eta}\tilde{g}_{\tilde{X}}\tilde{X} + i\tilde{p}_0(\hat{\eta}\tilde{g}_{\tilde{X}}\tilde{g}^2/\tilde{\alpha}^2 - \hat{\eta}\tilde{g}_{\tilde{X}}) = 0. \quad (4.1.14)$$

Now at fourth-order the controlling equations are found to be

$$i\tilde{u}_{31}(\tilde{h}_{\tilde{X}} - \bar{q}\tilde{g}) + \tilde{v}_{31\tilde{Y}} + i\tilde{w}_{31}\tilde{g} - \bar{q}\tilde{u}_{21\hat{\eta}} + \tilde{w}_{21\hat{\eta}} + i\tilde{u}_{11}\hat{\eta}\tilde{g}_{\tilde{X}} + \tilde{u}_{0\tilde{X}} = 0, \ \ (4.1.15a)$$

$$i\tilde{u}_{31}(\tilde{h} - \tilde{X}\tilde{h}_{\tilde{X}} + \tilde{Y}\tilde{h}_{\tilde{X}} - \tilde{Y}\bar{q}\tilde{g}) + \tilde{v}_{31} - \tilde{Y}\bar{q}\tilde{u}_{21\hat{\eta}} + i\tilde{u}_{11}\tilde{g}_{\tilde{X}}(\tilde{Y}-\tilde{X})\hat{\eta} +$$

$$\tilde{u}_0(-5/6 + i\tilde{h}_{\tilde{X}}\tilde{u}_{10} + i\tilde{g}\tilde{w}_{10} - \tilde{u}_{10}\bar{q}i\tilde{g}) + \tilde{u}_{0\tilde{X}}(\tilde{Y}-\tilde{X}) - (1/3)\hat{\eta}\tilde{u}_{0\hat{\eta}} + \tilde{v}_{10}\tilde{u}_{0\tilde{Y}}$$

$$+\tilde{v}_0\tilde{u}_{10\tilde{Y}} = -i\tilde{p}_{31}(\tilde{h}_{\tilde{X}} - \bar{q}\tilde{g}) + \bar{q}\tilde{p}_{21\hat{\eta}} - \tilde{p}_{11}i\hat{\eta}\tilde{g}_{\tilde{X}} - \tilde{p}_{0\tilde{X}}, \qquad (4.1.15b)$$

$$i\tilde{w}_{31}(\tilde{h} - \tilde{X}\tilde{h}_{\tilde{X}} + \tilde{Y}\tilde{h}_{\tilde{X}} - \tilde{Y}\bar{q}\tilde{g}) - \tilde{Y}\bar{q}\tilde{w}_{21\hat{\eta}} + i\tilde{w}_{11}\tilde{g}_{\tilde{X}}(\tilde{Y}-\tilde{X})\hat{\eta} +$$

$$\tilde{w}_0(-5/6 + i\tilde{h}_{\tilde{X}}\tilde{u}_{10} + i\tilde{g}\tilde{w}_{10} - \tilde{u}_{10}\bar{q}i\tilde{g}) + \tilde{w}_{0\tilde{X}}(\tilde{Y} - \tilde{X}) - (1/3)\hat{\eta}\tilde{w}_{0\hat{\eta}} + \tilde{v}_{10}\tilde{w}_{0\tilde{Y}}$$

$$+\tilde{v}_0\tilde{w}_{10\tilde{Y}} = -i\tilde{g}\tilde{p}_{31} - \tilde{p}_{21\hat{\eta}}, \qquad (4.1.15c)$$

from the continuity, streamwise and spanwise E term balances respectively. We examine $(4.1.15a - c)$ further in section 4.3.

The leading order mean-flow responses (E^0 contributions), meanwhile, are as follows. At second order we obtain

$$-\bar{q}\tilde{u}_{10\hat{\eta}} + \tilde{v}_{20\tilde{Y}} + \tilde{w}_{10\hat{\eta}} = 0 \qquad (4.1.16a)$$

$$-\tilde{Y}\bar{q}\tilde{u}_{10\hat{\eta}} + \tilde{v}_{20} = 0 \qquad (4.1.16b)$$

$$-\tilde{Y}\bar{q}\tilde{w}_{10\hat{\eta}} = 0 \qquad (4.1.16c)$$

from the continuity, streamwise and spanwise balances respectively; hence

$$\tilde{w}_{10} = 0, \quad \tilde{v}_{20} = \tilde{Y}\bar{q}\tilde{A}_{10\hat{\eta}}, \quad \tilde{u}_{10} = \tilde{A}_{10},$$

where the displacement function $\tilde{A}_{10}$ is unknown. At the next order, the controlling equations linking $(\tilde{u}_{30}, \tilde{v}_{40}, \tilde{w}_{30})$ are

$$\tilde{v}_{40} - \tilde{Y}\bar{q}\tilde{u}_{30\hat{\eta}} + \tilde{u}_{10\tilde{X}}(\tilde{Y} - \tilde{X}) - (1/3)\hat{\eta}\tilde{u}_{10\hat{\eta}} + \tilde{v}_{10}\tilde{u}_{10\tilde{Y}} - \tilde{u}_{10} + \Pi_1 = \bar{q}\tilde{p}_{10\hat{\eta}}, \quad (4.1.17a)$$

where

$$\Pi_1 = [-\bar{q}\tilde{u}_0\tilde{u}^*_{0\hat{\eta}} + \tilde{v}_{11}\tilde{u}^*_{0\tilde{Y}} + \tilde{v}_0\tilde{u}^*_{11\tilde{Y}} - \tilde{w}_{11}\tilde{u}^*_0 i\tilde{g} + \tilde{w}_0\tilde{u}^*_{0\hat{\eta}} - \tilde{w}_0\tilde{u}^*_{11} i\tilde{g} + c.c],$$

from the streamwise momentum balance, and

$$-\tilde{Y}\bar{q}\tilde{w}_{30\hat{\eta}} + \tilde{w}_{10\tilde{X}}(\tilde{Y} - \tilde{X}) - (1/3)\hat{\eta}\tilde{w}_{10\hat{\eta}} + \tilde{v}_{10}\tilde{w}_{10\tilde{Y}} - \tilde{w}_{10} + \Pi_2 = -\tilde{p}_{10\hat{\eta}}, \quad (4.1.17b)$$

where

$$\Pi_2 = [-\bar{q}\tilde{u}_0\tilde{w}^*_{0\hat{\eta}} + \tilde{v}_{11}\tilde{w}^*_{0\tilde{Y}} + \tilde{v}_0\tilde{w}^*_{11\tilde{Y}} + \tilde{w}_0\tilde{w}^*_{0\hat{\eta}} - \tilde{w}_0\tilde{w}^*_{11} i\tilde{g} - \tilde{w}_{11}\tilde{w}^*_0 i\tilde{g}$$

$$-\tilde{u}_{11}\tilde{w}^*_0 i\tilde{h}_{\tilde{X}} - \tilde{u}_0\tilde{w}^*_{11} i\tilde{h}_{\tilde{X}} + \tilde{u}_0\bar{q}\tilde{w}^*_{11} i\tilde{g} + \tilde{u}_{11}\bar{q}\tilde{w}^*_0 i\tilde{g} + c.c],$$

from the spanwise momentum balance. Following the pattern of section 2.6 we take the combination $\bar{q}$ times (4.1.17a) minus (4.1.17b), and then set $\tilde{Y} = 0$ in the resulting momentum equation to give

$$-\bar{q}\tilde{X}\tilde{A}_{10\tilde{X}} - \frac{1}{3}\bar{q}\hat{\eta}\tilde{A}_{10\hat{\eta}} - \bar{q}\tilde{A}_{10} + (\bar{q}^2+1)\Pi = (\bar{q}^2+1)\tilde{p}_{10\hat{\eta}}, \tag{4.1.18}$$

where

$$\Pi = -\frac{(\tilde{\alpha}^2+\tilde{g}^2)}{\tilde{\Phi}^2}(|\tilde{p}_0|^2)_{\hat{\eta}}.$$

Here we have made use of the solutions for $(\tilde{u}_0, \tilde{u}_{11}, \tilde{w}_0, \tilde{w}_{11})$ to obtain the expression for Π. We note that the mean-flow balance at first-order from the streamwise momentum equation is

$$\tilde{v}_{10} = 0,$$

consistent with the result $\tilde{v}_{10\tilde{Y}} = 0$ from the continuity equation (second order E^0 balances).

§4.2 EXTERNAL RELATIONS

From chapter 2 we have the pressure-displacement relation

$$p = -A_{xx}, \tag{4.2.1}$$

for the wall-jet case. Substituting the expansions (4.1.3d, e) into (4.2.1) yields the external relations as follows. From balancing mean-flow terms proportional to E^0 we obtain

$$\tilde{p}_{10} = -\bar{q}^2\tilde{A}_{10\hat{\eta}\hat{\eta}}, \tag{4.2.2}$$

linking $\tilde{p}_{10}$, $\tilde{A}_{10}$. Now balancing terms proportional to E we have

$$\tilde{p}_0 = \tilde{A}_0\tilde{\alpha}^2, \tag{4.2.3a}$$

at first order,

$$\tilde{p}_{11} = \tilde{A}_{11}\tilde{\alpha}^2 + 2i\bar{q}\tilde{A}_{0\hat{\eta}}\tilde{\alpha}, \tag{4.2.3b}$$

at second order,

$$\tilde{p}_{21} = \tilde{A}_{21}\tilde{\alpha}^2 + 2i\bar{q}\tilde{A}_{11\hat{\eta}}\tilde{\alpha} + 2\hat{\eta}\tilde{g}_{\tilde{X}}\tilde{A}_0\tilde{\alpha} - \bar{q}^2\tilde{A}_{0\hat{\eta}\hat{\eta}}, \tag{4.2.3c}$$

at third order,

$$\tilde{p}_{31} = \tilde{A}_{31}\tilde{\alpha}^2 + 2i\bar{q}\tilde{A}_{21\hat{\eta}}\tilde{\alpha} - \bar{q}^2\tilde{A}_{11\hat{\eta}\hat{\eta}} + 2\hat{\eta}\tilde{g}_{\tilde{X}}\tilde{A}_{11}\tilde{\alpha} - 2i\tilde{A}_{0\tilde{X}}\tilde{\alpha}$$

$$+2\bar{q}i\hat{\eta}\tilde{g}_{\tilde{X}}\tilde{A}_{0\hat{\eta}} + 2\bar{q}i\tilde{g}_{\tilde{X}}\tilde{A}_0 - \tilde{A}_0 i\tilde{h}_{\tilde{X}\tilde{X}}, \qquad (4.2.3d)$$

at fourth order. Coupling the external and internal pressure displacement relations above we then obtain the following eigenrelations;

$$\tilde{\Phi} = -\tilde{\alpha}^2\left(\tilde{\alpha} + \frac{\tilde{g}^2}{\tilde{\alpha}}\right), \qquad (4.2.4a)$$

from coupling the first-order relations (4.2.3a), (4.1.8), leaving $\tilde{p}_0$ arbitrary, and

$$-3\bar{q}\tilde{\alpha}^2 + 2\tilde{g}\tilde{\alpha} - \bar{q}\tilde{g}^2 = 0, \qquad (4.2.4b)$$

from coupling the second-order relations (4.2.3b), (4.1.11), leaving $\tilde{p}_0$ and $\tilde{p}_{11}$ arbitrary. This last eigenrelation yields

$$\tilde{\alpha} = \tilde{g}\bar{q}.$$

Coupling the third-order relations (4.2.3c), (4.1.14) we obtain the eigenrelation

$$-i\tilde{A}_{0\hat{\eta}\hat{\eta}}(-3\tilde{\alpha}\bar{q}^2 + 2\bar{q}\tilde{g} - \tilde{\alpha}) + i\tilde{A}_0(-\tilde{g}^2 + \tilde{X} - 3\tilde{\alpha}^2)\hat{\eta}\tilde{g}_{\tilde{X}} = 0, \qquad (4.2.4c)$$

leaving $\tilde{p}_{21}$, $\tilde{p}_{11}$ arbitrary. Substituting $\tilde{\alpha} = \tilde{g}\bar{q}$ into (4.2.4c) yields

$$\tilde{g} = \left(\frac{\tilde{X}}{2}\right)^{1/2}, \qquad (4.2.5)$$

which is used below.

§4.3 GOVERNING AMPLITUDE EQUATIONS OF THE $O(t)$ EDGE-LAYER

We now derive the main governing amplitude equation for the current $O(t)$ edge-layer region, using the fourth-order balances (4.1.15$a-c$).

Taking the derivative of (4.1.15b) with respect to $\tilde{Y}$ and substituting for $\tilde{w}_{31}$, $\tilde{v}_{31}$ gives

$$\tilde{u}_{31} = \tilde{A}_{31} - i\int_{\infty}^{\tilde{Y}} \tilde{\beta}^{-1}\bar{\tilde{Q}}_{31}d\tilde{Y}, \qquad (4.3.1)$$

subject to $\tilde{u}_{31} \to \tilde{A}_{31}$ as $\tilde{Y} \to \infty$ after some manipulation. Here

$$\bar{\tilde{Q}}_{31} = \mathcal{D}_1 + \mathcal{D}_2,$$

where

$$\mathcal{D}_1 = -\tilde{g}\tilde{\beta}^{-1}[\tilde{v}_{10}\tilde{w}_{0\tilde{Y}} + \tilde{v}_0\tilde{w}_{10\tilde{Y}} + i\tilde{\alpha}\tilde{w}_0\tilde{u}_{10} + i\tilde{g}\tilde{w}_0\tilde{w}_{10}]$$

$$-[i\tilde{\alpha}\tilde{u}_0\tilde{u}_{10} + i\tilde{g}\tilde{u}_0\tilde{w}_{10} + \tilde{v}_{10}\tilde{u}_{0\tilde{Y}} + \tilde{v}_0\tilde{u}_{10\tilde{Y}}]_{\tilde{Y}},$$

$$\mathcal{D}_2 = \tilde{w}_{21\hat{\eta}} + \tilde{Y}\bar{q}\tilde{u}_{21\hat{\eta}\tilde{Y}} - i\tilde{g}_{\tilde{X}}\hat{\eta}(\tilde{Y} - \tilde{X})\tilde{u}_{11\tilde{Y}} + \frac{5}{6}\tilde{u}_{0\tilde{Y}}$$

$$-(\tilde{Y} - \tilde{X})\tilde{u}_{0\tilde{X}\tilde{Y}} + \frac{1}{3}\hat{\eta}\tilde{u}_{0\hat{\eta}\tilde{Y}} - i\tilde{g}^2\tilde{\beta}^{-1}\tilde{p}_{31} - \tilde{g}\tilde{\beta}^{-1}\tilde{p}_{21\hat{\eta}} + \tilde{g}\tilde{\beta}^{-1}\tilde{Y}\bar{q}\tilde{w}_{21\hat{\eta}}$$

$$-i\tilde{g}\tilde{\beta}^{-1}\tilde{w}_{11}\tilde{g}_{\tilde{X}}(\tilde{Y} - \tilde{X})\hat{\eta} + \frac{5}{6}\tilde{g}\tilde{\beta}^{-1}\tilde{w}_0 - \tilde{g}\tilde{\beta}^{-1}\tilde{w}_{0\tilde{X}}(\tilde{Y} - \tilde{X}) + \frac{1}{3}\hat{\eta}\tilde{g}\tilde{\beta}^{-1}\tilde{w}_{0\hat{\eta}}.$$

Substituting this expression for $\tilde{u}_{31}$ into (4.1.15b) and taking the limit as $\tilde{Y} \to 0$ establishes the amplitude equation at fourth order as

$$\left(\frac{4}{3^{3/2}}\tilde{p}_{0\hat{\eta}\hat{\eta}} - \frac{1}{3}\hat{\eta}\tilde{p}_0\right)_{\hat{\eta}} = -i\tilde{\alpha}\tilde{p}_0\tilde{A}_{10}, \qquad (4.3.2a)$$

for $\tilde{p}_0$, after some working. Here we have made use of the expressions for the external relations (4.2.3a – c) amongst other details. As before we note here that the right-hand-side contains all the nonlinear effects. Therefore for a linear disturbance the amplitude equation again reduces to Airy's equation for $\tilde{p}_0$, giving the solution

$$\tilde{p}_0 \propto \tilde{A}_i(3^{1/6}4^{-1/3}\hat{\eta})\mathcal{S}(\tilde{X}), \qquad (4.3.2b)$$

in terms of the Airy function $\tilde{A}_i$, where $\mathcal{S}(\tilde{X})$ is determined by matching with the linear theory holding in between the edge layers. In the general nonlinear case we have two main governing partial differential equations (4.1.18), (4.3.2a) for $\tilde{A}_{10}$, $\tilde{p}_0$, which after further simplification are

$$\left(\frac{4}{3^{1/2}}\tilde{p}_{0\hat{\eta}\hat{\eta}} - \hat{\eta}\tilde{p}_0\right)_{\hat{\eta}} = -\frac{3^{1/2}}{2^{1/2}}\tilde{X}^{1/2}i\tilde{p}_0\tilde{A}_{10}, \qquad (4.3.3a)$$

$$-\tilde{X}\tilde{A}_{10\tilde{X}} - \frac{1}{3}\hat{\eta}\tilde{A}_{10\hat{\eta}} - \tilde{A}_{10} - \frac{3^{3/2}4}{\tilde{X}^2}|\tilde{p}_0|^2_{\hat{\eta}} = -\frac{4}{3^{3/2}}\tilde{A}_{10\hat{\eta}\hat{\eta}\hat{\eta}}. \qquad (4.3.3b)$$

So in general we have sets of nonlinear governing amplitude equations along the edge-layer which reduce to Airy's equation in the linear limit. The main reason for the present structure is that we have used the 'thin-layer' versions of the unsteady incompressible Euler equations throughout and the analysis has been restricted to 'large distances' $(x, z) \leq O(t)$. For larger distances beyond $O(t)$ we would expect the full Euler equations to apply again since locally the streamwise and spanwise scales would then be comparable with the normal coordinate scaling.

§4.4 $O(T)$ LINEAR THEORY

From section 2.2 we have, for the amplitude outside the edge-layer, the integral representation

$$\bar{A}(X, Z, T) = \frac{1}{4\pi^2} \int_{-\infty}^{\infty} \int_{-\infty}^{\infty} \tilde{Q}(\alpha, \beta) \exp[i\alpha X + i\beta Z - (\alpha^2 + \beta^2) i\alpha T] d\alpha d\beta. \tag{4.4.1}$$

So in the current $O(T)$ region we write

$$(X, Z) = T(\check{X}, \check{Z}) = TR(\cos\theta, \sin\theta), \quad (\alpha, \beta) = r(\cos\phi, \sin\phi), \tag{4.4.2}$$

in polars. It is observed that $\tilde{Q}(\alpha, \beta)$ affects the amplitude at leading order since α, β are now $O(1)$. For $\tilde{Q}(\alpha, \beta)$ we assume the Gaussian form

$$\tilde{Q}(\alpha, \beta) = \exp[-(\alpha^2 + \beta^2)], \tag{4.4.3}$$

as an example. Substituting (4.4.2), (4.4.3) into (4.4.1) and integrating with respect to ϕ we then obtain

$$\bar{A} = \frac{1}{2\pi} \int_0^{\infty} \gamma(r) J_0(T\bar{c}) r dr, \tag{4.4.4}$$

where

$$\bar{c} = (r^2 R^2 - 2r^4 R \cos\theta + r^6)^{1/2},$$

$$\gamma(r) = \exp(-r^2),$$

after some manipulation. Here J_0 is again the zeroth order Bessel function. As in section 2.2 we make the substitution $r = (\sigma R)^{1/2}$ for $R \gg 1$ and use the method of stationary phase to obtain

$$2^{1/2}\pi\bar{A} \sim$$
$$\frac{R}{(2T)^{1/2}}\left[\left(\frac{2\pi}{TR^{3/2}B_2^+}\right)^{1/2}\frac{1}{R^{3/4}B_1^{+1/2}}\exp(-R\sigma_1^+)\exp[iTR^{3/2}B_1^+ \pm \frac{i\pi}{4}]\right]$$
$$+\frac{R}{(2T)^{1/2}}\left[\left(\frac{2\pi}{TR^{3/2}B_2^-}\right)^{1/2}\frac{1}{R^{3/4}B_1^{-1/2}}\exp(-R\sigma_1^-)\exp[iTR^{3/2}B_1^- \pm \frac{i\pi}{4}]\right], \tag{4.4.5}$$

for $-\theta_c < \theta < \theta_c$ where

$$B_1(\theta) = (\sigma_1 - 2\sigma_1^2\cos\theta + \sigma_1^3)^{1/2},$$

$$B_2(\theta) = (-2\cos\theta + 3\sigma_1)B_1^{-1},$$

$$\sigma_1^{\pm}(\theta) = \frac{1}{3}[2\cos\theta \pm (4\cos^2\theta - 3)^{1/2}].$$

So the present amplitude decays exponentially far downstream in this $O(T)$ range. This effect is a direct consequence of the $O(1)$ contribution made by $\tilde{Q}(\alpha,\beta)$. We note also that the half-angle prediction remains the same, $\theta_c = 30°$. In detail (4.4.4) gives

$$\bar{A} \sim \frac{R^{-1/4}}{4\pi^{1/2}Tc^{5/4}}\left(\frac{3}{2}\right)^{3/4}\cos(B_1\check{X}^{3/2}T)\left(T2^{1/2}3\right)^{-1/3}e^{-\check{X}/c3^{1/2}}\tilde{A}_i(3^{1/6}2^{-2/3}\eta), \tag{4.4.6}$$

where

$$B_1 = \left[\left(\frac{2}{3}\right)^{3/2} + \frac{\eta T^{-2/3}}{2^{1/2}\check{X}}\right]$$

$$c = \frac{3^{1/2}}{2}, \text{ and } \eta, \check{X} \text{ are } O(1).$$

Once again we notice the factor $e^{-\check{X}/c3^{1/2}}$ which acts to damp down the amplitude sufficiently far downstream.

Now using $\tilde{p}_0 \sim \mathcal{S}(\tilde{X})|\hat{\eta}|^{-1/4}\cos[\frac{2}{3}|\hat{\eta}|^{3/2}]$ as $\hat{\eta} \to -\infty$ as our boundary condition, and matching with the linear result (4.4.5) in the centre of the wake region, we have that

$$\mathcal{S}(\tilde{X}) \propto \tilde{X}^{1/2}\exp(-\tilde{X}\sigma(\theta)/\cos\theta),$$

which may be used to simplify (4.3.3*b*) a little for small amplitudes as $\tilde{X} \to \infty$.

§4.5 SUMMARY

In this chapter we have derived the governing nonlinear amplitude equations $(4.3.3a, b)$ valid in the front-end caustic region of the spot. These equations are found to be analogous with those in the trailing-edge $O(t^{1/3})$ region of the spot further upstream, except that the amplitude is now damped by an exponentially decaying factor $e^{-\bar{X}/c3^{1/2}}$ in the edge layers. The other main conclusion is that we have sets of nonlinear amplitude relations along the edge layers for distances (x, z) up to $O(t)$.

CHAPTER 5

AMPLITUDE LEVEL III

NONLINEAR EFFECTS IN THE ENTIRE TRAILING EDGE REGION

§5.0 INTRODUCTION

This chapter presents the first half or so of work which is still in progress. The aim in this chapter is to consider raising the amplitude still further, leading in effect to a study of the entire trailing-edge region. The nonlinear interaction present now is found to become strongly nonlinear and, in contrast with the interactions addressed in the previous chapters, effectively all the higher harmonic fluctuations also play a significant role; see sections 5.1, 5.2, 5.3 below. As in previous chapters we derive a closed system of equations linking all the major unknown variables and in particular we establish analogues of $(3.6.1a-c)$; see section 5.3.

We show in section 5.3 that the leading-order equations for the wave term are related to the KDV equation and that the mean-flow balances at leading order involve 'Reynolds stresses', while the wave-term balances at the next order are needed in order to obtain a closed system.

The general method used is similar to that in chapter 2, except that since we are now concerned with the entire trailing edge region we work in polar coordinates. Also, since all the fluctuation terms are present at the current amplitude level we introduce Fourier expansions, as is seen in section 5.3.

We note that the results from the current work also hold in general for the case of the boundary-layer spot (Smith, Dodia and Bowles (1994)), partly because the mean pressure-amplitude law plays only a passive role for these higher levels of disturbance. The current analysis for the boundary-layer spot appears in a review paper by Smith, Dodia and Bowles (1994) in brief and will appear in detail in Bowles, Dodia and Smith (1994/5). Prof F. T. Smith and Dr R. G. A. Bowles are happy to confirm that this work was done jointly.

§5.1THE GOVERNING EQUATIONS AND EXPANSIONS

Since we are now examining the entire trailing edge region we work in polar coordinates. Defining $\bar{U}$ and $\bar{W}$ as our $R-$, $\theta-$ velocities, we have

$$\hat{U} = \bar{U}\cos\theta - \bar{W}\sin\theta,$$

$$\hat{W} = \bar{U}\sin\theta + \bar{W}\cos\theta,$$

so that our governing equations at the current amplitude level III which we need to address are

$$\bar{U}_R + \frac{\bar{U}}{R} + \bar{V}_{\hat{Y}} + \frac{\bar{W}_\theta}{R} = 0, \qquad (5.1.1a)$$

$$-\frac{2}{3}\bar{U} + \left(\bar{U} - \frac{1}{3}R\right)\bar{U}_R + \left(\bar{V} + \frac{2}{3}R\tilde{s}\right)\bar{U}_{\hat{Y}} + \frac{1}{R}(\bar{W})(\bar{U}_\theta - \bar{W}) = -\bar{P}_R, \quad (5.1.1b)$$

$$-\frac{2}{3}\bar{W} + \left(\bar{U} - \frac{1}{3}R\right)\bar{W}_R + \left(\bar{V} + \frac{2}{3}R\tilde{s}\right)\bar{W}_{\hat{Y}} + \frac{1}{R}(\bar{W})(\bar{W}_\theta + \bar{U}) = -\frac{\bar{P}_\theta}{R}, \quad (5.1.1c)$$

i.e the continuity, $R-$ momentum and $\theta-$ momentum equations. Our matching condition (2.3.3b) becomes

$$(\bar{U}, \bar{W}) \sim (\hat{Y} + \hat{A})(\cos\theta, -\sin\theta)$$

at large $\hat{Y}$. Also the normal scaling $\tilde{s}$ now equals $R^{-1}\hat{Y}$, of order unity, and is comparable with the previous s in section 2.4. From section 3.7 we have that as we raise the amplitude to the current level, $|A_{10}|$, $|u_{10}|$ increase to $O(\hat{X}^{3/2})$ and hence the mean flow correction becomes comparable with the basic flow $\hat{X}s$, while the fluctuating part $\propto \hat{X}^{-1/4}A_0$ increases to $O(\hat{X})$. So the expansions for the velocity variables at the current amplitude level are

$$\bar{U} = R(u_{0m}(\tilde{s},\theta) + u_{01}(F,\theta,\tilde{s})) + \ldots$$

$$+(Ru_{12}(F,\theta,\tilde{s}) + R^{-1/2}u_{11}(F,\theta,\tilde{s}) + R^{-1/2}u_{1m}) + \ldots$$

$$+(Ru_{23} + R^{-1/2}u_{22} + R^{-2}u_{21} + R^{-2}u_{2m}) + \ldots$$

$$+(Ru_{34} + R^{-1/2}u_{33} + R^{-2}u_{32} + R^{-7/2}u_{31} + R^{-7/2}u_{3m}) + \ldots, \qquad (5.1.2a)$$

$$\bar{V} = R^{5/2}v_{01} + \ldots + (R^{5/2}v_{12} + Rv_{11} + Rv_m) + \ldots$$

$$+(R^{5/2}v_{23} + Rv_{22} + R^{-1/2}v_{21} + R^{-1/2}v_{2m}) + \ldots$$

$$+(R^{5/2}v_{34} + Rv_{33} + R^{-1/2}v_{32} + R^{-2}v_{31} + R^{-2}v_{3m}) + \ldots, \qquad (5.1.2b)$$

$$\bar{W} = R(w_{0m} + w_{01}) + \ldots + (Rw_{12} + R^{-1/2}w_{11} + R^{-1/2}w_{1m}) + \ldots$$

$$+(Rw_{23} + R^{-1/2}w_{22} + R^{-2}w_{21} + R^{-2}w_{2m}) + \ldots$$

$$+(Rw_{34} + R^{-1/2}w_{33} + R^{-2}w_{32} + R^{-7/2}w_{31} + R^{-7/2}w_{3m}) + \ldots, \qquad (5.1.2c)$$

where

$$F \equiv R^{3/2}B(\theta),$$

and we have

$$\bar{P} = R^2p_{01} + \ldots + (R^2p_{12} + R^{1/2}p_{11} + R^{-1}p_{0m}) + \ldots, \qquad (5.1.2d)$$

$$\bar{A} = R(A_{0m} + A_{01}) + \ldots + (RA_{12} + R^{-1/2}A_{11} + R^{-1/2}A_{1m}) + \ldots, \qquad (5.1.2e)$$

for the pressure and amplitude respectively. The mean-flow terms with the subscripts m are functions of $\tilde{s}$, θ whereas the fluctuating terms depend also on the rapid variable F and represent in effect Fourier series in F. The expressions for $\tilde{s}$ and F yield the following transformations

$$\partial_R \to \partial_R + \frac{3}{2}R^{1/2}B\partial_F - \frac{\tilde{s}}{R}\partial_{\tilde{s}},$$

$$\partial_{\hat{Y}} \to R^{-1}\partial_{\tilde{s}},$$

$$\partial_\theta \to \partial_\theta + R^{3/2}B'\partial_F.$$

§5.2 THE CONTROLLING EQUATIONS

We now obtain the controlling equations from substituting $(5.1.2a-d)$ into $(5.1.1a-c)$. From the continuity equation at first order we have

$$\frac{3}{2}Bu_{01F}+v_{01\tilde{s}}+B'w_{01F}=0 \tag{5.2.1a}$$

from the wave-term contributions, while

$$-\tilde{s}u_{0m\tilde{s}}+2u_{0m}+v_{m\tilde{s}}+w_{0m\theta}=0 \tag{5.2.1b}$$

from the leading-order mean-flow term balance, and at second order we have

$$\frac{3}{2}Bu_{11F}+v_{11\tilde{s}}+B'w_{11F}-\tilde{s}u_{01\tilde{s}}+2u_{01}+w_{01\theta}=0, \tag{5.2.1c}$$

from the wave-term contributions. Now the R-momentum equation yields

$$(u_{0m}+u_{01}-\frac{1}{3})(\frac{3}{2}Bu_{01F})+v_{01}(u_{0m\tilde{s}}+u_{01\tilde{s}})+(w_{0m}+w_{01})B'u_{01F}=-\frac{3}{2}Bp_{01F}, \tag{5.2.2a}$$

from a leading $O(R^{5/2})$ balance;

$$\begin{aligned}-\frac{2}{3}(u_{0m}+u_{01})+(u_{0m}+u_{01}-\frac{1}{3})(u_{0m}+u_{01}-\tilde{s}u_{0m\tilde{s}}-\tilde{s}u_{01\tilde{s}}+\frac{3}{2}Bu_{11F})\\ +(u_{1m}+u_{11})(\frac{3}{2}Bu_{01F})+(u_{11\tilde{s}}+u_{1m\tilde{s}})v_{01}+(v_{11}+v_m+\frac{2}{3}\tilde{s})(u_{0m\tilde{s}}+u_{01\tilde{s}})\\ +(w_{0m}+w_{01})(u_{0m\theta}+u_{01\theta}+B'u_{11F}-w_{0m}-w_{01})+\\ (w_{11}+w_{1m})(B'u_{01F})=-\frac{3}{2}Bp_{11F}-2p_{01},\end{aligned} \tag{5.2.2b}$$

at $O(R)$; and the θ-momentum equation yields

$$(u_{0m}+u_{01}-\frac{1}{3})\frac{3}{2}Bw_{01F}+v_{01}(w_{0m\tilde{s}}+w_{01\tilde{s}})+(w_{0m}+w_{01})B'w_{01F}=-B'p_{01F}, \tag{5.2.3a}$$

from a $O(R^{5/2})$ balance; while

$$\begin{aligned}-\frac{2}{3}(w_{0m}+w_{01})+(u_{0m}+u_{01}-\frac{1}{3})(w_{0m}+w_{01}-\tilde{s}(w_{0m\tilde{s}}+w_{01\tilde{s}})+\frac{3}{2}Bw_{11F})\\ +(u_{1m}+u_{11})\frac{3}{2}Bw_{01F}+(w_{11\tilde{s}}+w_{1m\tilde{s}})v_{01}+(v_{11}+v_m+\frac{2}{3}\tilde{s})(w_{0m\tilde{s}}+w_{01\tilde{s}})\\ +(w_{0m}+w_{01})(w_{0m\theta}+w_{01\theta}+B'w_{11F}+u_{0m}+u_{01})+\end{aligned}$$

$$(w_{11} + w_{1m})B'w_{01F} = -B'p_{11F} - p_{01\theta}, \tag{5.2.3b}$$

at the next order. We now transform the pressure-displacement relation

$$P = -A_{XX},$$

into polar form, namely

$$\tilde{P} = -\left(c\partial_R - \frac{s}{R}\partial_\theta\right)^2 \tilde{A}, \tag{5.2.4}$$

where $c \equiv \cos\theta$, $s \equiv \sin\theta$. From substituting the expansions $(5.1.2d - e)$ into (5.2.4) we obtain the following controlling equations. At first order

$$-p_{01} = \left(\frac{3}{2}cB - sB'\right)^2 A_{01FF}; \tag{5.2.5a}$$

at second order

$$-p_{11} = \left(\frac{3}{2}cB - sB'\right)^2 A_{11FF} + \left(\frac{3}{2}B - 3scB' + s^2B'' + \frac{9}{4}c^2B\right) A_{01F}$$
$$+(2s^2B' - 3scB)A_{01F\theta}. \tag{5.2.5b}$$

These are used below.

§5.3 FOURIER SERIES EXPANSIONS

In section 5.1 above we noted that the fluctuating terms represent Fourier series in F. Below we examine this aspect in more detail and consider whether we have a closed system. Making the substitutions

$$u_{01} = \sum_{-\infty}^{\infty} a_n E^n, \quad v_{01} = \sum_{-\infty}^{\infty} b_n E^n, \quad w_{01} = \sum_{-\infty}^{\infty} c_n E^n, \quad p_{01} = \sum_{-\infty}^{\infty} g_n E^n,$$

with $a_0 = b_0 = c_0 = 0$, $a_{-n} = a_n^*, b_{-n} = b_n^*, c_{-n} = c_n^*, g_{-n} = g_n^*$ where $E \equiv e^{iF}$, we obtain from $(5.2.1a)$, $(5.2.2a)$, $(5.2.3a)$

$$\frac{3}{2}Bina_n + b_{n\tilde{s}} + B'inc_n = 0, \tag{5.3.1a}$$

$$(u_{0m} - \frac{1}{3})\frac{3}{2}Bina_n + u_{0m\tilde{s}}b_n + w_{0m}B'ina_n + \frac{3}{2}B\sum_j a_j a_{n-j} i(n-j) +$$

$$\sum_j b_j a_{n-j\tilde{s}} + B' \sum_j c_j a_{n-j} i(n-j) = -\frac{3}{2} B i n g_n, \qquad (5.3.1b)$$

$$(u_{0m} - \frac{1}{3})\frac{3}{2} B i n c_n + w_{0m\tilde{s}} b_n + w_{0m} B' i n c_n + \frac{3}{2} B \sum_j a_j c_{n-j} i(n-j) +$$

$$\sum_j b_j c_{n-j\tilde{s}} + B' \sum_j c_j c_{n-j} i(n-j) = -B' g_n i n. \qquad (5.3.1c)$$

$(5.3.1a-c)$ hold for all $n \neq 0$, and when $n = 0$ we have $0 = 0$ from $(5.3.1a)$

$$\sum_j b_j a^*_{j\tilde{s}} + B' \sum_j c_j a^*_j i(-j) = 0, \qquad (5.3.2a)$$

from $(5.3.1b)$ since $\frac{3}{2} B \sum_j a_j a^*_j i(-j) \equiv 0$,

$$\frac{3}{2} B \sum_j a_j c^*_j i(-j) + \sum_j b_j c^*_{j\tilde{s}} = 0, \qquad (5.3.2b)$$

from $(5.3.1c)$ since $B' \sum_j c_j c^*_j i(-j) \equiv 0$, which we assume later are satisfied. So taking the combination $\frac{3}{2} B * (5.3.1b) + B' * (5.3.1c)$ and setting $\tau_{0m} = \frac{3}{2} B u_{0m} + B' w_{0m}$, $\gamma_c^2 = (\frac{3}{2} B)^2 + B'^2$, $\tau_n = \frac{3}{2} B a_n + B' c_n$, we obtain

$$\left(\tau_{0m} - \frac{B}{2}\right) \tau_n i n + \sum_j \tau_j \tau_{n-j} i(n-j) + \sum_j \tau_{n-j\tilde{s}} b_j + \tau_{0m\tilde{s}} b_n = -\gamma_c^2 i n g_n, \quad (5.3.3a)$$

also the continuity equation becomes

$$i n \tau_n + b_{n\tilde{s}} = 0. \qquad (5.3.3b)$$

Further progress can be made by assuming that $\tau_{0m} = \alpha_1(\tilde{s} + A_{0m})$ so that

$$\tau_n = \alpha_1 A_{0n}, \quad b_n = -i n \tau_n \tilde{s}$$

is a solution where $\alpha_1 = (\frac{3}{2} B c - B' s)$. Substituting the above expressions for τ_{0m}, τ_n, b_n into $(5.3.3a)$ yields

$$\left[\alpha_1 A_{0m} - \frac{B}{2}\right] i n \alpha_1 A_{0n} + i \alpha_1^2 \sum_j (n-j) A_{0j} A_{0n-j} = -\gamma_c^2 i n g_n. \qquad (5.3.4a)$$

Coupling $(5.3.4a)$ with the pressure-displacement relation $(5.2.5a)$ we obtain

$$\left[\alpha_1 A_{0m} - \frac{B}{2}\right] n \alpha_1 A_{0n} + \alpha_1^2 \sum_j (n-j) A_{0j} A_{0n-j} = -\gamma_c^2 n^3 \alpha_1^2 A_{0n}. \qquad (5.3.4b)$$

This last relation is linked to the KDV type equation

$$\left[\alpha_1 A_{0m} - \frac{B}{2}\right] \alpha_1 A_F + \alpha_1^2 A A_F = \gamma_c^2 \alpha_1^2 A_{FFF}, \tag{5.3.5}$$

since substituting the form $A = \sum_j A_{0n} e^{inF}$ into (5.3.5) we obtain (5.3.4b) exactly. We now examine the mean-flow balances from (5.2.1b), (5.2.2b), (5.2.3b). Similarly to above we put

$$u_{11} = \sum_{-\infty}^{\infty} \hat{a}_n E^n, \quad v_{11} = \sum_{-\infty}^{\infty} \hat{b}_n E^n, \quad w_{11} = \sum_{-\infty}^{\infty} \hat{c}_n E^n, \quad p_{11} = \sum_{-\infty}^{\infty} \hat{g}_n E^n,$$

where $\hat{a}_0 = \hat{b}_0 = \hat{c}_0 = 0, \hat{a}_{-n} = \hat{a}_n^*, \hat{b}_{-n} = \hat{b}_n^*, \hat{c}_{-n} = \hat{c}_n^*, \hat{g}_{-n} = \hat{g}_n^*$. So our governing mean-flow balances from (5.2.1b), (5.2.2b), (5.2.3b) are

$$-\tilde{s} u_{0m\tilde{s}} + 2u_{0m} + v_{m\tilde{s}} + w_{0m\theta} = 0, \tag{5.3.6a}$$

$$-\frac{2}{3} u_{0m} + \left(u_{0m} - \frac{1}{3}\right)(u_{0m} - \tilde{s} u_{0m\tilde{s}}) + \left(v_m + \frac{2}{3}\tilde{s}\right) u_{0m\tilde{s}} + w_{0m}(u_{0m\theta} - w_{0m}) = \mathcal{F}_1, \tag{5.3.6b}$$

where

$$-\mathcal{F}_1 = \sum_{\bar{m}} [a_{\bar{m}}(a^*_{\bar{m}} - \tilde{s} a^*_{\bar{m}\tilde{s}}) + b_{\bar{m}} \hat{a}^*_{\bar{m}\tilde{s}} + \hat{b}_{\bar{m}} a^*_{\bar{m}\tilde{s}} + c_{\bar{m}}(-B' i\bar{m} \hat{a}^*_{\bar{m}} + a^*_{\bar{m}\theta} - c^*_{\bar{m}}) + \hat{c}_{\bar{m}}(-B' i\bar{m} a^*_{\bar{m}})] + c.c$$

$$-\frac{2}{3} w_{0m} + \left(u_{0m} - \frac{1}{3}\right)(w_{0m} - \tilde{s} w_{0m\tilde{s}}) + \left(v_m + \frac{2}{3}\tilde{s}\right) w_{0m\tilde{s}} + w_{0m}(w_{0m\theta} + u_{0m}) = \mathcal{F}_2, \tag{5.3.6c}$$

where

$$-\mathcal{F}_2 = \sum_{\bar{m}} [a_{\bar{m}}(-\frac{3}{2} B i\bar{m} \hat{c}^*_{\bar{m}} + c^*_{\bar{m}} - \tilde{s} c^*_{\bar{m}\tilde{s}}) + \hat{a}_{\bar{m}}(-\frac{3}{2} B i\bar{m} c^*_{\bar{m}}) + b_{\bar{m}} \hat{c}^*_{\bar{m}\tilde{s}} + \hat{b}_{\bar{m}} c^*_{\bar{m}\tilde{s}} + c_{\bar{m}}(c^*_{\bar{m}\theta} + a^*_{\bar{m}})] + c.c.$$

Here the $\mathcal{F}_1$, $\mathcal{F}_2$ give the 'Reynolds stresses'. Next we derive the equations governing the wave terms at next order from (5.2.1c), (5.2.2b), (5.2.3b). Namely

$$in\hat{\tau}_n + \hat{b}_{n\tilde{s}} + 2a_n - \tilde{s} a_{n\tilde{s}} + c_{n\theta} = 0, \tag{5.3.7a}$$

from (5.2.1c)

$$-\frac{2}{3}\tau_n+(u_{0m}-\frac{1}{3})(\tau_n-\tilde{s}\tau_{n\tilde{s}})+a_n(\tau_{0m}-\tilde{s}\tau_{0m\tilde{s}})+u_{1m}\frac{3}{2}Bin\tau_n+b_n\tau_{1m\tilde{s}}+$$

$$(v_m+\frac{2}{3}\tilde{s})\tau_{n\tilde{s}}+w_{0m}(\tau_{n\theta}-\frac{3}{2}Bc_n+B'a_n)+c_n(\tau_{0m\theta}-\frac{3}{2}Bw_{0m}+B'u_{0m})$$

$$+w_{1m}B'\tau_n in+(\tau_{0m}-\frac{1}{2}B)in\hat{\tau}_n+\hat{b}_n\tau_{0m\tilde{s}}$$

$$+\sum_{\bar{m}}[a_{\bar{m}}\left(\frac{3}{2}BiL\hat{\tau}_L+\tau_L-\tilde{s}\tau_{L\tilde{s}}\right)+\hat{a}_{\bar{m}}\frac{3}{2}BiL\tau_L+b_{\bar{m}}\hat{\tau}_{L\tilde{s}}+$$

$$\hat{b}_{\bar{m}}\tau_{L\tilde{s}}+c_{\bar{m}}\left(B'iL\hat{\tau}_L+\tau_{L\theta}-\frac{3}{2}Bc_L+B'a_L\right)+$$

$$\hat{c}_{\bar{m}}B'iL\tau_L]=-\gamma_c^2\hat{g}_n in-3Bg_n-B'g_{n\theta} \qquad (5.3.7b)$$

with $L=n-\bar{m}$, for $\bar{m}\neq n$ from combining (5.2.2b), (5.2.3b) as $\frac{3}{2}B*(5.2.2b)+B'*(5.2.3b)$. The next stage is to examine what happens when we take the real and imaginary parts of equations (5.3.7a,b). We may take this to be equivalent to regarding a_n, c_n, g_n as real and b_n as pure imaginary since

$$\tau_n=\alpha_1 A_{0n},\quad b_n=-in\tau_n\tilde{s}$$

is a solution, and similarly it follows that $\hat{a}_n$, $\hat{c}_n$, $\hat{g}_n$ may be regarded as real and $\hat{b}_n$ as pure imaginary. Therefore the real part of equation (5.3.7a) yields

$$2a_n-\tilde{s}a_{n\tilde{s}}+c_{n\theta}=0, \qquad (5.3.8a)$$

and the real part of equation (5.3.7b) yields

$$-\frac{2}{3}\tau_n+(u_{0m}-\frac{1}{3})(\tau_n-\tilde{s}\tau_{n\tilde{s}})+a_n(\tau_{0m}-\tilde{s}\tau_{0m\tilde{s}})+$$

$$(v_m+\frac{2}{3}\tilde{s})\tau_{n\tilde{s}}+w_{0m}(\tau_{n\theta}-\frac{3}{2}Bc_n+B'a_n)+c_n(\tau_{0m\theta}-\frac{3}{2}Bw_{0m}+B'u_{0m})$$

$$+\sum_{\bar{m}}[a_{\bar{m}}(\tau_L-\tilde{s}\tau_{L\tilde{s}})+c_{\bar{m}}\left(\tau_{L\theta}-\frac{3}{2}Bc_L+B'a_L\right)$$

$$=-3Bg_n-B'g_{n\theta}. \qquad (5.3.8b)$$

Hence as a consequence of carrying out this process we observe that the higher order terms u_{1m}, w_{1m}, τ_{1m}, $\hat{a}_n$, $\hat{b}_n$, $\hat{c}_n$, $\hat{g}_n$ have droped out. Our complete system, subject to the particular solutions and assumptions we have made,

controlling the major unknowns, namely the dominant fluctuations, the total mean flow and the phase function $B(\theta)$ is thus prescribed by equations $(5.2.5a)$, $(5.3.4a)$ plus $(5.3.6a, b, c)$ and $(5.3.8a, b)$, however the above analysis does need generalization. We note that the analogy we have made with amplitude level II suggests that the equations which are derived from the leading order wave balance, $(5.2.5a)$, $(5.3.4a)$, correspond to $(3.6.1a)$, and that $(5.3.6a, b, c)$, $(5.3.8a, b)$ from the mean flow and higher order wave balance respectively correspond to $(3.6.1c, b)$ respectively.

§5.4 SUMMARY

In this chapter we have studied the influence of higher amplitude nonlinear effects in the entire trailing edge region. As in previous chapters we again find that we have a mean flow/wave interaction. The KDV and Benjamin-Ono equations obtained for the wall-jet and boundary layer spot cases respectively, tend to imply that the 'spot structure' may be preserved as solitons retain their structure. A tentative link with the experimental observations of 'coherent structures' in turbulent boundary layers is suggested by Smith and Burggraf (1985), Kachanov et al (1993). Although the analysis is incomplete as yet, we do still find that the governing equations that we obtain are generally analogous with those at lower amplitudes in the caustic regions. Also the system is quite involved and complex and hence difficult to solve, but it is hoped that further follow-up study can be made.

CHAPTER 6

PLANE-POISEUILLE FLOW CASE

§6.0 INTRODUCTION

In this chapter we examine the case of a spot introduced into plane Poiseuille flow in a channel. The results of the linear theory in chapter 2 are used; there we noted that certain important properties are valid for both the channel and wall-jet cases; here we modify the nonlinear analysis of chapter 2, for the $x = O(t^{1/3})$ region.

One of the main differences between the present channel-flow case and the wall-jet case is that we have two wall-boundaries to consider, see figure 6.0.1, where the flow properties near the upper and lower channel walls interact through the pressure-displacement relation across the core. Naively we might expect to obtain more or less the same amplitude equations as in the wall-jet study. However we find instead that the symmetry of the geometry here acts to change the governing amplitude equations. In particular it is found that the nonlinear terms drop out eventually, although the remaining linear amplitude equations do match with the linear theory correctly, see sections 6.1, 6.2. In section 6.2 a method for overcoming this problem is suggested, although no details are presented. The main point of the above-mentioned modified approach is that we need to introduce an extra phase term in order to bring in nonlinear effects, this phase term implying a higher amplitude analysis as in Smith, Dodia and Bowles (1994). We describe the channel geometry and coordinate system as in Smith and Bowles (1992).

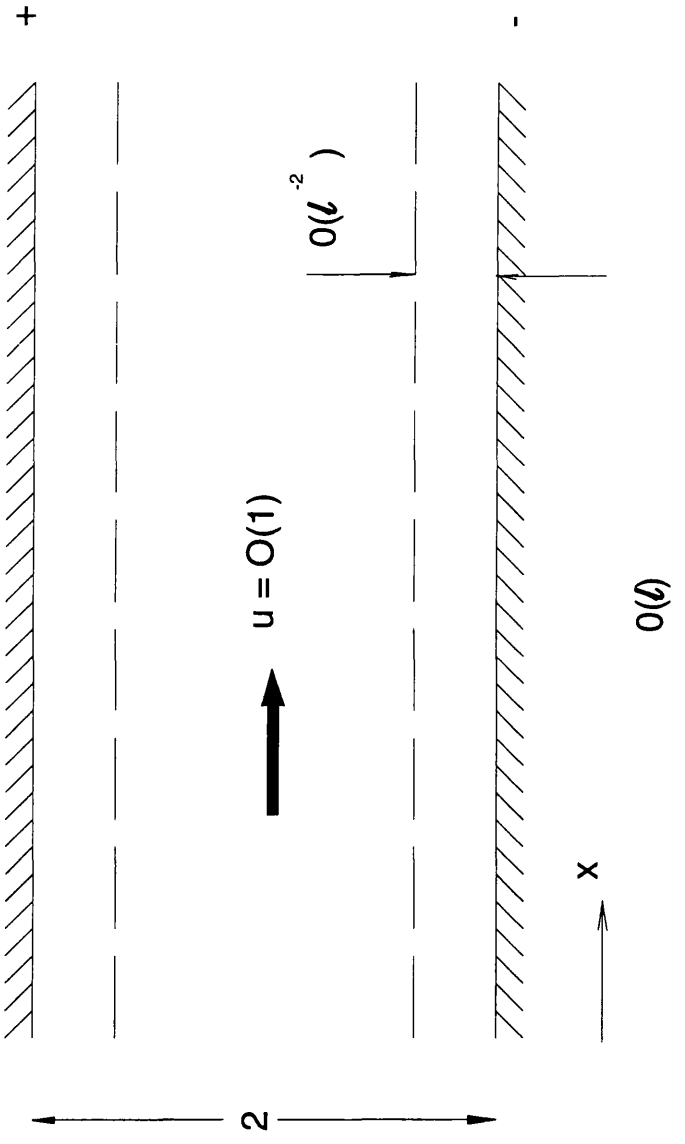

fig 6.0.1

Schematic diagram for the channel flow case.

§6.1 GOVERNING EQUATIONS

In the analysis which follows below we shall use the notation of chapter 2 for the velocity, pressure, amplitude and spatial variables. In addition we shall use the superscripts '+', '−' to denote properties holding near the upper and lower channel walls. (see figure 6.0.1). As in chapter 2 part I we start with the large-time equations

$$(\hat{U}_{\hat{X}} + \hat{V}_{\hat{Y}} + \hat{W}_{\hat{Z}})^{\pm} = 0, \tag{6.1.1a}$$

$$(-\frac{2}{3}\hat{U} + [\hat{U} - \frac{1}{3}\hat{X}]\hat{U}_{\hat{X}} + [\hat{V} + \frac{2}{3}\hat{Y}]\hat{U}_{\hat{Y}} + [\hat{W} - \frac{1}{3}\hat{Z}]\hat{U}_{\hat{Z}})^{\pm} = -\hat{P}^{\pm}_{\hat{X}}, \tag{6.1.1b}$$

$$(-\frac{2}{3}\hat{W} + [\hat{U} - \frac{1}{3}\hat{X}]\hat{W}_{\hat{X}} + [\hat{V} + \frac{2}{3}\hat{Y}]\hat{W}_{\hat{Y}} + [\hat{W} - \frac{1}{3}\hat{Z}]\hat{W}_{\hat{Z}})^{\pm} = -\hat{P}^{\pm}_{\hat{Z}}, \tag{6.1.1c}$$

subject to the main boundary conditions

$$\hat{V}^{\pm} = 0 \ \text{ at } \ \hat{Y} = 0, \tag{6.1.2a}$$

$$\hat{U}^{\pm} \sim \hat{Y} \mp \hat{A}, \ \ \hat{W}^{\pm} \to 0 \ \text{ as } \ \hat{Y} \to \infty \tag{6.1.2b}$$

The pressure-displacement relation is now given by

$$\hat{P}^{+} - \hat{P}^{-} = 2\hat{A}_{\hat{X}\hat{X}}, \tag{6.1.3}$$

see section 2.1. Also we use the same large-time expansions as for the wall-jet case namely

$$\hat{U}^{\pm} = \hat{X}s + (Eu_0^{\pm} + E^{-1}u_0^{*\pm})\hat{X}^{-1/4} + \ldots +$$

$$(E^2u_{12}^{\pm}\hat{X}^{-3/2} + Eu_{11}^{\pm}\hat{X}^{-3/4} + \hat{X}^{-1/2}u_{10}^{\pm} + c.c) + \ldots, \tag{6.1.4a}$$

$$\hat{V}^{\pm} = \hat{X}^{5/4}(Ev_0^{\pm} + E^{-1}v_0^{*\pm}) + \ldots$$

$$+\hat{X}^{3/2}(E^2v_{12}^{\pm}\hat{X}^{-3/2} + Ev_{11}^{\pm}\hat{X}^{-3/4} + \hat{X}^{-1/2}v_{10}^{\pm} + c.c) + \ldots, \tag{6.1.4b}$$

$$\hat{W}^{\pm} = \hat{X}^{-1/4}(Ew_0^{\pm} + E^{-1}w_0^{*\pm}) + \ldots$$
$$+\hat{X}^0(E^2 w_{12}^{\pm}\hat{X}^{-3/2} + Ew_{11}^{\pm}\hat{X}^{-3/4} + \hat{X}^{-1/2}w_{10}^{\pm} + c.c) + \ldots, \qquad (6.1.4c)$$

$$\hat{P}^{\pm} = \hat{X}^{3/4}(Eg_0^{\pm} + E^{-1}g_0^{*\pm}) + \ldots$$
$$+\hat{X}(E^2 g_{12}^{\pm}\hat{X}^{-3/2} + Eg_{11}^{\pm}\hat{X}^{-3/4} + \hat{X}^{-1/2}\hat{X}^{-1}g_{10}^{\pm} + c.c) + \ldots, \qquad (6.1.4d)$$

$$\hat{A} = \hat{X}^{-1/4}(EA_0 + E^{-1}A_0^*) + \ldots$$
$$+\hat{X}^0(E^2 A_{12}\hat{X}^{-3/2} + EA_{11}\hat{X}^{-3/4} + \hat{X}^{-1/2}A_{10} + \ldots) + \ldots. \qquad (6.1.4e)$$

We note that the expressions for the transformations and the oscillatory term E remain unchanged. Using a process similar to that in chapters 2, 4 we obtain the controlling equations for $(u_n^{\pm}, v_n^{\pm}, w_n^{\pm}, p_n^{\pm}, A_n)$, from the continuity, streamwise, spanwise momentum balances and from the pressure-amplitude relation, by substituting the large-time expansions $(6.1.4a-d)$ into the large-time asymptotes $(6.1.1a-c)$, and from substituting the expansions $(6.1.4d,e)$ into (6.1.3) respectively. As in the wall-jet case we find that we have an $E^0 - E^1$ interaction.

Below we show the external pressure-displacement relations. At first order

$$g_0^+ - g_0^- = -2A_0B^2, \qquad (6.1.5a)$$

at second order

$$g_{11}^+ - g_{11}^- = -2(A_{11}B^2 + 2\bar{q}iA_{0\hat{\eta}}B), \qquad (6.1.5b)$$

at third order

$$g_{21}^+ - g_{21}^- = -2(-\bar{q}^2 A_{0\hat{\eta}\hat{\eta}} + a_1\hat{\eta}A_0B + A_{21}B^2 + 2\bar{q}iBA_{11\hat{\eta}}), \qquad (6.1.5c)$$

and finally at fourth order

$$g_{31}^+ - g_{31}^- = -2(A_{31}B^2 + 2\bar{q}iA_{21\hat{\eta}}B - \bar{q}^2 A_{11\hat{\eta}\hat{\eta}} + a_1\hat{\eta}A_{11}B + i\bar{q}A_{0\hat{\eta}}a_1\hat{\eta} + \frac{1}{2}a_1\bar{q}iA_0), \qquad (6.1.5d)$$

from contributions proportional to E. Balancing mean-flow terms (i.e E^0 contributions) we obtain

$$g_{10}^{+} - g_{10}^{-} = -2A_{10\hat{n}\hat{n}}\bar{q}^2. \tag{6.1.5e}$$

Now we show the solutions/forms for the velocity variables.

At first order we obtain

$$u_0^{\pm} = \mp A_0 + \frac{a_1^2 g_0^{\pm}}{B\delta}, \tag{6.1.6a}$$

$$v_0^{\pm} = \pm iBA_0 s, \tag{6.1.6b}$$

$$w_0^{\pm} = -\frac{a_1 g_0^{\pm}}{\delta}, \tag{6.1.6c}$$

subject to

$$u_0^{\pm} \to \mp A_0 \ \text{ as } \ s \to \infty, \ \ v_0^{\pm} = 0 \ \text{ at } \ s = 0,$$

with the internal pressure-amplitude relation

$$A_0 = \mp \kappa g_0^{\pm}, \tag{6.1.6d}$$

where

$$\kappa \equiv 2b_1^{-1}B^{-1}(B^2 + a_1^2).$$

At second order

$$u_{11}^{\pm} = \mp A_{11} + \frac{i}{B}\left[\frac{\alpha}{\delta} + \frac{\beta}{2\delta^2}\right], \tag{6.1.7a}$$

where

$$\alpha = -ia_1^2 g_{11}^{\pm} - 2a_1(1 + \bar{q}a_1 B^{-1})g_{0\hat{\eta}}^{\pm},$$

and

$$\beta = -\bar{q}a_1^2 b_1 B^{-1} g_{0\hat{\eta}}^{\pm},$$

$$v_{11}^{\pm} = \bar{q}s\left[\frac{a_1^2 g_{0\hat{\eta}}^{\pm}}{B\delta} \mp A_{0\hat{\eta}}\right] - Big_{11}^{\pm} + \bar{q}g_{0\hat{\eta}}^{\pm} - i\delta u_{11}^{\pm}, \tag{6.1.7b}$$

$$w_{11}^{\pm} = -\left[\frac{a_1 g_{11}^{\pm} - ig_{0\hat{\eta}}^{\pm}}{\delta}\right] + \frac{is\bar{q}a_1 g_{0\hat{\eta}}^{\pm}}{\delta^2}, \tag{6.1.7c}$$

subject to

$$u_{11}^{\pm} \to \mp A_{11} \text{ as } s \to \infty, \quad v_{11}^{\pm} = 0 \text{ at } s = 0,$$

with the internal pressure-displacement relation

$$ib_1\kappa g_{11}^{\pm} = \mp ib_1 A_{11} + 2g_{0\hat{\eta}}^{\pm} B^{-1}(\frac{3}{2}b_1\bar{q} - \bar{q}^2 a_1 - 2a_1 - a_1^2\bar{q}B^{-1}). \qquad (6.1.7d)$$

At third order

$$u_{21}^{\pm} = \mp A_{21} - i\int_{\infty}^{s} \delta^{-1}[s\bar{q}u_{11\hat{\eta}s}^{\pm} + w_{11\hat{\eta}}^{\pm} - \frac{1}{2}(s-1)a_1\hat{\eta}iu_{0s}^{\pm}$$

$$+a_1\delta^{-1}[s\bar{q}w_{11\hat{\eta}}^{\pm} - \frac{1}{2}i(s-1)a_1\hat{\eta}w_0^{\pm} - g_{11\hat{\eta}}^{\pm} - ia_1 g_{21}^{\pm}]]ds, \qquad (6.1.8a)$$

$$v_{21}^{\pm} = -iBg_{21}^{\pm} + \bar{q}g_{11\hat{\eta}}^{\pm} - \frac{1}{2}a_1\hat{\eta}ig_0^{\pm} - \frac{1}{2}(s-1)a_1\hat{\eta}iu_0^{\pm} + s\bar{q}u_{11\hat{\eta}}^{\pm} - i\delta u_{21}^{\pm}, \quad (6.1.8b)$$

$$w_{21}^{\pm} = -i\delta^{-1}[s\bar{q}w_{11\hat{\eta}}^{\pm} - \frac{1}{2}i(s-1)a_1\hat{\eta}w_0^{\pm} - g_{11\hat{\eta}}^{\pm} - ia_1 g_{21}^{\pm}], \qquad (6.1.8c)$$

subject to

$$u_{21}^{\pm} \to \mp A_{21} \text{ as } s \to \infty, \quad v_{21}^{\pm} = 0 \text{ at } s = 0.$$

Finally at fourth order we have

$$w_{31}^{\pm} = -i\delta^{-1}[-g_{21\hat{\eta}}^{\pm} - ia_1 g_{31}^{\pm} + s\bar{q}w_{21\hat{\eta}}^{\pm} - \frac{1}{2}i(s-1)a_1\hat{\eta}w_{11}^{\pm} + \left[\frac{s}{4} + \frac{7}{12}\right]w_0^{\pm}$$

$$+(s-1)sw_{0s}^{\pm} + \frac{1}{3}\hat{\eta}w_{0\hat{\eta}}^{\pm} - v_0^{\pm}w_{10s}^{\pm} - v_{10}^{\pm}w_{0s}^{\pm} - iBu_{10}^{\pm}w_0^{\pm} - ia_1 w_{10}^{\pm}w_0^{\pm}], \quad (6.1.9a)$$

$$u_{31}^{\pm} = \left[\mp A_{31} - i\int_{\infty}^{s} \delta^{-1}\bar{\bar{B}}_{31}^{\pm} ds\right], \qquad (6.1.9b)$$

where

$$\bar{\bar{B}}_{31}^{\pm} = \bar{Q}_1^{\pm} + Q_2^{\pm},$$

and

$$\bar{Q}_1^{\pm} = a_1\delta^{-1}[-v_0^{\pm}w_{10s}^{\pm} - v_{10}^{\pm}w_{0s}^{\pm} - iBu_{10}^{\pm}w_0^{\pm} - ia_1 w_{10}^{\pm}w_0^{\pm}]$$

$$-[iBu_{10}^{\pm}u_0^{\pm} + v_{10}^{\pm}u_{0s}^{\pm} + v_0^{\pm}u_{10s}^{\pm} + w_{10}^{\pm}u_0^{\pm}a_1 i]_s,$$

$$Q_2^{\pm} = w_{21\hat{\eta}}^{\pm} - \frac{1}{2}(s-1)a_1\hat{\eta}iu_{11s}^{\pm} + s\bar{q}u_{21\hat{\eta}s}^{\pm} + (s^2-s)u_{0ss}^{\pm}$$
$$+\left(\frac{5}{4}s - \frac{5}{12}\right)u_{0s}^{\pm} + \frac{1}{3}\hat{\eta}u_{0\hat{\eta}s}^{\pm} + a_1\delta^{-1}[-g_{21\hat{\eta}}^{\pm} - ia_1g_{31}^{\pm} + s\bar{q}w_{21\hat{\eta}}^{\pm}$$
$$-\frac{1}{2}i(s-1)a_1\hat{\eta}w_{11}^{\pm} + \left(\frac{s}{4} + \frac{7}{12}\right)w_0^{\pm} + (s-1)sw_{0s}^{\pm} + \frac{1}{3}\hat{\eta}w_{0\hat{\eta}}^{\pm}].$$

So we find that the velocity variables are analogous with those from the wall-jet case. As before in chapter 2 we can manipulate the equations at fourth order and obtain the governing amplitude relation for A_0. The main difference now is that we have two sets of results holding near the upper and lower channel walls, which interact through the pressure-displacement relations $(6.1.5a-e)$. Before obtaining the above mentioned amplitude equation (in section 6.2) however, we derive the eigenrelations from the internal and external pressure-displacement relations. First $(6.1.5a)$ with $(6.1.6d)$ gives

$$b_1 = 2B(B^2 + a_1^2),$$

which is effectively the dominant eigenrelation leaving $g_0^{\pm}$ arbitrary. Second coupling $(6.1.5b)$ with $(6.1.7d)$ gives the eigenrelation

$$\bar{q}B(B^2 - a_1^2) = -\bar{q}b_1 + 2a_1B^2$$

leaving $g_0^{\pm}$, $g_{11}^{\pm}$ arbitrary. We note that these eigenrelations are identically equal to those for the wall-jet case, and hence for the constant $\bar{q} = 1/3^{1/2}$ corresponding to the half-angle $\theta_c = 30°$ we find that the other constants remain the same. These results are used in the working leading to the amplitude equation for A_0.

Finally in this section we examine the mean-flow term balances obtained from the continuity and momentum equations. At second order we obtain

$$-\bar{q}u_{10\hat{\eta}}^{\pm} + v_{20s}^{\pm} + w_{10\hat{\eta}}^{\pm} = 0, \qquad (6.1.10a)$$

$$v_{20}^{\pm} - s\bar{q}u_{10\hat{\eta}}^{\pm} = 0, \qquad (6.1.10b)$$

$$-s\bar{q}w^{\pm}_{10\hat{\eta}} = 0, \tag{6.1.10c}$$

from the continuity, streamwise and spanwise momentum balances respectively; hence

$$w^{\pm}_{10} = 0, \quad v^{\pm}_{20} = \mp s\bar{q}A_{10\hat{\eta}}, \quad u^{\pm}_{10} = \mp A_{10}.$$

At the next order the controlling equations linking $(u^{\pm}_{30}, v^{\pm}_{40}, w^{\pm}_{30})$ are

$$(2/3)su^{\pm}_{10_s} - (1/3)\hat{\eta}u^{\pm}_{10\hat{\eta}} - (1/2)su^{\pm}_{10} - (1/2)u^{\pm}_{10} + v^{\pm}_{40} - s\bar{q}u^{\pm}_{30\hat{\eta}}$$

$$v^{\pm}_{10}u^{\pm}_{10_s} - (s - (1/3))su^{\pm}_{10_s} + f^{\pm}_1 = \bar{q}g^{\pm}_{10\hat{\eta}}, \tag{6.1.11a}$$

where

$$f^{\pm}_1 = [v^{\pm}_0 u^{*\pm}_{11_s} + v^{\pm}_{11}u^{*\pm}_{0_s} - w^{\pm}_0 a_1 i u^{*\pm}_{11} - w^{\pm}_{11}a_1 i u^{*\pm}_0 + w^{\pm}_0 u^{*\pm}_{0\hat{\eta}} - u^{\pm}_0 \bar{q}u^{*\pm}_{0\hat{\eta}} + c.c],$$

$$sw^{\pm}_{10_s} - s^2 w^{\pm}_{10_s} - (1/3)\hat{\eta}w^{\pm}_{10\hat{\eta}} - (1/2)w^{\pm}_{10} - (1/2)sw^{\pm}_{10}$$

$$-s\bar{q}w^{\pm}_{30\hat{\eta}} + v^{\pm}_{10}w^{\pm}_{10_s} + f^{\pm}_2 = -g^{\pm}_{10\hat{\eta}}, \tag{6.1.11b}$$

where

$$f^{\pm}_2 = [v^{\pm}_0 w^{*\pm}_{11_s} + v^{\pm}_{11}w^{*\pm}_{0_s} + w^{\pm}_0 w^{*\pm}_{0\hat{\eta}} - iBu^{\pm}_0 w^{*\pm}_{11} - iBu^{\pm}_{11}w^{*\pm}_0 - u^{\pm}_0 \bar{q}w^{*\pm}_{0\hat{\eta}} + c.c],$$

from the streamwise and spanwise balances respectively. Following the pattern of chapter 2 and using (6.1.5e) we can take the combination $\bar{q}$ times (6.1.11a) minus (6.1.11b) and then set $s = 0$ in the resulting equation to give

$$-2\bar{q}^2 A_{10\hat{\eta}\hat{\eta}\hat{\eta}} = \frac{\bar{q}}{(\bar{q}^2+1)}\left[\frac{2}{3}\hat{\eta}A_{10\hat{\eta}} + A_{10}\right] + \tilde{\Omega},$$

where

$$\tilde{\Omega} \equiv -4b_1^{-2}(B^2 + a_1^2)[g^+_0 g^{+*}_0 - g^-_0 g^{-*}_0]_{\hat{\eta}},$$

but we have from (6.1.6d) that

$$g^{\pm}_0 = \mp\kappa^{-1}A_0,$$

so $\tilde{\Omega} \equiv 0$, and we are eventually left with

$$-2\bar{q}^2 A_{10\hat{\eta}\hat{\eta}\hat{\eta}} = \frac{\bar{q}}{(\bar{q}^2+1)}\left[\frac{2}{3}\hat{\eta}A_{10\hat{\eta}} + A_{10}\right]. \tag{6.1.12}$$

So comparing with the wall-jet case we see that the term proportional to $|g_0|^2$ has dropped out. It is felt that this is due to the symmetry of the channel geometry.

§6.2 GOVERNING AMPLITUDE EQUATION

In this section we show the main amplitude equation governing A_0. As for the wall-jet case this equation is obtained from the fourth order continuity, streamwise and spanwise momentum balances, using the external pressure-displacement equations to eliminate the $(g_0^{\pm}, g_{11}^{\pm}, g_{21}^{\pm}, g_{31}^{\pm})$ terms. After some manipulation we find as a solvability condition the amplitude equation

$$\frac{4}{3^{3/2}}A_{0\hat{\eta}\hat{\eta}\hat{\eta}} - \frac{1}{3}\hat{\eta}A_{0\hat{\eta}} - \frac{1}{3}A_0 = 0, \tag{6.2.1}$$

for A_0 which reduces to Airy's equation for $A_0(\hat{\eta})$ after an integration with respect to $\hat{\eta}$. Comparing with the wall-jet amplitude equation (2.7.3) we see that there is no longer a nonlinear contribution present, again this effect is attributed to the symmetry in the geometry of the channel. So we have two main governing equations (6.1.12), (6.2.1), with no nonlinear terms present. A possible way to resolve this difficulty is to consider an extra phase effect in the wave contribution term, i.e

$$E \equiv \exp[i(b_1\hat{X}^{3/2} + a_1\hat{X}^{1/2}\hat{\eta} + \hat{X}^{\iota}\tilde{f}(\hat{\eta})]$$

say, where ι needs to be determined and $\tilde{f}(\hat{\eta})$ is the phase. This in a sense corresponds to examining higher amplitude effects, so $\hat{\eta}$ in the above wave term expression needs to be increased (cf. Smith, Dodia and Bowles (1994)).

§6.3 SUMMARY

Modifying the earlier analysis of chapter 2, we have examined, as far as is possible now, a spot disturbance in a channel flow. The amplitude equations that we obtain are linear; the nonlinear terms that are present in the wall-jet case drop out in the current analysis because of the symmetry of the channel.

Our conclusion is that higher amplitudes need to be taken into account, as in Smith, Dodia and Bowles (1994), by introducing an extra phase effect. However other details may need consideration.

CHAPTER 7

SUMMARY & CONCLUSIONS

§7.0 SUMMARY & CONCLUSIONS

In this thesis we have presented a theoretical study on the properties of spots in wall-jets and channel flows. In chapter 2 we addressed a linear model, and it was found that for large-scaled distances, $X = O(T^{1/3})$ where T denotes scaled time, the beginning of a confined wake with a half-angle of 30° can be distinguished. Also the maximum amplitude occurs near the edges of the wake, the amplitude having an Airy function dependence within the thin edge-layer(s), and decaying exponentially outside the wake region, but with multiple waves in-between the two edges.

A nonlinear model built up from the linear theory is also presented in chapter 2. The aim of the nonlinear study is to understand how the nonlinear effects which enter the edge-layer(s) first affect the trailing region of the spot, and to obtain some guidance on 3D amplitude dependent effects in spot development, so that we may build up a picture of the flow structure in a typical nonlinear spot. Outside the edge-layer(s) we find that the linear properties continue to hold, leading in particular to the 30° half-angle prediction, as the flow solution matches back to the linear theory. However at higher amplitudes we have a full nonlinear set of amplitudes equations holding near the edge-layer(s). Numerical solutions for these equations confirm that the amplitude decays exponentially outside the edge-layer(s) and algebraically inside. Unfortunately there seems to be no experimental work to compare with as regards spots in wall-jet flows, as far as we know, although we would expect that in practice spots in boundary-layer flows and plane Poiseuille flows in channels would have properties similar to those of spots in wall-jets, in broad terms. So comparing the results mentioned so far with a channel flow spot say, e.g Carlson, Widnall and Peeters (1982), the half-angle prediction is over estimated, even though the overall structure is in agreement. Although we note cautiously that the 'reversed' arrowhead shape found in practice in channel flows, is not predicted by the theory.

In chapter 3 we consider raising the amplitude further analytically and

investigate the effects of stronger nonlinearity. The governing equations that we obtain are difficult to solve and so a modified system of equations suitable for a phase-plane analysis is studied. For this modified system we find that three critical points are present, see section 3.4, but a unique solution for a particular selected set of initial conditions is possible. This information is used to find numerical solutions for the actual system, a Runge-Kutta shooting method being used. The main conclusion drawn from this chapter is that nonlinear effects move inwards towards the centre of the spot disturbance, and hence the spread angle is reduced, a property which is not so well confirmed from the numerical results for the amplitude level I equations.

In chapter 4 we examine the edge-layer properties further downstream at streamwise and spanwise distances of $O(t)$. In this zone we find that the initial disturbance $\bar{A}(X, Z, O)$ acts to change the solution amplitude at leading order, see section 4.4. In particular for the detailed distribution $\tilde{Q}(\alpha, \beta) = \exp(-[\alpha^2 + \beta^2])$ (see section 4.4), the amplitude is damped by an exponentially decaying factor $e^{-\tilde{X}/c3^{1/2}}$. We note that the spread half-angle is again 30° in the linear limit because our investigation is aimed specifically at the unsteady thin-layer Euler equations and also the governing amplitude equations are analogous with those in the $O(t^{1/3})$ region. We draw the conclusion that along the edge-layers up to distances of $O(t)$, sets of nonlinear amplitude equations apply, which in general require a computational treatment

Increasing the amplitude further still from that of chapter 3 we find that nonlinearity floods the entire trailing-edge, $O(t^{1/3})$, region. We find that the dominant fluctuations are represented by a modified KDV equation, the Benjamin-Ono equation being the corresponding traveling wave equation obtained for the boundary-layer spot study in Smith, Dodia and Bowles (1994). These equations verify the existence of nonlinear multiple waves. We should however note that a simplification is made by assuming the skewed mean flow component τ_{0m} to be equal to a uniform shear, i.e $\tau_{0m} = \alpha_1(\tilde{s} + A_{0m})$, see section 5.3. The other main feature of the work in chapter 5 is that Reynolds

stress terms proportional to the square of the typical amplitudes of the dominant fluctuations are present, which is encouraging, since they are generally associated with 'turbulence', see section 1.0. A fuller study on this amplitude level III is to be presented in Bowles, Dodia and Smith (1994/5).

Finally as regards this thesis, the corresponding analysis for the plane Poiseuille flow spot is shown in chapter 6. Briefly, we find that since the geometry of the channel is symmetric, the nonlinear terms at amplitude level I cancel out, although it is felt that by increasing the amplitude we may yet find nonlinear effects playing a significant role. The linear theory, on the other hand, does predict a 30° half-angle for the wake as for the wall-jet case and also the amplitude is dominant near the edges of the wake, again as for the wall-jet study.

At distances beyond $O(t)$, $x = O(t^\gamma)\tilde{x}$, where $\gamma > 1$ say, we would expect the full Euler equations to hold, since in the local region $\tilde{x}$ under investigation short-scale effects become active. In essence we would have an interaction between long and short length scales, as in Smith, Dodia and Bowles (1994). All of this implies a large numerical task. Other important factors which we have so far neglected are:

- compressibility,
- viscosity,
- short-scale effects.

From the studies of Doorly and Smith (1992), Smith (1992), Smith, Dodia and Bowles (1994), Bowles and Smith (1994), it seems clear that in order to obtain a full knowledge of the physics of transitional/turbulent spots, most of these factors need to be incorporated along with nonlinearity already introduced.

As in Smith, Dodia and Bowles (1994) we note here that the theory tentatively appears to fall in line with some of the experimental findings outlined in chapter 1, i.e

1. much of the dynamics in a spot resembles closely that in a fully turbulent boundary-layer/channel flow,

2. a turbulent spot develops fast, typically from localized disturbances with large initial amplitude,

3. the spanwise growth of the spot greatly exceeds the growth normal to the surface.

These features are all implicit in the present theory. However as regards the spot spread angle, the agreement with experiments is poor, although as mentioned previously above, short-scale effects need consideration and the solutions at amplitude level III and beyond may prove to be useful.

We end this study by noting that although transitional/turbulent spots in general, in many different contexts, e.g, airfoil flows, turbomachinery, are very interesting and important coherent structures which need detailed investigation, they are by no means the only important quantities in the transition process leading to turbulence.

REFERENCES

1. Acheson, D.J. Elementary Fluid Dynamics: Oxford applied mathematics and computing science series (1990).

2. Alavyoon, F., Henningson, D.S. and Alfredsson, P.H. Turbulent spots in plane Poiseuille flow-flow visualization. *Phys.Fluids* (1986), **29** 1328-1331.

3. Benny, D. J. and Bergeron, R. F., Stud. Appl. Math. **48**, 181-204 (1969).

4. Bodonyi, R. J., Smith, F. T. and Gajjar, J. S. B. IMA J. Appl. Math. **30**, 1-19 (1983).

5. Bowles, R.G.A., Dodia, B.T. and Smith, F.T., In preparation. (1994).

6. Bowles, R.G.A., Smith, F.T., Short-scale effects on model boundary-layer spots. Submitted to *J.Fluid.Mech.* (1994).

7. Chambers, F.W. and Thomas, A.S.W. Turbulent spots, wave packets and growth. *Phys.Fluids* (1983) **26**, 1160-1162.

8. Carlson, D.R., Widnall, S.E. and Peeters, M.F. A flow visualization study of transition in plane Poiseuille flow. *J.Fluid.Mech.* (1982) **121**, 487-505.

9. Chapman, G.T. and Tobak, M. Observations, Theoretical Ideas, and Modeling of Turbulent flows - Past, Present and Future. Applied Mathematical Sciences series. **58** Theoretical Approaches to Turbulence. Chapter II *pp* 19-49.

10. Cheng, H.K. and Johnson, E.R., Inertial waves above an obstacle in an unbounded, rapidly rotating fluid. *Proc. Roy. Soc.* A 383 (1982) 71 - 87.

11. Dodia, B.T., Bowles, R.G.A. and Smith, F.T., In preparation. (1994/5).

12. Doorly, D.J. and Smith, F.T., Initial-value problems for spot disturbances in incompressible or compressible boundary layers. *J.Engng.Math.* (1992) **26**, 87-106.

13. Emmons, H.W., The laminar-turbulent transition in a boundary layer, Part I *J.Aero.Sci.* (1951) **18**, 490-498.

14. Gaster, M. and Grant, I., An experimental investigation of the formation and development of a wave packet in a laminar boundary layer. *Proc. Roy. Soc.* A 347 (1975) 253-269

15. Gaster, M., A theoretical model of a wave packet in the boundary layer on a flat plate. *Proc. Roy. Soc.* A 347 (1975) 271-289.

16. Gaster, M., The nonlinear phase of wave growth leading to chaos and breakdown to turbulence in a boundary layer as an example of an open system. *Proc. Roy. Soc.* A 430 (1990) 3-24.

17. Glezer, A., Katz, Y. & Wygnanski, I.J., On the breakdown of the wave packet trailing a turbulent spot in a laminar boundary layer. *J.Fluid.Mech.* (1989) **198**, 1-26.

18. Goldstein, M.E. and Choi, S,-W., Nonlinear evolution of interacting oblique waves on two-dimensional shear layers. *J.Fluid.Mech.* (1989), **207** 97-120 & corrigendum *J.Fluid.Mech.* (1990), **216** 659-663.

19. Hall, P. and Smith, F.T. On strongly nonlinear vortex/wave interactions in boundary-layer transition. *J.Fluid.Mech.* (1991), **227** 641-666.

20. Henningson, D.S. and Kim, J., On turbulent spots in plane Poiseuille flow. *J.Fluid.Mech.* (1991) **228**, 183-205.

21. Henningson, D.S., Spalart, P. and Kim, J. Numerical simulation of turbulent spots in plane Poiseuille and boundary layer flows. *Phys.Fluids A.*, (1989), **30** 2914-2931.

22. Kachanov, Y.S., Ryzhov, O.S. and Smith, F.T. Formation of solitons in transitional boundary layers: theory and experiment. *J.Fluid.Mech.* (1993), **251** p 273.

23. Klebanoff, P.S., Tidstrom, K.D. and Sargent, L.M., The three dimensional nature of boundary layer transition. *J.Fluid.Mech.* **12**, 1-34.

24. Lindberg, P.A., Fahlgren, E.M., Alfredsson, P.H. and Johansson, A.V. An experimental study of the structure and spreading of turbulent spots. In *Laminar-turbulent transition* (ed. V.V. Kozlov). Springer, Berlin (1984), 617-641.

25. Narasimha, R. On the distribution of intermittency in the transition region of a boundary layer. *J.Aero.Sci.*, **24** p 711.

26. Ovid, Metamorphoses. Penguin classics, translated by Mary Innes.

27. Patera, A. and Orzag, S. Subcritical transition to turbulence in plane shear flows. In *Transition to turbulence* (ed. R.E. Meyer), Academic Press, New York (1981), 127-175.

28. Pedlosky, J. Geophysical Fluid Dynamics. (second edition) Springer-Verlag (1987).

29. Reynolds, W.C and Potter, M.C. Finite amplitude instability of parallel shear flows. *J.Fluid.Mech.*, (1967) **27** p 465.

30. Schubauer, G.B. and Klebanoff, P.S. Contributions on the mechanics of boundary layer transition. (1956) *NACA* Rep. no. **128**.

31. Smith, C.R., Walker, J.D.A., Haidari, A.H., Sobrun, U On the dynamics of near-wall turbulence. *Trans. Roy. Soc.* A 336 (1991) 131-175.

32. Smith, F.T., On nonlinear effects near the wing-tips of an evolving boundary-layer spot *Phil.Trans.R.Soc.Lond.* A340 (1992), 131-165.

33. Smith, F.T. and Bowles, R.I. Transition theory and experimental comparisons on (I) amplification into streets and (II) a strongly nonlinear break-up criterion. *Proc. Roy. Soc.* A 439 (1992) 163 - 175.

34. Smith, F.T., Brown, S.N. and Brown, P.G. Initiation of three- dimensional nonlinear transition paths from an inflectional profile. *Eur. J. Mech.* (1993) **12** no. 4 447.

35. Smith, F.T. and Burggraf, O.R., On the development of large-sized short-scaled disturbances in boundary layers. *Proc. Roy. Soc.* A 399 (1985) 25-35.

36. Smith, F.T., Dodia, B.T. and Bowles, R.G.A., On global and internal dynamics of spots: a theoretical approach. *J.Engng.Math.* (1994) **28**, 73-91.

37. Smith, F.T., Doorly, D.J. and Rothmayer, A.P., On displacement thickness, wall-layer and mid-flow scales in turbulent boundary layers, and slugs of vorticity in pipes and channels. *Proc. Roy. Soc.* A 428 (1990) 255-281.

38. Stewart, P.A., and Smith, F.T., Three-dimensional nonlinear blow-up from a nearly planar initial disturbance, in boundary-layer transition: theory and experimental comparisons. *J.Fluid.Mech.* (1992) **244**, 79-100.

39. Stuart, J.T. *Laminar boundary layers* (ed. L. Rosenhead), ch IX. Oxford University Press (1963).

40. Stuart, J.T. On the nonlinear mechanics of wave disturbance in stable and unstable parallel flow. *J.Fluid.Mech., Pt 1*, (1960) **9** p 355.

41. Widnall, S.E. Growth of turbulent spots in plane Poiseuille flow. In *Turbulence and Chaotic Phenomena in Fluids.* (ed. T. Tatsumi), Elsevier (1984), 93-98.

42. Wygnanski, I.J., Haritonides, J.H. and Kaplan, R.E. On a Tollmien-Schlichting wave packet produced by a turbulent spot *J.Fluid.Mech.* (1979) **92**, 505-528.

43. Wygnanski, I.J., Sokolov, M. and Friedman, D. On a turbulent spot in a laminar boundary layer. *J.Fluid.Mech.* (1976) **78**, 785-819.

44. Young, A.D. Boundary layers, B.S.P Professional books (1989).